To the Graduate Council:

I am submitting herewith a thesis written by Tara Liyana Mallison entitled "Comparing In Situ Submerged Jet Test Device and Laboratory Flume Methods to Estimate Erosional Properties of Cohesive Soils for Bank Stability Models." I have examined the final electronic copy of this thesis for form and content and recommend that it be accepted in partial fulfillment of the requirements for the degree of Master of Science, with a major in Environmental Engineering.

_____
John S. Schwartz
Major Professor

We have read this thesis
and recommend its acceptance:

_____
Larry D. McKay

_____
Randall W. Gentry

Accepted for the Council:

_____
Carolyn R. Hodges
Vice Provost and Dean of
the Graduate School

Comparing In Situ Submerged Jet Test Device and Laboratory Flume Methods to Estimate Erosional Properties of Cohesive Soils for Bank Stability Models

A Thesis
Presented for the
Master of Science
Degree
The University of Tennessee, Knoxville

Tara Liyana Mallison
May 2008

Acknowledgements

Earning a masters degree in Environmental Engineering has been an arduous process and I could not have accomplished the goal without support from the University of Tennessee (UT), professors, family, and friends. First and foremost, I would like to thank the UT Center for Environmental Biotechnology (CEB) and the UT Institute for a Secure and Sustainable Environment (ISSE) for funding this research. I would especially like to thank my major professor, Dr. John Schwartz, for his intelligence, guidance, support, and motivation. When the research reached frustrating obstacles, he was present to turn things around and move things forward. Dr. Schwartz paid attention to my strengths and weaknesses so that he could best utilize and improve upon my abilities as a graduate student. Dr. Larry McKay and Dr. Randy Gentry have contributed their time and resources to help reach the research objectives. I would like to thank the two of them for serving on my committee and providing resources and guidance.

Thanks to Andrew Simon, Brian Bell, and the rest of the crew at the National Sedimentation Laboratory for the use of their resources, equipment, and for the direction they provided, and to Dr. Tess Wynn in the Biological Systems Engineering Department at Virginia Tech for providing her expert opinion on the research topic. Larry Roberts and Ken Thomas have contributed a lot to this project. I would like to thank them for their incredible shop abilities in the construction and alteration phases of the flume. And, special thanks go to M. Patrick Massey for his unwavering support in the field and ability to keep things under control in the Perkins office. In the future, even though he won't need it, Patrick will have me as a good reference for his character, quality of work, and determination. William Tyler Mallison, Nancy Roberts, Amanda Dunnavant, Keil Neff,

and Dan Carter also helped with data acquisition or laboratory testing procedures. I appreciate their assistance with the research collection and analysis process.

Finally, I would especially like to thank my husband again, William Tyler Mallison, and my parents, Andy & Loretta Liyana and Tom & Sharron Mallison, for being supportive of continuing education and challenging me to succeed and attempt to learn as much as they already know. Without their love and continual support, I would not have had the time, strength, or determination to reach my goal of graduating from the University of Tennessee's Environmental Engineering Masters program.

Abstract

In order to accurately predict the stability of riverbanks, model input parameters must be reliable bank failure estimators. Currently, bank stability models require two input parameters to predict bank erosion: critical erosion shear stress and erodibility coefficient. The investigation's purpose was to compare two erosion estimation methods and improve the bank stability models for cohesive soil commonly found on the banks.

To accomplish the objective, critical shear stresses and erodibility coefficients obtained using the in situ submerged jet test device (SJT) were measured against results from the closed-loop laboratory flume method for 12 cohesive bank sites. Additionally, SJT critical shear stress values were compared to values found via empirical relationships found in literature that incorporate plasticity index, median particle diameter, percent silt-clay or percent clay content to compute critical shear stress. Particle size analysis and Atterberg limit determinations were run classify the sediment type collected.

The critical shear stress values obtained ranged from 0.09 to 5.84 Pa and SJT erodibility coefficients varied from 0.37 to 10.07 $cm^3/N{\cdot}s$. From flume observations, cohesive soil erosion was influenced by interparticle forces and occurred in aggregate pieces and particle-by-particle. A few critical shear stress values appeared to be unreliable considering the critical shear stress threshold of 1.83 Pa found using the laboratory flume analysis and the limited erosion witnessed. Study results also indicated that sediment properties did not correlate directly with the SJT critical shear stress values or with each other.

Flume observations and variations among experimental results suggest other influential factors exist besides critical shear stress and the erodibility coefficient when

quantifying the cohesive sediment erosivity. When empirical results were lower than the flume's critical shear stress threshold, it was possible the mechanical soil property could not be transferred to the soil types tested or estimates incorrectly assumed zero physical and chemical influences. Because of its complexities, traditional experimental design may not reliably measure cohesive soil erosion. Only through the continued collaboration of various field and advanced degree professionals and the detailed, high-quality documentation of as many influential parameters as possible per project can the goal of estimating cohesive sediment erosion be accomplished.

Table of Contents

1 Introduction 1
2 Literature Review 5
2.1 Noncohesive Material 6
2.1.1 Shields Parameter 6
2.1.2 Alternate Form of Shields Diagram 8
2.2 Cohesive Material 9
2.2.1 Flume Experiments 10
2.2.2 Submerged Jet Test Device 15
2.2.3 Cohesive Strength Meter 19
2.2.4 Relating Critical Shear Stress & Erosion Rate to Soil Properties 20
2.2.5 Simple Relations 23
2.3 Additional Effects on Erosion 23
3 Device Descriptions 26
3.1 Submerged Jet Test Device 26
3.2 University of Tennessee Closed-Loop Laboratory Flume 27
4 Methodology 31
4.1 Test Locations 31
4.2 Submerged Jet Test Device 36
4.2.1 Field Setup & Data Collection 36
4.2.2 Data Analysis 37
4.3 Laboratory Flume 38
4.3.1 Soil Sampling 38
4.3.2 Data Collection 39
4.3.3 Data Analysis 41
4.4 Critical Shear Stress Values Obtained from Empirical Relations 43
5 Results 45
5.1 Submerged Jet Test Device Results 45
5.1.1 Critical Shear Stress 45
5.1.2 Erodibility Coefficient 45
5.2 Closed-loop Laboratory Flume Results 47
5.3 Critical Shear Stress Results from Empirical Equations found in Literature 48
5.4 Compilation of Critical Shear Stress Results 49
5.5 Critical Shear Stress Correlations with Sediment Properties 49
6 Discussion 53
References 57
Appendix 63
Appendix A: Flume Construction and Initial Activation 64
Flume Construction 64
Equilibrium Test 68
Velocity Profiles 75
Bed Shear Computation 89

List of Tables

Table 1. List of parameters used to characterize cohesive material excluding biological effects (Winterwerp *et al.* 1990). 11
Table 2. Critical shear stress coefficients to account for vegetation (Julian and Torres 2006). 22
Table 3. Site information. 31
Table 4. Median critical shear stress determined from submerged jet test device field data. 46
Table 5. Median erodibility coefficients by site for the submerged jet test. 47
Table 6. Submerged jet test critical stress shown with brief flume observations and root presence. 48
Table 7. Critical shear stress values determined from empirical sediment relationships. 49
Table 8. Critical shear stress result summary. 50
Table 9. Percent difference between submerged jet test device critical shear stress and the analytical values. 51
Table 10. Sediment properties determined for each test location. 51
Table 11. Multivariate correlations for submerged jet test device critical shear stresses and soil properties. 52
Table 12. Velocity data for trolling motor with half propeller on setting #1 75
Table 13. Velocity data for trolling motor with half propeller on setting #2 77
Table 14. Velocity data for trolling motor with half propeller on setting #3 78
Table 15. Velocity data for trolling motor with half propeller on setting #4 80
Table 16. Velocity data for trolling motor with half propeller on setting #5 81
Table 17. Velocity data for trolling motor with full propeller on setting #1. 83
Table 18. Velocity data for trolling motor with full propeller on setting #2. 84
Table 19. Velocity data for trolling motor with full propeller on setting #3. 86
Table 20. Velocity data for trolling motor with full propeller on setting #4. 87
Table 21. Flume bed shear stress values. 117

List of Figures

Figure 1. The Shields diagram as updated by Yalin and Karahan (1979). 7
Figure 2. An alternate form of the Shields diagram for direct determination of critical shear stress (Sturm 2001). 9
Figure 3. Core sediment sample subjected to flow in a laboratory flume schematic (Julien 1998). 11
Figure 4. Plan and elevation view of in situ erosion flume (Krishnappan and Droppo 2006). 14
Figure 5. In situ flume (Debnath *et al.* 2007). 15
Figure 6. Field testing of Beaver Creek Site #4 with the multiangle submerged jet test device. 26
Figure 7. University of Tennessee closed-loop laboratory flume schematic. 28
Figure 8. University of Tennessee closed-loop laboratory flume utilized for sediment research. 29
Figure 9. Acoustic Doppler Velocimeter 5.3-cm above sediment core sample 30
Figure 10. Overall site map developed from Google Earth software. 32
Figure 11. Closer view of the northern-most test sites compiled from Google Earth images. 33
Figure 12. Defined Google Earth image of the Beaver Creek locations next to Halls Crossroads. 33
Figure 13. Initial inspection of three sediment core samples from upstream Beaver Creek. 34
Figure 14. Facing upstream of Beaver Creek site #4. 35
Figure 15. Beaver Creek site #2 off of Dry Gap Road. 35
Figure 16. Beaver Creek site #3 off Afton Road. 36
Figure 17. Extruder utilized to extract sediment core samples from stainless steel cylinders. 39
Figure 18. Initial photo of soil sample #1 from Beaver Creek downstream site. 40
Figure 19. Sample from Beaver Creek Site #6 in the unconfined compressive strength test device. 44
Figure 20. Five samples during hydrometer analysis. 44
Figure 21. One-way analysis of critical shear stress from submerged jet test by site location. 45
Figure 22. One-way analysis of erodibility coefficient from submerged jet test by site location. 46
Figure 23. Graphical representation of shear stress values obtain by submerged jet test device and soil parameter relationships. 50
Figure 24. Scatterplot matrix for multivariate correlation data. 52
Figure 25. Typical velocities for the deposition, transport, and erosion of various particle sizes (Pidwirny 2006). 54
Figure 26. Support structure for flume with sediment bed cut-out and hydraulic jack section. 64
Figure 27. Sediment core jack system. 65
Figure 28. Polyvinyl chloride utilized to weld the sheets of PVC together. 65

Figure 29. Construction of the inside wall and the first vane. 66
Figure 30. Closed-loop flume during testing procedure. 67
Figure 31. Acoustic Doppler Velocimeter over cylindrical test section with plexiglass window. 68
Figure 32. Equilibrium profile for trolling motor setting #1. 69
Figure 33. Equilibrium profile for trolling motor setting #2. 70
Figure 34. Equilibrium profile with trolling motor setting #3. 71
Figure 35. Equilibrium profile with trolling motor setting #4. 72
Figure 36. Long duration equilibrium profile with trolling motor on setting #3. 74
Figure 37. Velocity profile for trolling motor with half propeller on setting #1. 76
Figure 38. Velocity distribution for trolling motor with half propeller on setting #1. 76
Figure 39. Velocity profile for trolling motor with half propeller on setting #2. 77
Figure 40. Velocity distribution for trolling motor with half propeller on setting #2. 78
Figure 41. Velocity profile for trolling motor with half propeller on setting #3. 79
Figure 42. Velocity distribution for trolling motor with half propeller on setting #3. 79
Figure 43. Velocity profile for trolling motor with half propeller on setting #4. 80
Figure 44. Velocity distribution for trolling motor with half propeller on setting #4. 81
Figure 45. Velocity profile for trolling motor with half propeller on setting #5. 82
Figure 46. Velocity distribution for trolling motor with half propeller on setting #5. 82
Figure 47. Velocity profile for trolling motor with full propeller on setting #1. 83
Figure 48. Velocity distribution for trolling motor with full propeller on setting #1. 84
Figure 49. Velocity profile for trolling motor with full propeller on setting #2. 85
Figure 50. Velocity distribution for trolling motor with full propeller on setting #2. 85
Figure 51. Velocity profile for trolling motor with full propeller on setting #3. 86
Figure 52. Velocity distribution for trolling motor with full propeller on setting #3. 87
Figure 53. Velocity profile for trolling motor with full propeller on setting #4. 88
Figure 54. Velocity distribution for trolling motor with full propeller on setting #4. 88

List of Equations

Equation 1. Dimensionless particle number. 8
Equation 2. Critical shear stress for noncohesive sediment. 9
Equation 3. K factor developed by Hanson. 18
Equation 4. Erosion rate. 18
Equation 5. Shear stress related to plasticity index 20
Equation 6. Critical shear stress related to the dispersion ratio. 20
Equation 7. Critical shear stress related to the mean particle size. 20
Equation 8. Critical shear stress related to the percentage of clay 20
Equation 9. Neill's equation. 21
Equation 10. Critical shear stress based on silt-clay content. 22
Equation 11. Estimate of soil erodibility coefficient. 23
Equation 12. Logarithmic definition of dimensionless “y” to solve for the ultimate scour depth. 37
Equation 13. Logarithmic definition of dimensionless “x” to solve for the ultimate scour depth. 37
Equation 14. Logarithmic velocity distribution. 41
Equation 15. Region where viscous-sublayer velocity distribution applies. 42

1 Introduction

Considering the significant role of sediment in water quality and management of river systems nationally, there is an urgent need to improve sediment erosion models for the complexities of cohesive soils (Huang *et al.* 2006). Heavy metals, pesticides, nutrients, and harmful bacteria can absorb to cohesive materials on banks and disperse in surface water when that riverbank fails (Huang *et al.* 2006). Certain levels of sediments themselves can reduce the presence of aquatic life in rivers and can raise water treatment costs (Huang *et al.* 2006). From the output of bank stability model results, stream conditions can be properly restored by evaluating sediment best management practices such as: landuse management alternatives, amount of vegetation, streamside buffers, and in-stream grade control structures (Langendoen 2000). Because several studies have found up to 90% of the sediment in streams are from bank erosion sources, improving the bank stability components to these models are critical to the success of stream restoration or maintenance projects (Prosser and Winchester 1996; Wallbrink *et al.* 1998; Wasson *et al.* 1998).

River mechanics, stream morphology, and sediment transport concepts are the basic components of erosion models (Langendoen 2000). To specifically estimate channel erosion, bank stability models use the excess shear equation which can be related to flow hydraulics (Langendoen 2000). To estimate channel sediment erosion, the bank stability models require two input parameters, the critical erosion shear stress (τ_c) and erodibility coefficient (k_d), which, unfortunately, can be difficult to estimate or measure for cohesive sediment (Langendoen 2000). Critical shear stress is the primary factor in determining whether soil will resist the forces of a concentrated flow, and the erodibility

rate determined from the erodibility coefficient, applied, and critical shear stress defines how quickly fine-grained sediments will erode (Sturm 2001). Currently, critical erosion shear stress and erodibility coefficients are estimated from empirical relationships developed from flume studies that related critical shear stress to basic soil properties, or determined by available testing methods, including the in situ submerged jet test device (Smerdon and Beasley 1961; Hedges 1990; Stein *el al.* 1993; Hanson and Simon 2001; Mazurek 2001; Julian and Torres 2006; Wynn and Mostaghimi 2006a; Clark and Wynn 2007) and subjecting a sediment core sample to an erosion test in a specially-design flume (Briaud *et al.* 2004; Huang *et al.* 2006; Krishnappan and Droppo 2006; Debnath 2007). The typical critical shear stress range for cohesive sediment found by the Transportation Research Board during their pier and scour depth study on cohesive soils was 0.5 N/m^2 to 5 N/m^2 (Briaud *et al.* 2004). The range was comparable to the critical shear stress values commonly obtained for sands (Briaud *et al.* 2004).

The objective of this research was to compare and evaluate two methods of collecting critical shear stress and the erodibility parameter of cohesive sediment to enhance the erosive input parameters of bank stability models. To reach this goal of improving the erosion model input, the critical shear stresses and erodibility coefficients obtained using the in situ submerged jet test device were compared to results from the laboratory flume method for twelve cohesive test sites in East Tennessee. Three study locations were used for this investigation: Beaver Creek (Knox County, TN), Hines Branch (Knox County, TN), and Abrams Creek (Blount County, TN). All locations were second to third-order streams with cohesive riverbanks and each of the twelve sites are in Watts Bar Lake watershed. At least four runs were performed with the submerged jest

test device at each site to account for the variability of bank material. Twelve 6-inch long, 2-inch diameter core samples were collected at each of the 12 locations for closed-loop flume method and soil analysis. In addition to that comparison, the submerged jet test device's critical shear stress values were weighed against values found via empirical relationships found in literature based on flume and soil property experiments (Smerdon and Beasley 1961; Julian and Torres 2006). The properties related to the hydraulic erosion of cohesive sediment utilized to compute critical shear stresses are plasticity index, median particle diameter, percent silt-clay and percentage of clay present. Correlations were explored between the submerged jet test critical shear stresses and sediment properties to explore connections between the outcome of this research and past projects.

Because each of the methods exhibit strengths and weaknesses during the data collection process, the procedure and outcome of each testing method are presented. As presented later in this paper, the in situ procedure uses a submerged jet test device to generate a scouring jet stream of water perpendicular to the bank. Besides the intense jet impact on the sediment surface, the placement of the submerged jet test device can affect the values obtained. Vegetation, habitat, soil structure, and soil gradation under the footprint of the device can lead to under- or over-estimated critical erosion shear stress and erodibility rates. Another test used to determine the erosive properties of cohesive sediment utilized was a sediment core subjected to flow in a laboratory flume. The flume test is not run on-site, but incorporates the hydraulic flow field and the viscous sublayer present in stream networks. While it is important to consider the hydraulics involved in data collection of erosive input parameters, erosion tests on cohesive material that do not

incorporate the soil and water chemistry influences are questionable due to the manner in which cohesive soil erodes (Wynn and Mostaghimi 2006a).

From the comparison of methods and results obtained, the cohesive sediment erosion phenomenon was explored and recommendations towards finding a reliable method to estimate cohesive soil erosional properties were made. The erosive properties produced from two testing procedures and the computed empirical values were further evaluated by exploring the hydraulics of the river systems and effects present to influence the process of cohesive sediment erosion. Hydraulic engineers and fluvial geomorphologists involved in river restoration projects will be able to utilize the investigation results to enhance computer models incorporating the differences between noncohesive, semi-cohesive, and cohesive bank stability input parameters.

2 Literature Review

To better understand the concept of critical shear stress and its applicability, the topic is presented for both noncohesive and cohesive material. Features of cohesive sediment that set it apart from noncohesive sediment are its high composition of clay-sized material and strong interparticle forces (Huang *et al.* 2006). The high strength of interparticle forces is a result of surface ionic charges (Huang *et al.* 2006). Interparticle forces become the dominant factor affecting the behavior of sediment rather than gravity as the particle size decreases because the specific surface area (i.e. surface area per unit volume) increases concurrently (Huang *et al.* 2006). A clear boundary between cohesive and noncohesive does not exist, but particle sizes less than 2 μm are commonly labeled cohesive clays (Huang *et al.* 2006). Particles larger than 60 μm are cohesionless coarse sediment and sediment sizes in between 2 μm and 60 μm are classified as silts (Huang *et al.* 2006). Notably, silt sediment is between cohesive and cohesionless soils (Huang *et al.* 2006).

Since the presence of clay is mostly responsible for cohesive properties of silt sediment, practicing engineers consider both silt and clay as cohesive material (Huang *et al.* 2006). Included in this section is a detailed study of methods to determine the erosion parameters of cohesive and noncohesive sediment including Shields parameter, submerged jet test device, laboratory flume methods, and experimentally-derived soil parameter relationships. In addition to the procedures available to determine the critical shear stress and erodibility rate of site-specific sediment, additional factors that effect streambank erosion of cohesive soils are discussed.

2.1 Noncohesive Material

Most erodibility experiments have been preformed on noncohesive sand, stream beds where flume and field methodology is clear (Haan 1994; Huang *et al.* 2006). From experience, Shields parameter, the ratio of the shear stress to a particle's submerged weight per unit of surface area at critical conditions, is a reliable tool to provide a precise estimate of critical shear stress for noncohesive sediment (Shields 1936; Haan 1994). As described below, the behavior of noncohesive sediment erosion is well-defined and predictive models from those inputs are assumed reliable. Therefore, Shields parameter is typically used to determine the critical shear stress of cohesionless soils in practice. First, one indirect and then one direct method of obtaining critical shear stress using Shield's parameter is presented in this section.

2.1.1 Shields Parameter

A noncohesive soil's resistance to the critical shear stresses caused by a concentrated flow of water has been studied extensively both in the field and laboratory. As a result, the critical shear stress of a noncohesive soil can be ascertained from a few soil and fluid properties. Because the submerged specific weight of the sediment, sediment grain size, fluid density and dynamic viscosity have been found to control the erodibility of noncohesive soil, Shields parameter (τ_{*c}) can be utilized to determine the critical shear stress (Sturm 2001). The parameter is dimensionless and developed from the compilation of various flume experiments on a wide range of grain sizes (Shields 1936).

Shields, the American that collected, developed, and presented critical shear stress results for various grain sizes, concluded that the noncohesive particles begin rolling and

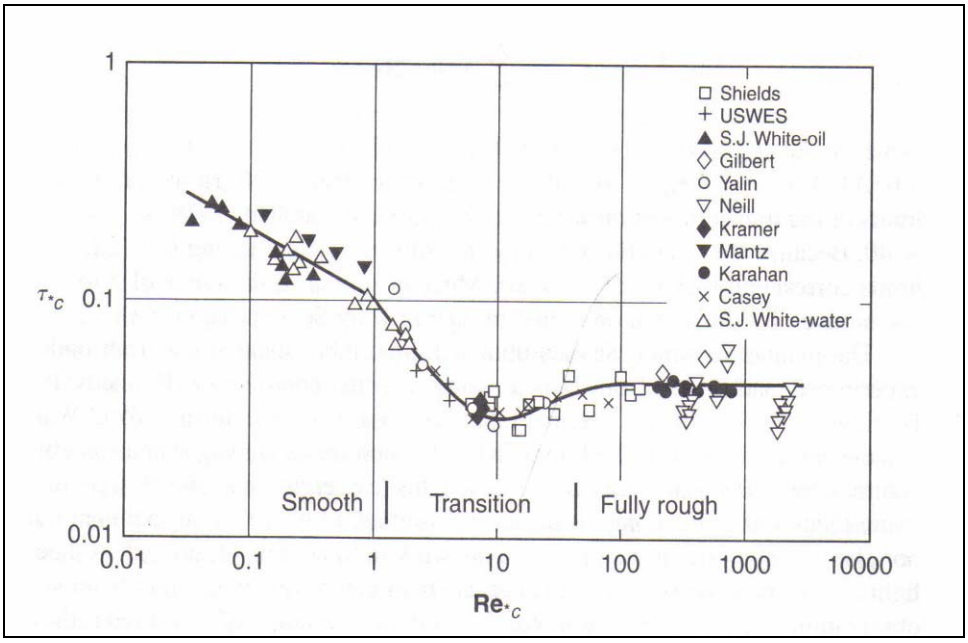


Figure 1. The Shields diagram as updated by Yalin and Karahan (1979).

sliding at various locations along the soil face, just as the threshold of sediment movement is exceeded (Sturm 2001). Illustrated in Figure 1, he created the Shields diagram that presented results obtained during the experiments. While the original diagram did not account for particles with low specific gravity and small particle diameter, Mantz (1977) altered the graph to include smaller sediment sizes. The information needed to determine Shields parameter can be found from soil and water variables.

According to Sturm (2001), a weakness of Shields diagram is that how incipient motion was defined by Shield's to compute the critical shear stresses is unknown. Two ways that determine the value are: (1) visual observation of the initiation of movement, or (2) extrapolation of measured sediment transport rates to zero (Sturm 2001). In addition to uncertainties of which method Shield used, other controversies in using Shields

parameter (τ_{*c}) are his use of both mean and median grain sizes and the presence of bed forms in part of the data (Sturm 2001). The diagram was based on a representative particle diameter and assumes zero influences between individual particles (Clark and Wynn 2007). Since the variability among sediment sizes is great, interaction between particles exist, and the bed form inclusion can lead to overestimation of τ_c, Shields diagram is considered very generalized for the initiation of motion (Clark and Wynn 2007).

2.1.2 Alternate Form of Shields Diagram

Julien (1995) proposed an alternate form of the Shields diagram in order to directly compute the critical shear stress. Rather than having to iterate between critical shear stress and Reynolds number which both contain Shields parameter, an additional dimensionless parameter was introduced. First to compute the critical shear stress, a dimensionless particle number must be calculated utilizing Equation 1:

$$d_* = \left[\frac{(SG-1)g{d_{50}}^3}{\nu^2} \right]^{1/3} \quad (1)$$

in which d_* = dimensionless particle number, SG = specific gravity of sediment, g = gravitational constant, d_{50} = particle size with 50% passing, and ν = kinematic viscosity of the fluid.

Then, the ratio of shear stress to the submerged weight of a particle per unit of surface area at critical conditions, τ_{*c}, is obtained from the diagram presented in Figure 2. And, the corresponding critical shear stress using Shields parameter, the unit weight of soil, unit weight of the fluid, and the diameter with 50% passing, can be found using the

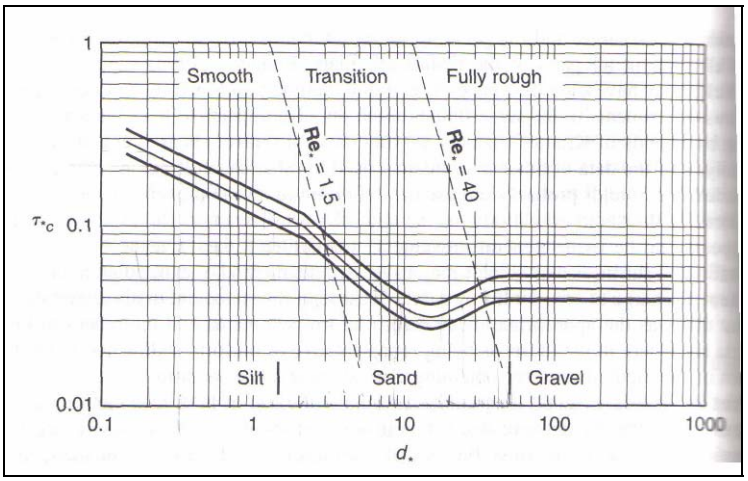


Figure 2. An alternate form of the Shields diagram for direct determination of critical shear stress (Sturm 2001).

relationship in Equation 2 (Sturm 2001):

$$\tau_c = (\gamma_s - \gamma) d_{50} \tau_{*c} \tag{2}$$

where τ_c = critical shear stress, γ_s = unit weight of sediment, γ = unit weight of the fluid, d_{50} = diameter with 50% passing, and τ_{*c} = dimensionless critical shear stress.

Even though the alternative form obviously contains the same limitations of Shields parameter, this relationship between specific unit weight and particle size has become a widely used practice for determining the critical shear stress of noncohesive sediment (Haan 1994).

2.2 Cohesive Material

Values of critical shear stress and erodibility rates are more complicated for cohesive soils than noncohesive sediment because of surface charge forces (Huang *et al.* 2006). Due to the effects from soil shear strength, soil salinity, moisture content, percentage of clay, particle size and other related parameters on the resistance to shearing

forces, the method used to analyze cohesive sediment erosive properties should incorporate soil and site water conditions (Wynn and Mostaghimi 2006a). Judging from the methods presented below, the flume and field experiments utilized during the development of Shields parameter that does not apply to fine-grained sediment and the concept of critical shear stress set a precedence for designing experiments involving cohesive sediment (Shields 1936). Therefore, during the research projects preformed on the erosive properties of cohesive sediment, considerations were not always made for the 28 parameters in Table 1 that currently characterize cohesive soil (Winterwerp *et al.* 1990). With the erosive behavior of noncohesive soils in mind, the following methods were developed for determining the erosional parameters of fine-grained soils.

2.2.1 Flume Experiments

2.2.1.1 Laboratory Open-Channel Flow Test

For cohesive soils, a laboratory open-channel flow test with a soil sample on the bed is an erosion measurement technique to determine the critical shear stress and erodibility rate of cohesive sediment. Figure 3 illustrates the experimental setup. After the soil sample is placed in a flume and the test has begun, the critical shear stress can be determined visually or graphically (Clark and Wynn 2007). A weakness with the visual method is that the point of failure is difficult to observe and even harder to separate from the individual's definition of failure. The visual point is a subjective observation. In the paper, *Methods for Determining Streambank Critical Shear Stress and Soil Erodibility: Implications for Erosion Rate Predictions*, Clark and Wynn (2007) summarized three different interpretations of the point of failure from various sources. Dunn (1959) determined that the critical shear stress was met as "the water becomes cloudy."

Table 1. List of parameters used to characterize cohesive material excluding biological effects (Winterwerp *et al.* 1990).

Physico-chemical properties of the overflowing fluid	(19) specific surface
(1) chlorinity	(20) mineralogical composition
(2) temperature	(21) grain size distribution and sand content
(3) oxygen content	**Characteristics of bed structure**
(4) redox potential	(22) consolidation a. consolidation curve and density profile b. permeability c. pore pressure and effective stress
(5) pH	
(6) Na-, K-, Mg-, Ca-, Fe-, Ai- ions	
(7) sodium adsorption ratio (SAR)	
(8) suspended sediment concentration	(23) rheological parameters a. upper and lower yield stress b. Bingham viscosity c. equilibrium slope of mud deposits
Physico-chemical properties of the mud	
(9) chlorinity	
(10) temperature	
(11) oxygen content	(24) Atterberg limits (liquid and plastic limit)
(12) redox potential	**Water – bed exchange processes**
(13) pH	(25) settling velocity a. as a function of sediment concentration and floc density b. as a function of salinity
(14) gas content	
(15) organic content	
(16) Na-, K-, Mg-, Ca-, Fe-, Ai- ions	(26) critical shear stress for deposition
(17) cation exchange capacity (CEC)	(27) critical shear stress for erosion
(18) bulk density (density profile)	(28) erosion rate

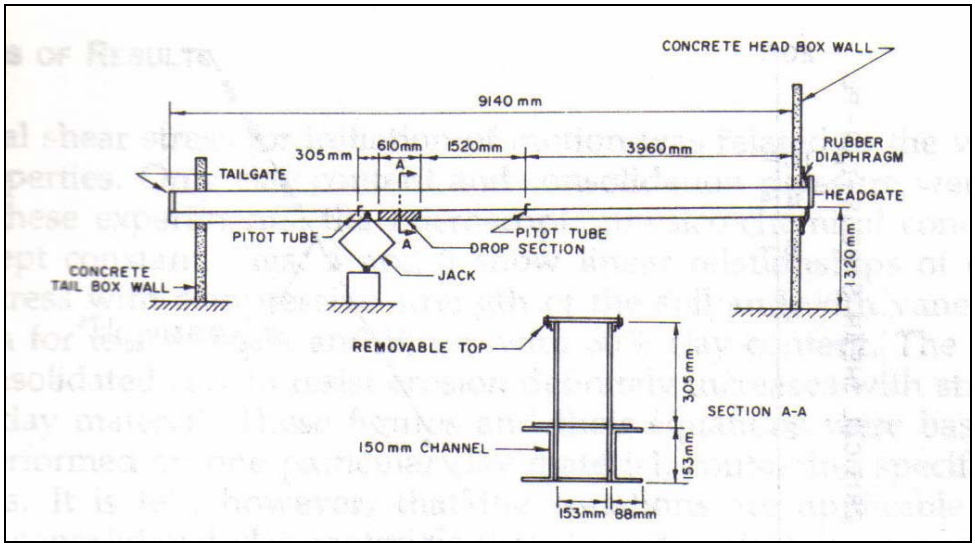


Figure 3. Core sediment sample subjected to flow in a laboratory flume schematic (Julien 1998).

Alternatively, Smerdon and Beasley (1961) observed the critical shear stress when "general movement of the soil composing the channel bed was observed." Many years later, Kamphuis and Hall (1983) reported that the critical value was reached at "pitting of the surface" during their flume observations. In order to avoid this subjectivity, Clark and Wynn (2007) determined it was best to graphically represent the erosion rate versus the shear stress.

To graphically represent the erosion rate versus the shear stress, the variables to obtain the parameters from the laboratory flume method must be defined. The depth of sample eroded and the time passed from start to finish of erosion period is necessary to determine the erodibility rate (Briaud *et al.* 2004). And, using measurements of velocities and respective elevations, the vertical velocity profile can be developed (Briaud *et al.* 2004). The velocity profile is utilized as a major component of the calculation of critical shear stress (Briaud *et al.* 2004). Through the addition of a best-fit line, a value that equals the critical stress can be found where the line crosses the x-axis (Clark and Wynn 2007).

Overall, laboratory flumes enable researchers to control the environmental and flow conditions more easily than field tests; however, it is impossible to transport the bank material into a flume without causing disturbance (Hanson *et al*. 1999; Hanson and Cook 2004). Also, erosion tests on cohesive material that do not incorporate the soil and water chemistry influences are questionable due to the manner in which cohesive soil erodes (Clark and Wynn 2007). In situ experimental processes that do not require the disturbance of the fine-grained soil and incorporate the exact physical, chemical and

biological state of the field, more easily and adequately represent the critical shear stress and erodibility rate of cohesive sediment (Krishnappan and Droppo 2006).

2.2.1.2 In Situ Flumes

Benthic in situ flumes are set up over stream sediment to measure erosive properties of cohesive soils (Black and Paterson 1997). The procedure is similar to the laboratory flume test, but the sediment samples do not require transport (Black and Paterson 1997). Even though the in situ flumes are a good approach, many uncontrollable influences can lead to uncertainty of soil parameter estimates (Julian and Torres 2006). Published in a 2006 issue of *Geomorphology*, Julian and Torres (2006) dealt with the lack of controls by choosing a study site based upon the location of the water table, soil with low silt-clay content and an entrenched channel, low vegetation component, and warm climactic region without the freeze-thaw component. During their in-situ flume study, bank erosion measurements were collected from cohesive banks over a 14-month duration (Julian and Torres 2006). From prior bank cohesive bank erosion studies, a conceptual model was developed that defined three categories (Julian and Torres 2006). When the channel banks contain greater than 40% of silt-clay content, the erosion was controlled by sub-aerial erosion and the hydraulic shear considered negligible (Julian and Torres 2006). When the silt-clay percentage was between 20% and 40%, a combination of the subaerial and shear stresses had an impact on the erosion of channel banks (Julian and Torres 2006). Lastly, hydraulic shear stress became the controlling erosional process of silt-clay soils with less than 20% of fines (Julian and Torres 2006). Utilizing the conceptual model with the three categories of erosivity influences and the data collected

using the in-situ flume, Julian and Torres (2006) found for sites with moderate τ_c (1.93-4.08 N/m^2), event peak is strongly related to bank erosion, while low τ_c (0.95 N/m^2) values indicated a stronger correlation of variability with bank erosion.

A Canadian in situ flume study by Krishnappan and Droppo (2006) involved a submerged pump attached and underwater video camera mounted onto a field flume setup. The plan and elevation view of the in situ erosion flume (Figure 4) shows the components of the instrument (Krishnappan and Droppo 2006). While this research project was a bed study and not bank testing, the outcome is influential towards understanding the effect of sediment deposition on erosion. Also, the experimental setup is similar to that of in situ flume bank erosion testing. The two sites measured in Hamilton Harbour found density variations as the explanatory variable for erosion rates.

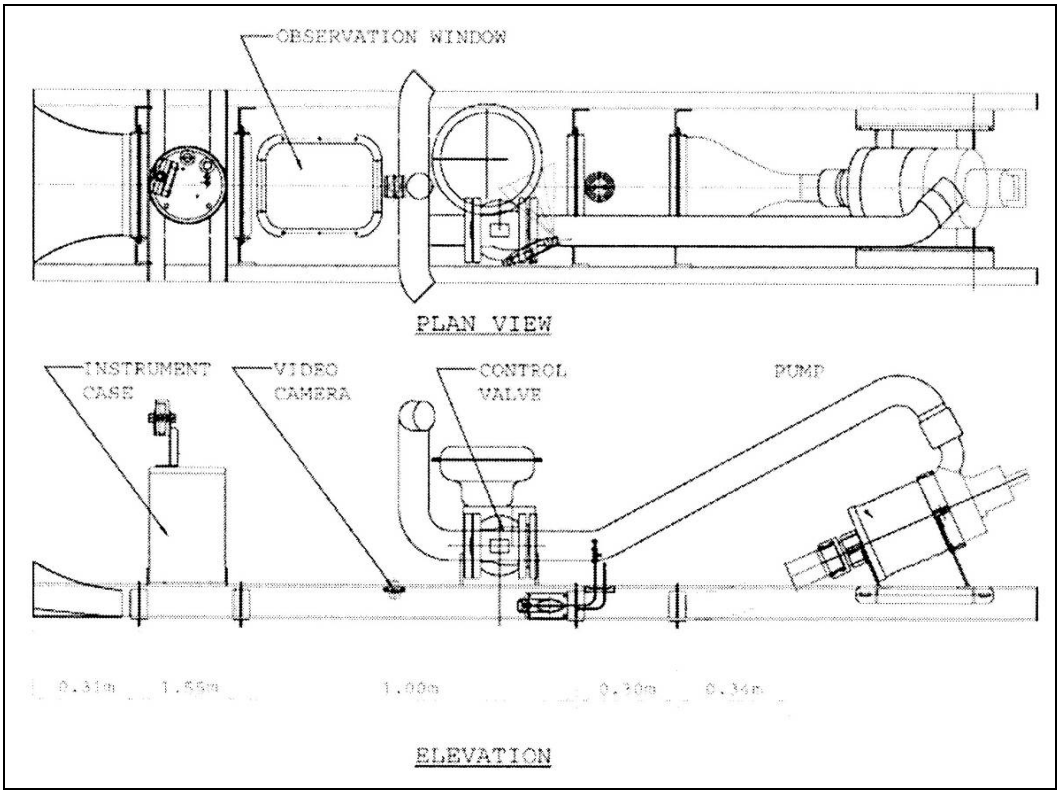


Figure 4. Plan and elevation view of in situ erosion flume (Krishnappan and Droppo 2006).

The density variations were a result of gas accumulation, biofilm development/degradation, and bioturbation (Krishnappan and Droppo 2006). Also, Krishnappan and Droppo (2006) found it prudent to run in situ tests because of the difficultly of mimicking the physical, chemical, and biological state of the sediment and the exact function of all on-site influences.

From an in situ flume study, Debnath *et al.* (2007) concluded that the spatial and temporal variation of the sediment on the bed controlled the rate of erosion. The physical properties of the flume in Figure 5 did not have an effect. The data also showed an exponential decrease in the erodibility rate after the bed shear stress is reached depending on clay content, dry bulk density, and conductivity (Debnath *et al.* 2007).

2.2.2 Submerged Jet Test Device

Studies have been performed with the submerged jet test device on cohesionless sediment. Yet, as mentioned earlier, Shields parameter as a method to determine critical

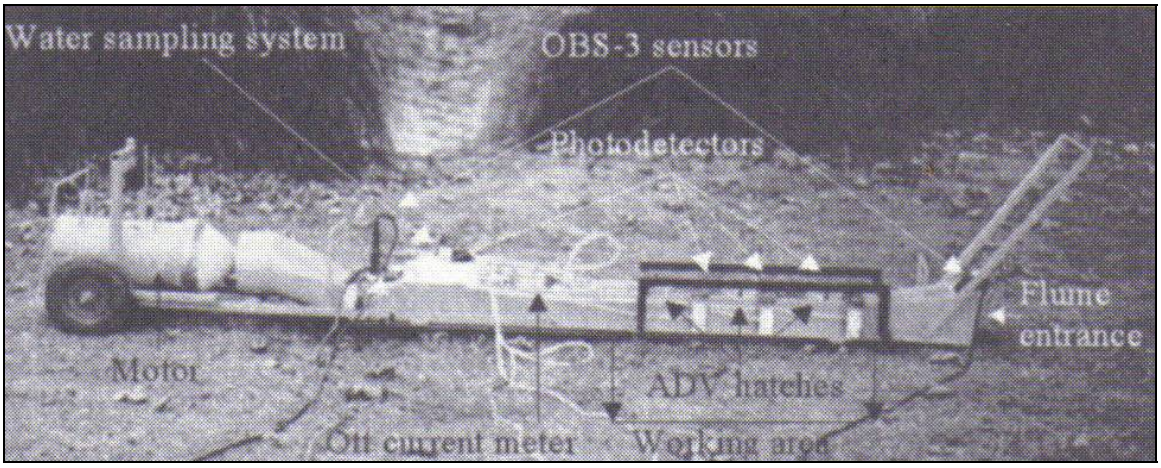


Figure 5. In situ flume (Debnath *et al.* 2007).

shear stress is more common. So, other researchers have begun to explore the complexities of testing cohesive soils with and exploring the scour properties of the submerged jet test device (Dunn 1959; Moore and Masch 1962; Mirstkulava *et al.* 1967; Dash 1968; Bhasin *et al.* 1969; Hollick 1976; Blaisdell *et al.* 1981; Stein 1993; Hanson 1990; Hedges 1990; Mazurek *et al.* 2001). By determining critical shear stresses and erodibility coefficients from a wide range of submerged jet test results and determining the properties of the sediment at each of the test sites, some of the data collected was used to observe relationships between the soil properties and the erosivity of cohesive soil (Hanson and Simon 2001; Clark and Wynn 2007). While others observed the scouring effects of the jet test device such as the shape of the scouring hole formed, maximum scour depth, and the shear stress distribution underneath the jet (Blaisdell *et al.* 1981; Mazurek *et al.* 2001; Ansari 2003).

Hanson and Simon (2001) analyzed the critical shear stress and erodibility coefficients from 83 submerged jet test runs in the Midwestern United States. The outcome of their testing resulted in critical shear stresses from 0.0 to 400 Pa and an erodibility coefficient of 0.001 to 3.75 $cm^3/N \cdot s$ (Hanson and Simon 2001). Hanson and Simon (2001) determined a large variation in the values of critical shear stress and erodibility coefficients. The loess soils in the Midwest varied among erosion resistance within streambeds, from streambed to streambed, and across regions (Hanson and Simon 2001). Clark and Wynn (2007) compared the submerged jet test device results against estimated critical shear stress values obtained from Shields diagram and empirical equations relating the τ_c to soil properties for 25 field sites near Blacksburg, Virginia. For the Virginia testing locations, the submerged jet test critical shear stress results were

larger than all of the other values obtained except for the silt-clay estimate (Clark and Wynn 2007).

In depth research has been performed to study the scour properties of the device. Consistent with the relationship presented by Moore and Masch (1962) and assumptions of scour analysis made by Blaisdell *et al.* (1981), there exists a linear relationship between scour depth and logarithm of time. Dunn (1959) observed that the erosion first occurs away from the centerline of the jet nozzle and Moore and Masch (1962) describe the jet erosion of cohesive or consolidated clays as a process of mass erosion. Considering the pattern of submerged jet test erosion, two types of scour holes were observed by Moore and Masch (1962) and Hollick (1976): wide and shallow or narrow and deep. While Moore and Masch related the height of the jet above the sediment surface and the diameter of the nozzle to the hole type, Hollick found that other parameters influence the type of scour hole.

2.2.2.1 Jet Test Erosion Coefficient

An erodibility coefficient (k_d) which is used to calculate an erodibility rate (ε) can be produced from the data collected of a submerged jet test device. In the 1990 *Transactions of the ASAE*, G. J. Hanson wrote about the development of the submerged jet test device. While his design with an inner cylindrical baffle and a pin profiler is slightly different than the one being utilized for this research, the mechanics of the scour are the same. Four different soil types were analyzed and the data collected was used to calibrate the device based upon the Reynolds number of the submerged jet device (Hanson 1990). Summary tables of the soils' physical properties and average compacted densities were tabulated and the experiment led to the development of the equation to

estimate the erodibility of other soils. Equation 3 developed by Hanson (1990) is used to solve for the K factor:

$$K = \left(\frac{\sqrt[3]{Vol} / h}{0.00436 \left(\frac{\rho V d}{\mu} \right)^{0.67} \left(\frac{\mu t}{\rho d^2} \right)^{0.065}} \right)^{7.25} \times \frac{d}{\mu} \quad (3)$$

where K = coefficient of erodibility, Vol = volume of material removed during a jetting event, h = elevation of jet above the soil surface, d = diameter of the jet nozzle, V = jet velocity, ρ = the mass density of the fluid, μ = absolute viscosity of the fluid, and t = time.

The K factor is then related to the Reynolds number of the jet and the time factor and represented by a linear relationship on a logarithmic scale. In situ tests are compared against predicted values and the results are accurately represented. Clark and Wynn (2007) also used this least squares method. Their jet test scour depth data was fitted to the excess shear stress equation and the erodibility coefficient, k_d, was produced (Clark and Wynn 2007). Along with the applied shear stress on the boundary and the critical shear stress determined from submerged jet test data, the erodibility coefficient can be plugged into Equation 4 and an erosion rate can be determined (Clark and Wynn 2007):

$$\varepsilon = k_d (\tau_a - \tau_c)^a \quad (4)$$

where ε = erodibility rate (m/s), k_d = erodibility coefficient ($m^3/N \cdot s$), a = exponent typically assumed to equal 1, τ_a = applied shear stress on the soil boundary (Pa), and τ_c = critical shear stress (Pa).

For the Blacksburg, Virginia sites, the erodibility results collected using a submerged jet test device were effected by freeze/thaw cycling, root density, field moisture content, soil

texture and soil pore water in contact with stream water had influence on the streambank erosion (Clark and Wynn 2007).

2.2.3 Cohesive Strength Meter

2.2.3.1 Critical Shear Stress

Since it is a fairly new *in situ* device, few researchers have performed experiments on soils utilizing the Cohesive Strength Meter (CSM). Set up on the exposed intertidal sediment, the claim is that the CSM can measure critical erosion shear stress (Paterson 1989). The experimental set-up and hydraulics of the CSM are similar to the submerged jet test device. A 3-cm wide chamber is carefully pushed in perpendicular to the soil surface and filled with site water. Incrementally, the jet pressure, calibrated with a standard manometer, increases and the vertical jet causes erosion over a 700 mm^2 area. The light transmission is read periodically to detect the increase of sediment in the chamber water caused by the erosion. As the amount of sediment increases within the chamber, the turbidity level increases which causes the light transmissivity to decrease. From the plot of transmission versus pressure, the critical erosion threshold is found when the light transmission falls just below 90% (Widdows *et al*. 2007). Eroding pressure is plugged into an empirical equation and used to determine the equivalent horizontal shear stress (Tolhurst *et al*. 1999). Widdows (2001) found no correlation with the CSM critical erosion shear stresses compared to the four other intertidal erosion devices. The four other devices analyzed were: (1) Plymouth Marine Laboratory's (PML) annular flume (diameter 64 cm; area 0.17 m^2), (2) PML's mini-annular flume (diameter 19 cm; area 0.026 m^2), (3) National Oceanography Centre Southampton's (NOC) EROMES erosion device (diameter 10 cm; area 0.0079 m^2), and (4) NOC's annular mini-

flume (diameter 30.5 cm; area 0.032 m^2). The CSM values were repeatedly higher than the others' measurements (Widdows *et al.* 2007).

2.2.3.2 Erodibility Rate

Inferred by Widdows (2001), the CSM is not capable of measuring a rate of erosion. The device does not contain a sensitive optical backscatter sensor (OBS) and the intervals of the recording of the suspended sediment concentration (SSC) are not small enough.

2.2.4 Relating Critical Shear Stress & Erosion Rate to Soil Properties

2.2.4.1 Critical Shear Stress

Smerdon and Beasley (1961) related critical shear stress to the plasticity index, dispersion ratio, mean particle size, and percentage of clay present from data collected during a flume study on eleven cohesive sediment types in Missouri. The equations that were developed by Smerdon and Beasley (1961) are shown in Equations 5 through 8:

$$\tau_c = 0.16(I_w)^{0.84} \quad (5)$$

$$\tau_c = 10.2(D_r)^{-0.63} \quad (6)$$

$$\tau_c = 3.54 \times 10^{-28.1 D_{50}} \quad (7)$$

$$\tau_c = 0.493 \times 10^{0.0182 P_c} \quad (8)$$

in which τ_c = critical shear stress (Pa), I_w = plasticity index, D_r = dispersion ratio, D_{50} = mean particle size (m), and P_c = percent clay by weight (%) (Smerdon and Beasley 1961).

In *Design Hydrology and Sedimentology for Small Catchments*, Foster (1982) suggested the foundation of the Smerdon and Beasley equation be the dispersion ratio (Equation 6),

while Hirschi and Barfield (1988a) suggested the equation be based on percentage clay (Equation 8) (Haan 1994). Clark and Wynn (2007) considered the relationship between critical shear stress and plasticity index or dispersion ratio to be the best estimate since they found the two properties were directly related to the sediment's ability to resist erosion.

An experiment by Neill (1967) involved six particle sizes of graded gravels, uniform glass balls of two different sizes, and cellulose acetate balls. The cellulose acetate balls were of various diameters (6 to 30 mm) for a uniform flow over a wide channel with no slope (Neill 1967). Equation 9, which represented critical shear stress in terms of specific gravity, median particle diameter, and water depth, was developed from his experimental data (Neill 1973):

$$\tau_c = 0.76090\gamma(SG-1)D_{50}{}^{2/3}d^{1/3} \quad (9)$$

in which τ_c = critical shear stress (Pa), γ = specific weight of water (N/m^3), SG = specific gravity of soil, D_{50} = mean particle size (m), d = depth of flow (m) (Neill 1973).

A limitation of Neill's equation is that it considered the flow conditions in addition to the soil properties. Therefore, studies have concluded that Neill's equation is difficult to compare to other estimation processes (Clark and Wynn 2007).

From work presented by Dunn (1959) and Vanoni (1977), Julian and Torres (2006) related critical shear stress to the percentage of silt and clay (SC), which are defined by particles sizes less than 0.063 mm. Equation 10 is the third order polynomial fitted to the critical shear stress and silt-clay content data:

$$\tau_c = 0.1 + 0.1779(SC) + 0.0028(SC)^2 - 2.34E - 5(SC)^3 \quad (10)$$

where τ_c = critical shear stress (N/m^2), SC = silt-clay (<0.063 mm) content (%), and E = erodibility rate (cm/s) (Julian and Torres 2006).

The critical shear stress in Equation 10 could also be multiplied by a coefficient to account for vegetation. Table 2 lists the vegetation coefficient which ranges from 1 to 19.20 (Julian and Torres 2006).

In the "USDA Water Erosion Prediction Project: Hillslope Profile Model Documentation," authors relate the critical shear stress of cohesive soils to shear strength, soil salinity, and moisture content (Alberts *et al.* 1989). Alternatively, Lyle and Smerdon (1965) related the erosive parameter to percentage clay, mean particle size, dispersion ratio, vane shear strength, organic matter content, cation exchange capacity, and calcium-sodium ratio.

2.2.4.2 Erosion Rate

Typically, the erodibility rate of fine-grained sediment is predicted using Equation 4. However, the parameters that affect the critical shear stress such as moisture content and percent clay can also affect the erosion rate, causing the critical shear stress and erodibility coefficient to be variable (Clark and Wynn 2007).

Table 2. Critical shear stress coefficients to account for vegetation (Julian and Torres 2006).

Bank vegetation	τ_c coefficient
None	1.00
Grassy	1.97
Sparse trees	5.40
Dense trees	19.20

2.2.5 Simple Relations

2.2.5.1 Critical Shear Stress Assumed Zero

Considering a worst-case condition, the critical shear stress can be considered zero. One approach to determining the erosive properties of sediment does just that (Clark and Wynn 2007). Because many people believe it is difficult to define the point of incipient motion, critical shear stress is often assumed to be insignificant and set equal to zero (Foster et al. 1977; Hanson 1990; Temple 1992; Hanson et al. 1999), or assigned a constant value base upon soil properties as suggested in earlier sections of this literature review.

2.2.5.2 Erodibility coefficient function to determine erodibility rate

In the Midwestern U.S. where the stream beds were 50% to 80% silt, an intensive jet test study was performed by Hanson and Simon (2001). The critical shear stresses ranged from 0.0 to 400 Pa and the erodibility coefficient varied from 0.001 to 3.75 $cm^3/N{\cdot}s$. From the analysis of the data set, Hanson and Simon (2001) identified that k_d was inversely related to τ_c and determined that the following equation could be utilized as an estimate of the erodibility coefficient:

$$k_d = 0.2\tau_c^{-0.5} \tag{11}$$

in which k_d = erodibility coefficient ($cm^3/N{\cdot}s$) and τ_c = critical shear stress (Pa). For other projects where the erodibility coefficient was not available, Equation 11 provided a good approximation (Hanson and Simon 2001).

2.3 Additional Effects on Erosion

Other pertinent studies involved the effects of vegetation, soil structure, soil gradation, soil chemistry, and water chemistry on streambank erosion (Wynn and

Mostaghimi 2006a). When studying the erosivity of cohesive sediment banks, the factors cannot be avoided (Wynn and Mostaghimi 2006a). Using a submerged jet test device to study the effect of soil vegetation on the erodibility properties of sediment, Wynn and Mostagimi (2006a) ran 48 submerged jet test device runs in a variety of Virginian soils. During the study, cohesive soils tended to erode by aggregates so the stability of the particle compounds had an effect on the critical shear stress (Wynn and Mosaghimi 2006a). The salinity of the soil pore water influenced the clayey soils' dispersion (Wynn and Mosaghimi 2006a). Therefore, the soil and water chemistry was found to affect the pattern of bank erosion (Wynn and Mosaghimi 2006a). Clark and Wynn (2007) also determined the soil chemistry, structure, and water chemistry affected the pattern at which a bank sample erodes.

Specifically, a few of the cohesive properties of cohesive sediment have been studied. Bulk density was found to impact the critical shear stress value obtained significantly (Wynn and Mosaghimi 2006a). Previous research by Asare *et al.* (1997) found that as the bulk density increases, the shear strength of sediment increases concurrently. Root density, soil freezing, and soil texture have also been found to impact the erodibility of soils (Wynn and Mosaghimi 2006a). In addition, the range of particles diameters found by soil classification methods affects the erosion of soils. As the amount of sand size particles decreases, the critical shear stress of cohesive sediment is increased (Wynn and Mosaghimi 2006a). The results of an in situ erosion test by Debnath *et al.* (2007) showed an exponential decrease in the erodibility rate after the bed shear stress is reached depending on clay content, dry bulk density, and conductivity.

In addition to the sediment property impacts on erosion results, the footprint of the device or size of sample used for analysis can also affect results. Investigations of various in-situ and laboratory erosion experiments made by Cornelisse *et al.* (1994) determined that the as the surface area of the test increased, the reproducibility also improves. Both the shear stress of cohesive and cohesionless sediment can be influenced by the presence of vegetation, freeze-thaw cycles, and soil texture; however, the amount of factors impacting erosion increases with cohesive soils when considering the critical shear stress and the erodibility coefficient (Wynn and Mosaghimi 2006a).

3 Device Descriptions

In order to understand the procedures utilized to collect the soil erosional properties for this study, a detailed description of the equipment is necessary. The following information summarizes the device components and capabilities.

3.1 Submerged Jet Test Device

A method of utilizing a submerged vertical circular turbulent impinging jet device exists to determine the erodibility of cohesive sediments. The multi-angle submerged jet test device, shown in Figure 6, scours the bank sediment with a highly turbulent jet stream of water at a 90 degree angle from the soil surface. A submerged jet test requires the following components: pump & motor, steel cylinder with a diameter of 30.5 cm, outer jet tube, nozzle, point gauge, and hammer. The system also requires tubing for the inlet, outlet, and jet components and gate valves for head control.

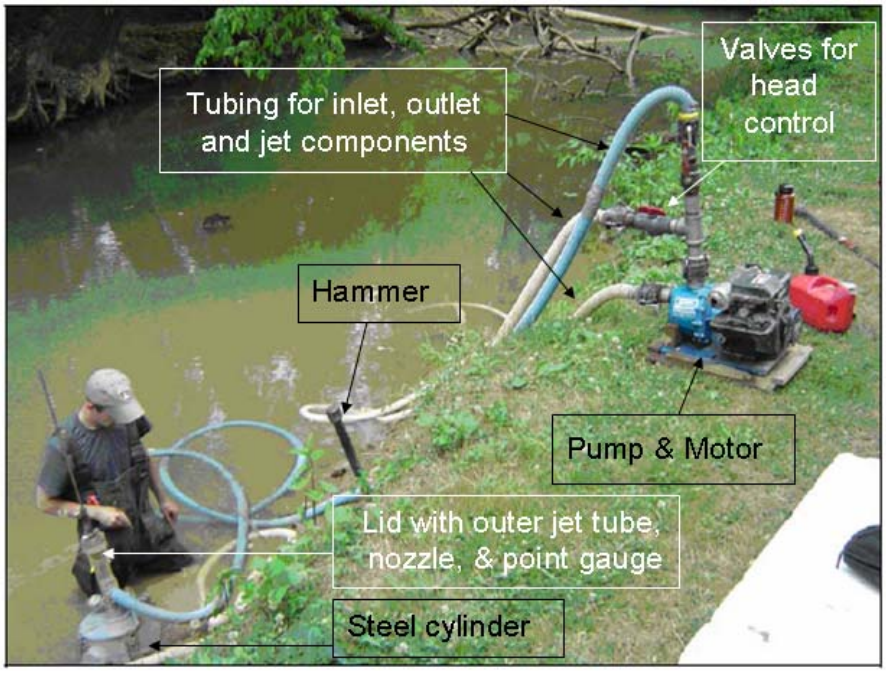


Figure 6. Field testing of Beaver Creek Site #4 with the multiangle submerged jet test device.

The steel cylinder is pounded into the soil 7.6 cm with a hammer and the inflow, outflow, and jet hoses are attached to the pump. After the initial setup, the pump is turned on and a constant jet stream of water begins scouring the riverbank. In theory, the velocity of the water coming out of the jet nozzle remains constant and causes shear stress on the sediment surface. The pressure head created by the pump system controls the applied shear stress. At regular intervals, the scour depth is measured with a point gage until a maximum depth or the final time period is reached.

While the device allows for direct field measurements, the amount of equipment required adds a level of difficultly when considering the widespread use of the submerged jet test device. Moreover, vertical or steep riverbanks can restrict the placement of the pump motor. Depending upon the elevation of the streambank and the placement of the intake, a restriction can be placed on the minimum pressure head allowed which leads an unavoidable increase in applied shear stress during testing. Also, because of the turbulent nature of the flow perpendicular to the bank, the submerged jet test device is criticized. The jet stream of water impinges perpendicular to the streambank ignores the presence of the viscous sublayer.

3.2 University of Tennessee Closed-Loop Laboratory Flume

Recently, a small-scale hydraulic flume was built to facilitate the project. Figure 7, the schematic of the closed-loop laboratory flume, shows the aerial view of the outside and inside wall dimensions along with key features of the design. Additional images of the flume during construction phases and initial testing can be viewed in Appendix A. As

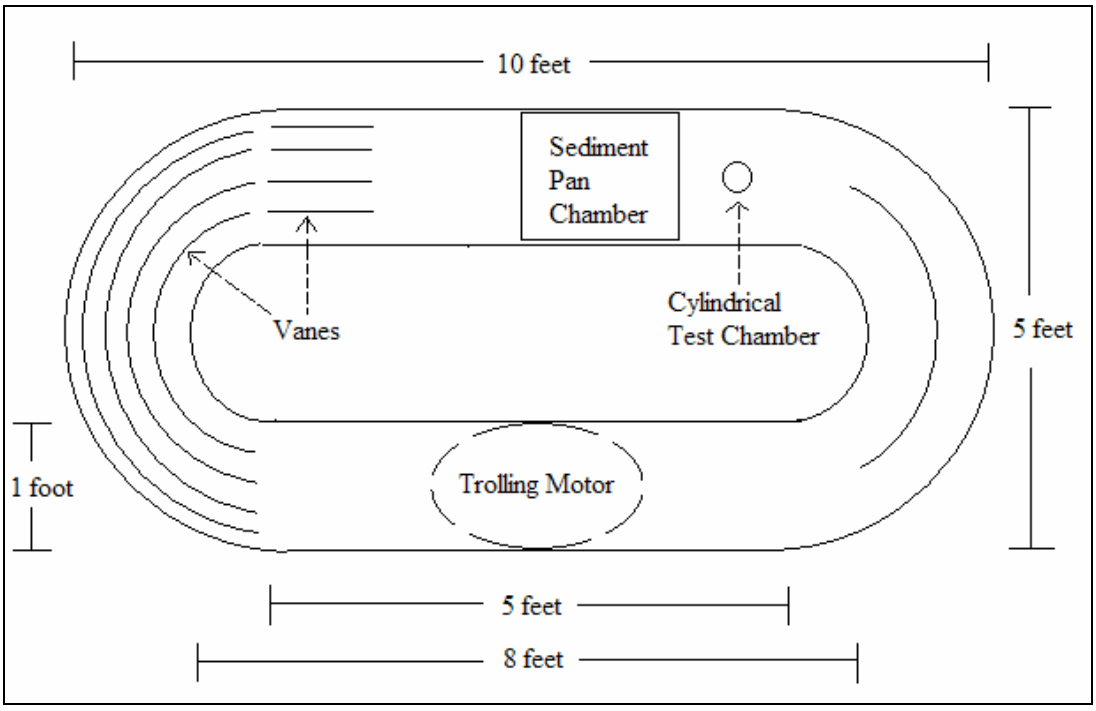


Figure 7. University of Tennessee closed-loop laboratory flume schematic.

seen in the development of velocity profiles and the calculation of bed shear stresses in Appendix A, the flume is capable of producing bed shear stresses (τ_b) from 0.34 to 1.83 Pa.

The table that supports the flume is 11-feet by 6-feet. The outside length and width of the widest portions of the flume are 10-feet by 5-feet. The inside diameter of the semi-circular segments are 3-feet in diameter. As seen in Figure 8, four major vanes are located around the bend prior to the test section to prevent differential local velocities and vortexes from forming. Each of the vanes was spaced to allow an equal area of flow and lined on the bottom with gravel to increase bed roughness. At the start of the test section, eight-inch vanes were placed to aid in the development of laminar flow. Approximately 23-inches after the test section, one major vane was located around the second bend in the

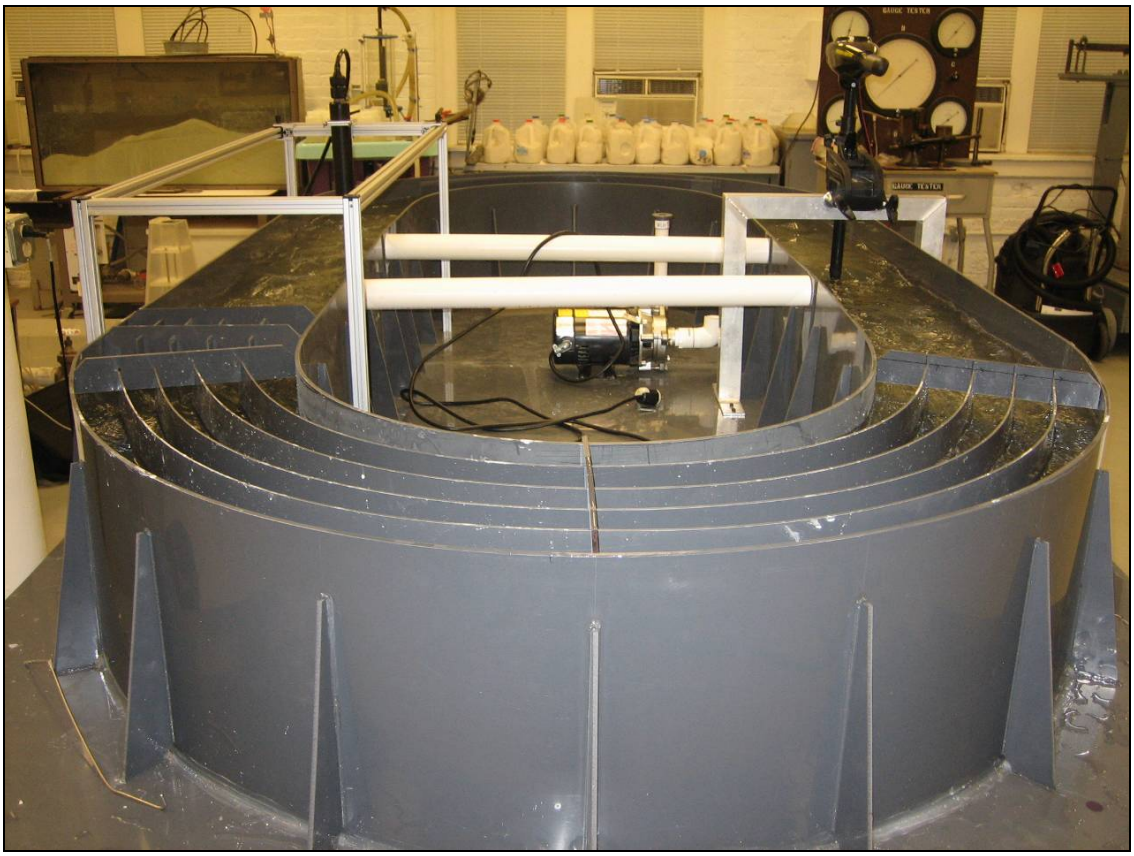


Figure 8. University of Tennessee closed-loop laboratory flume utilized for sediment research.

flume to facilitate the flow pattern. The closed-loop design enables the mimicking of river hydraulics without varying flow rates or highly turbulent flows. It is important to note that sediment can be recirculated through the flume without much disturbance if necessary. The test section is 5-feet in length by about 1-foot in width and is free from flow impedance. A 2-inch diameter cylindrical test chamber is located 55-inches from the beginning of the test section and a 17-inch long, 11.8-inch wide, and 2-inch deep sediment chamber is located 30-inches from the beginning of the test section. When sediment pans are not being tested, a removable plate that is flush with the flume bed is placed over the sediment box.

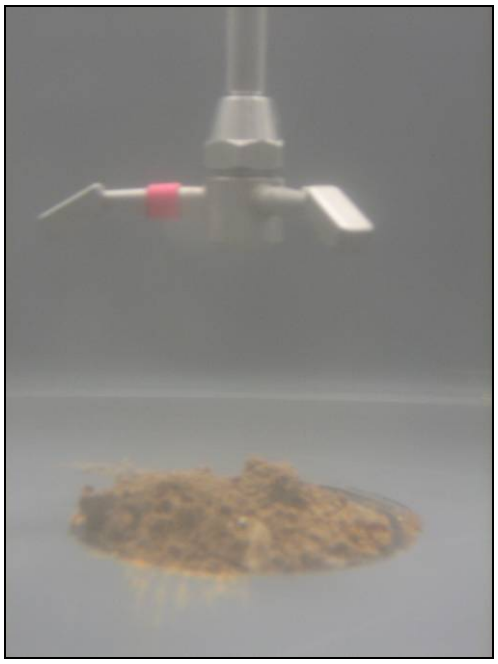


Figure 9. Acoustic Doppler Velocimeter 5.3-cm above sediment core sample.

A SonTek Acoustic Doppler Velocimeter (ADV), shown 5.3-cm above the sample volume in Figure 9, was used to measure the local mean flow and turbulence in three-dimensions. The Acoustic Doppler Velocimeter's sample volume is 5-cm down from the probe head and the ADV has the ability to measure a sample volume within 2-mm of the boundary. The last two components of the closed-loop flume is an 8-Ton hydraulic bottle jack which was utilized to raise the 2-inch cylindrical soil sample into the flow field and Minn Kota trolling motor.

4 Methodology

Twelve field sites were chosen in East Tennessee to perform the submerged jet tests and collect soil samples for soil characterization and laboratory flume analysis. The test locations are described below and the procedure for data collection is presented.

4.1 Test Locations

The streams chosen were second to third-order streams with cohesive riverbanks. All 12 sites have the hydrologic unit code in the Watts Bar Lake watershed of 06010201 (USGS 2007). The selected locations have a longitude between 35°35’30.52” N and 36°4’55.14” N and latitude between 83°49’34.83” W and 84°8’15.04” W. A description, latitude, longitude, and the side of bank tested for each site is listed in Table 3.

Table 3. Site information.

Site Designation	Description	Latitude	Longitude	Bank Tested
Abrams Creek	Abrams Creek	35°35'30.52" N	83°49'34.83" W	Left
BC_DS	Beaver Creek, Downstream	36°4'55.14" N	83°55'27.87" W	Left
BC_Site2	Beaver Creek, Site 2	36°3'30.33" N	83°58'26.06" W	Left
BC_Site3	Beaver Creek, Site 3	36°4'47.22" N	83°56'0.86" W	Left
BC_Site4	Beaver Creek, Site 4	36°1'38.65" N	84°1'37.99" W	Left
BC_Site5	Beaver Creek, Site 5	35°59'50.46" N	84°5'5.26" W	Right
BC_Site6	Beaver Creek, Site 6	35°58'18.99" N	84°8'15.04" W	Right
BC_US1	Beaver Creek, Upstream #1	36°4'51.22" N	83°55'23.83" W	Right
HB_DS	Beaver Creek at Halls, Downstream	36°4'47.22" N	83°55'12.74" W	Right
HB_Site1	Hines Branch, Site 1	36°4'7.37" N	83°56'35.94" W	Left
HB_US	Beaver Creek at Halls, Upstream	36°4'47.28" N	83°55'10.82" W	Right
HB_USB	Beaver Creek at Halls, US of bridge	36°4'47.28" N	83°55'11.16" W	Right

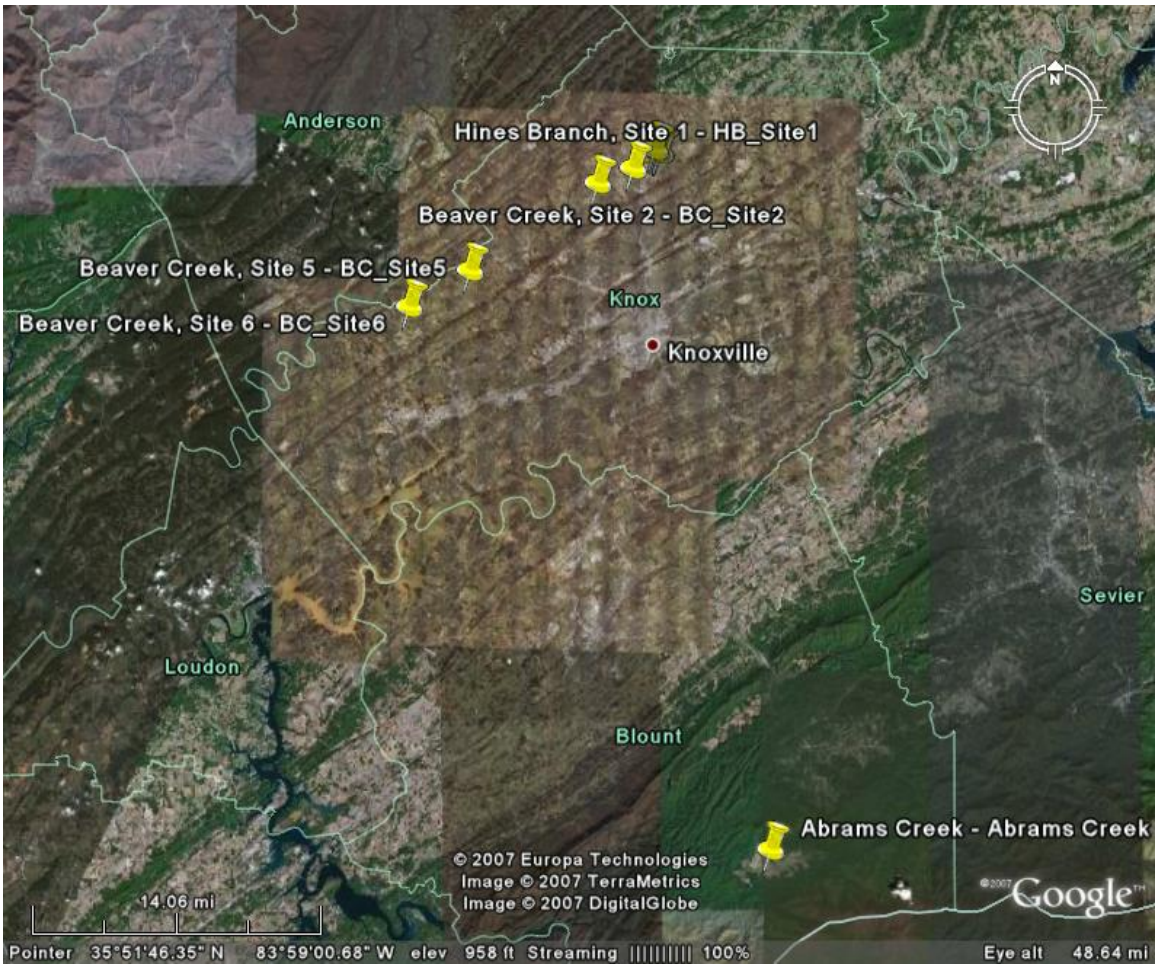


Figure 10. Overall site map developed from Google Earth software.

More specifically, eleven of the locations are in the Beaver Creek Watershed which is in Knox County, Tennessee (USGS 1). The predominant landuse observed of these Knox County stream areas tested is residential/urbanized. Labeled a third-order stream, Abrams Creek is the only test site located outside of Knox County and is part of the Great Smoky Mountain National Park river system (USGS 1). The predominant landuse around the site tested is forested. An overall site map (Figure 10) depicts the locations the sites. Due to the extent of the locations, Figure 11 shows a closer view of the northern-most sites and Figure 12 is more defined picture of the Beaver Creek locations next to Halls Crossroads.

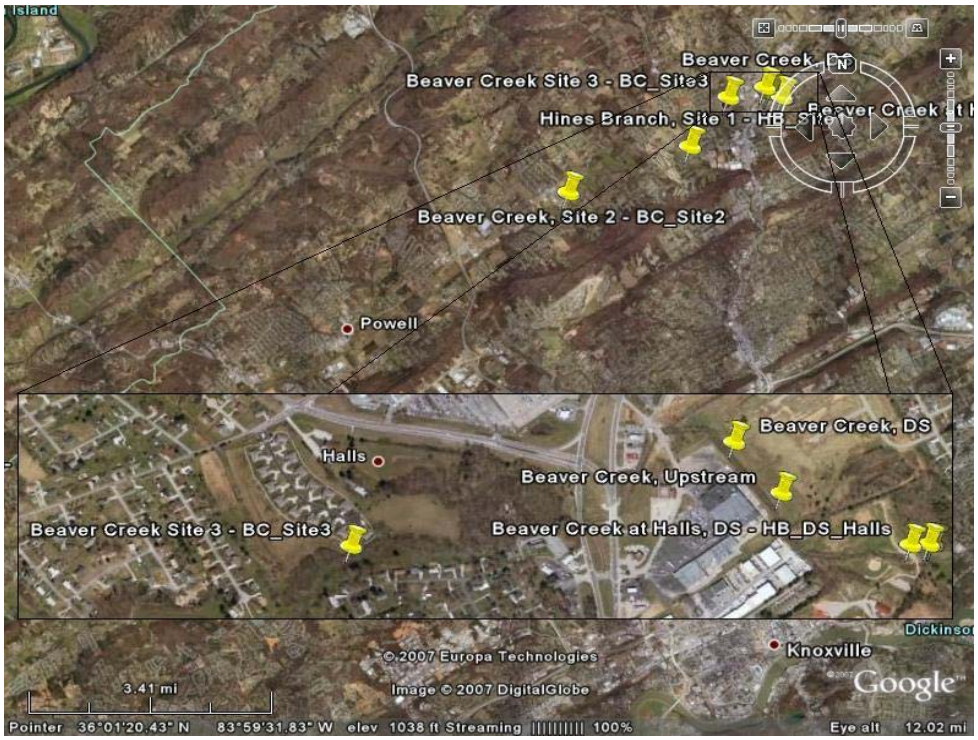


Figure 11. Closer view of the northern-most test sites compiled from Google Earth images.



Figure 12. Defined Google Earth image of the Beaver Creek locations next to Halls Crossroads.

Each study site location was at least 5 m wide and was visually inspected for homogeneity. Later, the homogeneity was checked via soil tests and observation of the soil samples. The first time the soil samples' depth can be checked visually was after extrusion (Figure 13). According to the data collected and the triangular classification chart introduced by the U.S. Bureau of Reclamation (1974), bank materials ranged from clay, silty clay, and sandy & silty clay. Figure 14, Figure 15, and Figure 16 provide a visual of typical study sites' physical characteristics. The bank angles where the submerged jet test device is placed ranges from 20-75°, and the amount of vegetation present where testing occurred ranged from none to low. The tests and samples collected avoided contact with roots unless otherwise noted on the data sheets. Runs with apparent vegetative influences are discarded from data analysis.



Figure 13. Initial inspection of three sediment core samples from upstream Beaver Creek.



Figure 14. Facing upstream of Beaver Creek site #4.



Figure 15. Beaver Creek site #2 off of Dry Gap Road.



Figure 16. Beaver Creek site #3 off Afton Road.

Each of the submerged jet test and sample collection location is carefully chosen to avoid contact with roots or habitat. However, the three previous figures displayed the difficultly encountered when choosing a wide enough, visually homogeneous area to perform four complete jet tests and accrue twelve 6-inch long, 2-inch diameter samples.

4.2 Submerged Jet Test Device

4.2.1 Field Setup & Data Collection

In order to remain in close proximity to the moisture content of the soil samples tested within the flume and in situ methods, the submerged jet tests were limited to the submerged bank or toe of the bank. Therefore, the soil under each footprint of the test had a high moisture content. Every multi-angle submerged jet test device run had a 30 minute

duration with reading intervals every minute. Each time the reading was taken with a point gage, the gage tip plugged the nozzle opening; therefore scour ceased during those measurements. At least four jet test device runs were conducted at each of the field sites. In cases where vegetation, soil strength, or habitat influenced the outcome of the tests, additional information was collected.

4.2.2 Data Analysis

Since the maximum scour depth can take hours or days to reach, the critical shear stress can be computed from the data collected by utilizing the Blaisdell Method (Blaisdell *et al*. 1981; Hanson and Cook 1997). As suggested by Blaisdell *et al.* (1981), the hyperbolic logarithmic method of analysis is utilized to provide the best-fit equation and produce a prediction of the ultimate scour depth based on data collected in the early stages of the scour. The basic equations for the submerged jet data processing are provided as Equation 12 and Equation 13:

$$y = \log \frac{\frac{Z_m}{D_P}}{\frac{V_p t}{D_p}} = \log \frac{Z_m}{D_p} - \log \frac{V_p t}{D_p} \tag{12}$$

$$x = \log \frac{V_p t}{D_p} \tag{13}$$

in which Z_m = the maximum depth of scour measured from the tailwater surface, V_p and D_p = the jet velocity and diameter at the point where the jet plunges in to the tailwater surface, and t = the time passed since the beginning of the scour.

Utilizing a least squares method, an erodibility coefficient (k_d) can be produced from the data collected of a submerged jet test device (Hanson and Cook 1997). In most cases, the bank angles restricted the placement of the pump and motor; therefore, the applied shear stress was relatively high.

4.3 Laboratory Flume

Seven soil samples were collected at each site for testing in the laboratory flume. A major difference between the flume and submerged jet device methods was the location of testing. A submerged jet test was run at the field site and the laboratory flume required an undisturbed sample to be taken and bought back to the laboratory for analysis. In addition to the testing location difference, the hydraulic component of the equipment varied. While the submerged jet test device impinged a jet stream of water at a 90-degree angle, the flume allowed for the flow to run horizontally over the sample and did not directly interfere with the viscous sublayer.

4.3.1 Soil Sampling

For the laboratory flume method, seven 2-inch diameter sediment cores were collected from each of the field sites with 6-inch soil stainless steel tubes, a sampler head, and hammer. Immediately after collection, each sample was sealed with a labeled plastic cap and duct tape around the cap provided another means of preventing moisture loss. The samples were placed in labeled Ziploc bag and drove back to the laboratory where they were extracted by standard methods. As depicted in Figure 17, each sediment core sample was extracted from stainless steel cylinders using an extruder. Then, the



Figure 17. Extruder utilized to extract sediment core samples from stainless steel cylinders.

samples were sealed back into labeled Ziploc bags and brought immediately to a moisture room. In the moisture room, the sediment cores were placed vertically with the top of the soil sample facing upward and stored until testing.

4.3.2 Data Collection

Per equilibrium and velocity tests that were conducted on the University of Tennessee's closed-loop flume, the following procedures were followed to determine the soil erosional properties of critical shear stress and erodibility rate using a laboratory flume.

1. Clean flume prior to use and fill 12 inches with tap water.
2. Shear one-inch off the top of the soil sample and discard the one-inch trimming.

3. Place the rest of the sample in flume for at least 12 hours to promote saturation. Make sure the top of the sample collected is at the highest elevation within the test cylinder.
4. Set up Acoustic Doppler Velocimeter directly over the test cylinder to measure the mean velocity 10-cm above flume bed.
5. Record the initial temperature of the water.
6. Turn the trolling motor on to the position necessary for the shear stress required and wait 5 minutes for equilibrium within the flume.
7. Take an initial turbidity measurement.
8. Crank the soil sample up using the 8-ton hydraulic jack until the soil is 1.5-mm above the flume bed, take an initial photo similar to Figure 18, and start timing the scour rate.
9. Begin recording the mean velocity with the ADV for approximately 10 minutes at the beginning of the test.



Figure 18. Initial photo of soil sample #1 from Beaver Creek downstream site.

10. When the soil sample is eroded approximately 1.5-mm, take an additional picture and crank the soil sample up an additional 1.5-mm. Record the time interval each time the soil sample is raised.
11. Repeat steps 1 through 10 until an accurate erodibility rate is obtained.
12. Record the mean velocity with the ADV for approximately a 10 minute duration during the end of the testing process.
13. Take final temperature and turbidity readings.
14. Turn off equipment, extrude soil sample from flume, and repeat the procedure for the next soil sample.

As seen by the calculations present in Appendix A, the flume has the capability of producing bed shear stresses in a range of 0.3 to 1.83 Pa. Depending on the soil sample, a range of values were tested in order to predict a critical shear stress for the site. For this process, one to seven values of critical shear stress should be tested per site for solving or categorizing the critical value.

4.3.3 Data Analysis

From modern fluid mechanics research on turbulent mixing length by Prandtl and von Karman's hypothesis of turbulence similarity, the law of the wall (Equation 14) was developed (Sturm 2001):

$$\frac{u}{u_*} = \frac{1}{\kappa} \ln \frac{z}{z_o} \tag{14}$$

where u_* = shear velocity, κ = von Karman's constant = 0.40, z_o = constant of integration, and u and z are the point velocity and distance from the wall, respectively.

The law of the wall presents a logarithmic distribution of velocities from the bed to the near-wall region where z/h < 0.2 (Sturm 2001). The "h" in the near-wall region considers the boundary-layer thickness and z is the point distance from the wall. The region where the equation applies is not the full thickness of the flow, but the transition between the viscous sublayer and the region where turbulent shear stresses govern entirely. Because the viscous sublayer is a region where only viscous shear applies, the thickness is determined via Equation 15 and then the logarithmic overlap layer between the viscous sublayer and the fully turbulent region is utilized to find the logarithmic best-fit line and solve for the bed shear stress (Sturm 2001):

$$\frac{u_* z}{v} < 5 \tag{15}$$

where u_* = shear velocity, z = point distance from the wall, and v = kinematic viscosity of the fluid (Sturm 2001).

Because the selection of depth for the no-slip (zero velocity) condition strongly influences the estimated bed shear, Equation 15 is applied and the thickness of the viscous sublayer is computed for 70°F, the average temperature of the fluid during testing. Considering the bed shear stress is the shear stress acting on the soil sample, the bed shear value computed from the law of the wall equation in the transition zone between the viscous sublayer and turbulent flow is the critical shear stress for each flow rate.

An erodibility rate was measured simply by measuring the depth of sediment eroded and dividing the depth by the time passed. Many depth and time measurements

were required to account for variability in sediment samples. Also, three samples were tested at a single flow rate to test for repeatability.

4.4 Critical Shear Stress Values Obtained from Empirical Relations

In order to classify the sediment collected and compute critical shear stress values relating to soil properties, the following soil analyses were preformed: Standard Test Methods for Unconfined Compressive Strength of Cohesive Soil (ASTM D 2166-00), Standard Test Methods for Liquid Limit, Plastic Limit, and Plasticity Index of Soils (ASTM D 4318-00), and Standard Test Method for Particle-Size Analysis of Soils (ASTM D 422-63). Each of tests is run according to the ASTM standard and documented accordingly.

The unconfined compressive strength test device is shown with a sample from Beaver Creek Site #6 in Figure 19 and the hydrometer analysis setup is depicted in Figure 20. Due to the inconsistency of results from the unconfined compressive strength, possibly a result of strain rate, only the physical properties and characteristics of the site obtained during preparation of the unconfined compressive strength samples were utilized in characterizing the soil samples.

As mentioned earlier, other studies have found relationships between critical shear stress and soil parameters such as plasticity index and percentage of clay present. The parameters collected during soil characterization are plugged into the respective equation (Equation 5, Equation 7, Equation 8, or Equation 10) and critical shear stress values were computed for each site.



Figure 19. Sample from Beaver Creek Site #6 in the unconfined compressive strength test device.

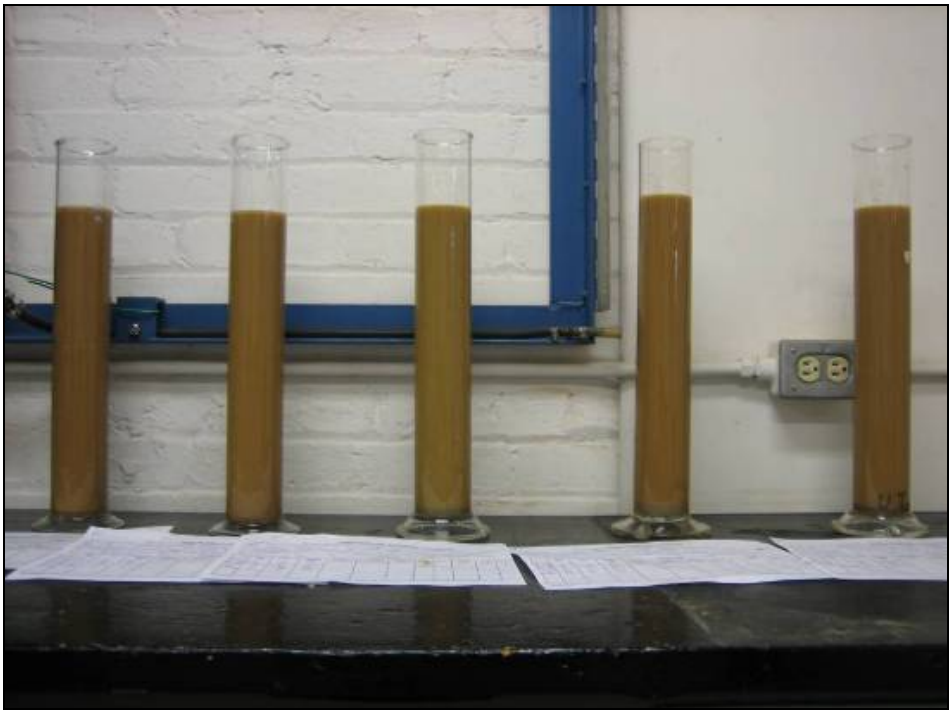


Figure 20. Five samples during hydrometer analysis.

5 Results

5.1 Submerged Jet Test Device Results

5.1.1 Critical Shear Stress

In order to determine the presence of outliers affecting the submerged jet test results, a one-way analysis of the four test runs for each test site is preformed. The graphical results are depicted in Figure 21 and the values in Table 4 present the median critical shear stresses determined from the submerged jet test device. The values outside of the 95% confidence interval were considered outliers and a result of vegetative or habitat influences on the test run. In all cases, three out of four test runs were compiled to compute the average critical shear stress for each location.

5.1.2 Erodibility Coefficient

Erodibility coefficients were computed from the submerged jet device

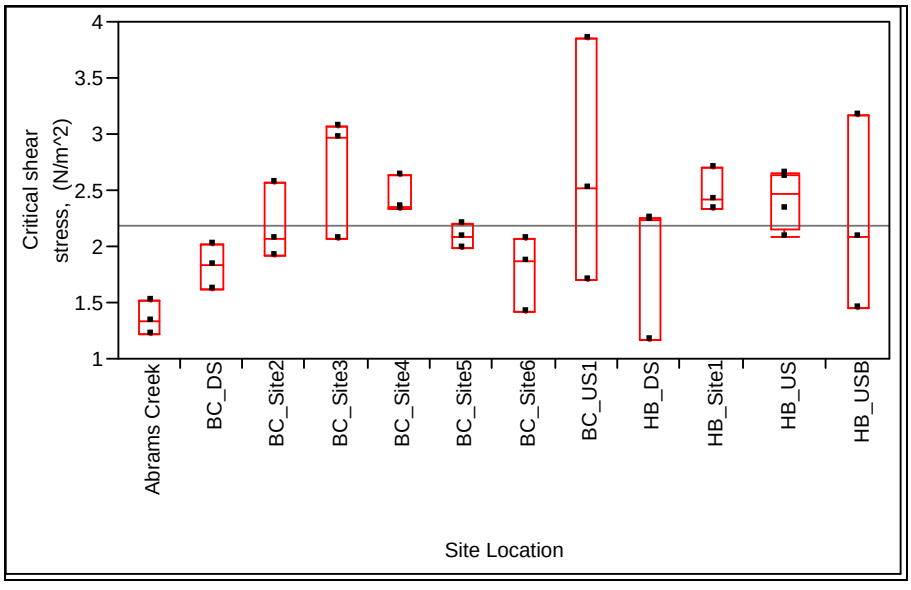


Figure 21. One-way analysis of critical shear stress from submerged jet test by site location.

measurements. The erodibility coefficients are visually presented in a quartile plot (Figure 22) and presented numerically in Table 5.

Table 4. Median critical shear stress determined from submerged jet test device field data.

Site Location	$\tau_{c,\ SJT}$ (N/m^2)
Abrams Creek	1.33
BC_DS	1.84
BC_US1	2.06
BC_Site2	2.96
BC_Site3	2.35
BC_Site4	2.09
BC_Site5	1.86
BC_Site6	2.51
HB_DS	2.23
HB_Site1	2.41
HB_US	2.48
HB_USB	2.09

*Note: SJT = submerged jet test device.

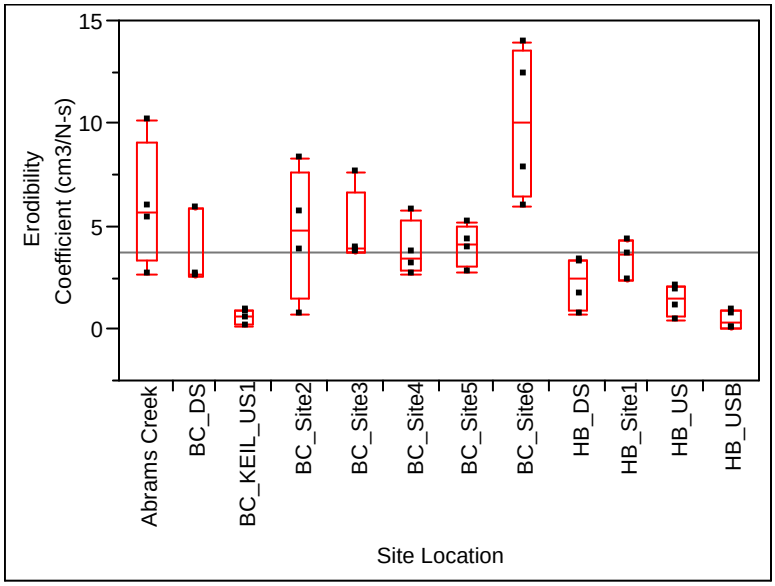


Figure 22. One-way analysis of erodibility coefficient from submerged jet test by site location.

Table 5. Median erodibility coefficients by site for the submerged jet test.

Site Location	Submerged Jet Test Device Erodibility Coefficient ($cm^3/N*s$)
Abrams Creek	5.66
BC_DS	2.63
BC_Site2	0.66
BC_Site3	4.77
BC_Site4	3.89
BC_Site5	3.43
BC_Site6	4.13
BC_US1	10.07
HB_DS	2.45
HB_Site1	3.59
HB_US	1.52
HB_USB	0.37

5.2 Closed-loop Laboratory Flume Results

During the experimental procedure of the flume method, the values of bed shear stress are found to be insufficient to provide a numerical comparison between the values obtained during the jet test data collection and the values computed from empirical soil parameter relationships. However, the observation and experience during the laboratory flume method is valuable and summarized next to the submerged jet test device results in Table 6. Generally, the soil samples did not continue to erode throughout the flume testing; therefore, the critical shear stress of each of the sites tested is assumed to be greater than 1.83 Pa. Critical shear stresses at three sites, as determined by the submerged jet tester were within the range of τ_c that the flume could generate, however only minimal disturbance was observed during the flume tests.

Table 6. Submerged jet test critical stress shown with brief flume observations and root presence.

Site Location	Submerged Jet Test τ_c (Pa)	Erosion Observation in Closed Loop Flume*	Roots Presence, (Y or N)*
Abrams Creek	1.33	Disturbance-induced on 2/3^{rds} of the samples. None on 1/3rd.	N
BC_DS	1.84	High erosion on 1/3rd of the samples. None on 2/3^{rds}.	N
BC_Site2	2.06	Minimal disturbance-induced on 2/3^{rds} of the samples. None on 1/3rd.	N
BC_Site3	2.96	None	N
BC_Site4	2.35	None	(1/3) Y (2/3) N
BC_Site5	2.09	None	N
BC_Site6	1.86	Disturbance-induced on 2/3^{rds} of the samples. None on 1/3rd..	N
BC_US1	2.51	High erosion on 1/3rd of the samples. None on 2/3^{rds}.	(1/3) Y (2/3) N
HB_DS	2.23	Disturbance-induced on 2/3^{rds} of the samples. None on 1/3rd.	N
HB_Site1	2.41	Each sample had few aggregate pieces erode followed by no erosion.	(1/3) Y (2/3) N
HB_US	2.48	High erosion on 1/3rd of the samples. Minimal erosion on 2/3^{rds}.	N
HB_USB	2.09	None	Y

* Note: Fractions are used to represent portion of samples that did or did not experience erosion and amount of samples tested where roots were encountered during flume testing.

5.3 Critical Shear Stress Results from Empirical Equations found in Literature

From the soil properties obtained by the Unconfined Compressive Strength of Cohesive Soil (ASTM D 2166-00), Standard Test Methods for Liquid Limit, Plastic Limit, and Plasticity Index of Soils (ASTM D 4318-00), and Standard Test Method for Particle-Size Analysis of Soils and the erodibility rate obtained using the jet tester, the following critical shear stresses in Table 7 were computed. As mentioned previously, the empirical equations were developed by Smerdon and Beasley (1961) and Julian and Torres (2006).

Table 7. Critical shear stress values determined from empirical sediment relationships.

Site Location	$\tau_{c, PI}$ (N/m^2)	$\tau_{c, D50}$ (N/m^2)	$\tau_{c, PC}$ (N/m^2)	$\tau_{c, SC}$ (N/m^2)
Abrams Creek	1.62	1.93	2.64	3.91
BC_DS	2.28	2.34	3.84	4.42
BC_US1	1.86	2.52	5.84	4.29
BC_Site2	2.05	2.29	4.01	4.77
BC_Site3	1.88	2.51	4.64	3.32
BC_Site4	2.49	2.06	3.39	2.18
BC_Site5	1.64	1.26	2.42	3.85
BC_Site6	0.82	2.03	3.39	4.84
HB_DS	2.52	2.10	3.69	4.56
HB_Site1	0.09	1.18	1.59	2.52
HB_US	0.29	1.74	2.99	4.70
HB_USB	0.16	2.03	3.84	3.67

*Note: PI = plasticity index, D50 = median particle diameter (mm), PC = percent clay, and SC = percent silt-clay.

5.4 Compilation of Critical Shear Stress Results

All of the critical shear stress result are compiled in Table 8 and presented graphically in Figure 23. Then, the percent differences between the critical shear stress determined from submerged jet test device and the empirical equation results. By site location, the percent differences are summarized in Table 9.

5.5 Critical Shear Stress Correlations with Sediment Properties

Previous research had shown a strong relationship between critical shear stress and bulk density or other soil characteristics. In order to determine if the presence of similar findings exists for this project, data was collected to determine the sediment properties summarized in Table 10. Then, multivariate correlations were found for the submerged

jet test device critical shear stresses and soil properties. The correlation results are listed in Table 11 and Figure 24 is a scatterplot matrix depicting the correlations.

Table 8. Critical shear stress result summary.

Site Location	$\tau_{c\ Threshold,\ CLF}$ (N/m^2)	$\tau_{c,\ SJT}$ (N/m^2)	$\tau_{c,\ PI}$ (N/m^2)	$\tau_{c,\ D50}$ (N/m^2)	$\tau_{c,\ PC}$ (N/m^2)	$\tau_{c,\ SC}$ (N/m^2)
Abrams Creek	1.83	1.33	1.62	1.93	2.64	3.91
BC_DS	1.83	1.84	2.28	2.34	3.84	4.42
BC_US1	1.83	2.06	1.86	2.52	5.84	4.29
BC_Site2	1.83	2.96	2.05	2.29	4.01	4.77
BC_Site3	1.83	2.35	1.88	2.51	4.64	3.32
BC_Site4	1.83	2.09	2.49	2.06	3.39	2.18
BC_Site5	1.83	1.86	1.64	1.26	2.42	3.85
BC_Site6	1.83	2.51	0.82	2.03	3.39	4.84
HB_DS	1.83	2.23	2.52	2.10	3.69	4.56
HB_Site1	1.83	2.41	0.09	1.18	1.59	2.52
HB_US	1.83	2.475	0.29	1.74	2.99	4.70
HB_USB	1.83	2.09	0.16	2.03	3.84	3.67

*Note: CLF = closed-loop laboratory flume, SJT = submerged jet test, PI = plasticity index, D50 = median particle diameter (mm), PC = percent clay, and SC = percent silt-clay.

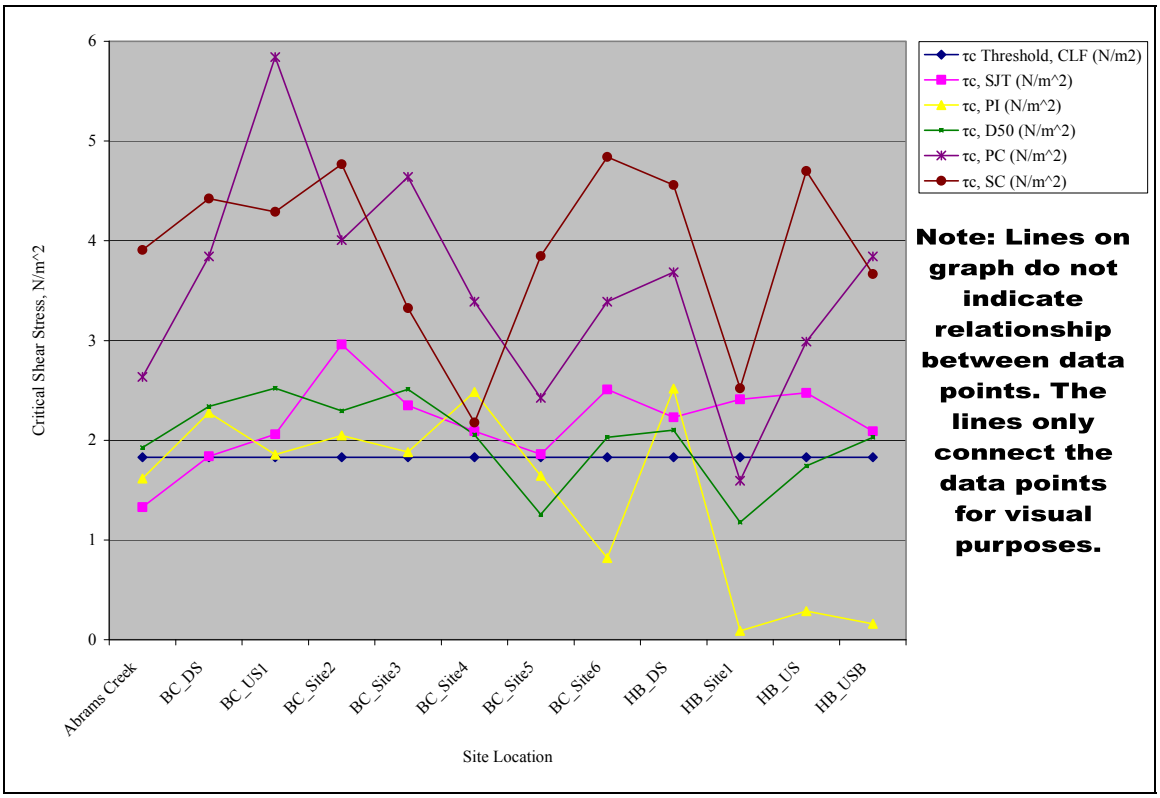


Figure 23. Graphical representation of shear stress values obtain by submerged jet test device and soil parameter relationships.

Table 9. Percent difference between submerged jet test device critical shear stress and the analytical values.

Site Location	$\tau_{c, SJT}$ (N/m^2)	$\tau_{c, PI}$ Difference (%)	$\tau_{c, D50}$ Difference (%)	$\tau_{c, PC}$ Difference (%)	$\tau_{c, SC}$ Difference (%)
Abrams Creek	1.33	9.73	18.33	32.92	49.22
BC_DS	1.84	10.61	11.96	35.24	41.25
BC_US1	2.06	-5.21	10.05	47.87	35.12
BC_Site2	2.96	-18.21	-12.66	15.03	23.40
BC_Site3	2.35	-11.07	3.34	32.76	17.17
BC_Site4	2.09	8.65	-0.83	23.71	2.04
BC_Site5	1.86	-6.20	-19.34	13.16	34.81
BC_Site6	2.51	-50.73	-10.59	14.90	31.70
HB_DS	2.23	6.06	-2.94	24.60	34.31
HB_Site1	2.41	-92.85	-34.32	-20.38	2.27
HB_US	2.475	-79.26	-17.35	9.40	30.99
HB_USB	2.09	-85.78	-1.47	29.54	27.39
Average Percent Difference (%)		-26.19	-4.65	21.56	27.47

*Note: SJT = submerged jet test, PI = plasticity index, D50 = median particle diameter (mm), PC = percent clay, and SC = percent silt-clay.

Table 10. Sediment properties determined for each test location.

Site Location	Bulk Density (g/cm^3)	D_{50} (mm)	G	LL (%)	PL (%)	PI (%)	Percent silt (%)	Percent clay (%)	Percent silt-clay (%)
Abrams Creek	1.93	0.00940	2.93	43	27	16	50	40	90
BC_DS	1.85	0.00640	2.80	47	23	24	45	49	94
BC_Site2	1.88	0.00670	2.50	41	20	21	43	50	93
BC_Site3	1.93	0.00530	2.59	43	24	19	43	54	97
BC_Site4	1.60	0.00840	2.65	57	31	26	39	46	85
BC_Site5	1.98	0.01600	2.93	33	17	16	35	38	73
BC_Site6	1.83	0.00860	2.44	31	24	7	44	46	90
BC_US1	1.89	0.00525	2.31	40	21	19	38	59	97
HB_DS	2.00	0.00805	2.55	47	20	27	47	48	95
HB_Site1	1.88	0.01700	2.40	27	26	1	49	28	77
HB_US	2.02	0.01095	2.59	26	24	2	53	43	96
HB_USB	1.97	0.00860	2.39	25	24	1	39	49	88

*Note: D_{50} = mean particle diameter, G = specific gravity, LL = liquid limit, PL = plastic limit, and PI = plasticity index.

Table 11. Multivariate correlations for submerged jet test device critical shear stresses and soil properties.

	Critical Shear Stress, SJT (N/m^2)	Bulk Density (g/cm^3)	D_{50} (mm)	G	PI (%)	Percent silt (%)	Percent clay (%)	Percent silt-clay (%)
Critical Shear Stress, SJT (N/m^2)	1.0000	0.0156	-0.0884	-0.4751	-0.0237	-0.1518	0.2671	0.1690
Bulk Density (g/cm^3)	0.0156	1.0000	0.1821	0.0390	-0.3520	0.2852	-0.0549	0.1410
D_{50} (mm)	-0.0884	0.1821	1.0000	0.2157	-0.5082	0.1142	-0.9192	-0.8638
G	-0.4751	0.0390	0.2157	1.0000	0.3520	0.0483	-0.2978	-0.2720
PI (%)	-0.0237	-0.3520	-0.5082	0.3520	1.0000	-0.2845	0.4602	0.2751
Percent silt (%)	-0.1518	0.2852	0.1142	0.0483	-0.2845	1.0000	-0.3739	0.3084
Percent clay (%)	0.2671	-0.0549	-0.9192	-0.2978	0.4602	-0.3739	1.0000	0.7669
Percent silt-clay (%)	0.1690	0.1410	-0.8638	-0.2720	0.2751	0.3084	0.7669	1.0000

Note: D_{50} = mean particle diameter, G = specific gravity, and PI = plasticity index.

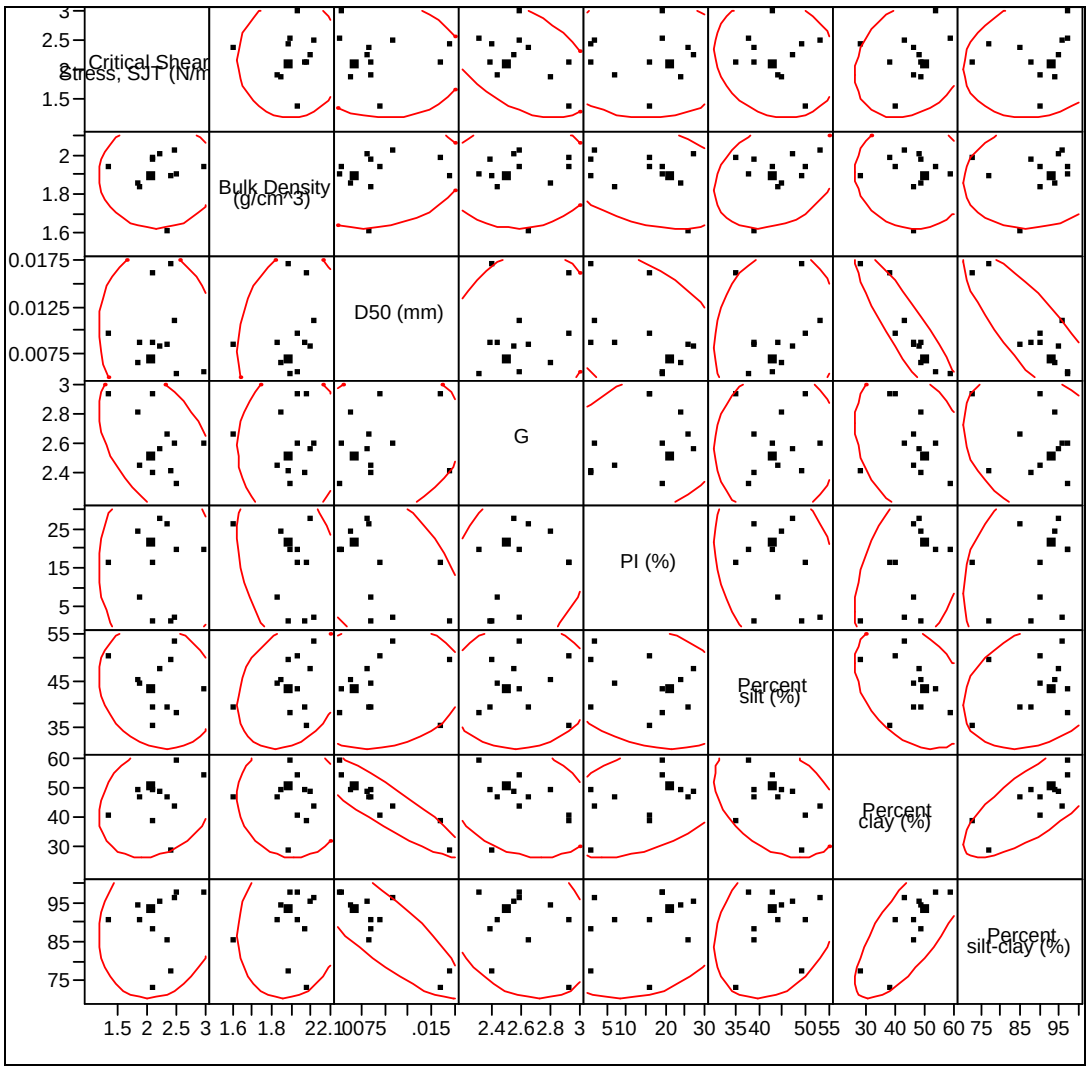


Figure 24. Scatterplot matrix for multivariate correlation data.

6 Discussion

Due to the low bed shear stress values produced in the laboratory flume, percent differences between the critical shear stresses and erodibility parameters produced by the submerged jet test device method and laboratory flume method could not be determined. However, the submerged jet test results could be compared to the laboratory flume's threshold. The in situ test produced an estimate above the laboratory flume's threshold at each test site location except for Abrams Creek, and two Beaver Creek sites were near the flume maximum τ_c. Even though none of the complete flume test runs continually eroded at the max shear stress applied, the flow rate within the flume had the ability to transport gravel placed on the bottom of the flume for roughness. Because the velocity required to transport some gravel sizes is less than the speed needed to cause erosion in clay and silt sediment, the ability of the flume to transport gravel without causing erosion in the core sample can be explained. The illustration in Figure 25 of deposition, transport, and erosion velocities for different particles sizes best represents the flume's ability to move gravel particles without eroding the sediment core sample. The transport of gravel can occur at lower flow velocities than erosion of clay particles. During the initial rise of the cylinder, when aggregate eroded quickly and then the sample remained intact, the cause was assumed to be a drag force induced.

When considering the concept of shear stress and erodibility coefficient being the controlling factor of the erosion of cohesive sediment, this flume study found that it did not adequately describe the pattern of cohesive sediment erosion. In fact, the soil sample face and the moisture level affected the ability of the flume to erode the sediment. If a

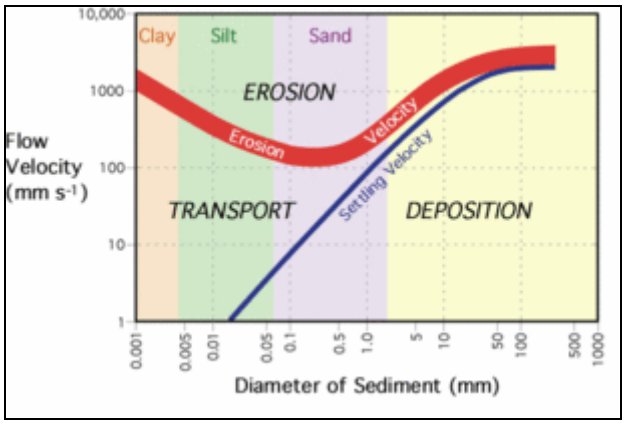


Figure 25. Typical velocities for the deposition, transport, and erosion of various particle sizes (Pidwirny 2006).

sample had a jagged face or high moisture content, the weak plane of soil sheared most times. When another sediment core from the same site had a smooth face or lower moisture content, no erosion would occur, not even in the initial rise of the cylinder. According to the flume observations and outcome witnessed, cohesive sediment erosion estimates should incorporate the effects of soil structure, gradation, physical and chemical properties which have been found to effect cohesive sediment erosion.

With the submerged jet test device, the presence of organic matter and habitat affected the runs and accounted for part of the variability within the results. While some wildlife presence was accounted for by correcting the data collected for crawfish holes or moving the jet test cylinder's location when roots were encountered, the field testers may not realize other wildlife impacts. Also, the jet test device eroded sediment very quickly and aggregate collected on the bottom of the scour hole. From both an objective and subjective standpoint, this piling effect could also affect scour rates and measurements. Limitations aside, the submerged jet test data returned similar critical shear stresses and erodibility rates in three out of the four test runs per site.

Considering the empirical estimates of critical shear stress, the values obtained from the percent clay or percent silt-clay parameters returned the highest estimates of the erosive property. Also, the plasticity index equation to find critical shear stress produced the lowest critical shear stress at a few of the test sites. Apparently, the equation based on plasticity index did not apply to half of the sediments sample collected because they were considerably lower than the flume's critical shear stress threshold. Erosion was not usually witnessed in the flume from the samples collected at those sites. The critical shear stress calculated from the mean particle diameter was closest to the submerged jet test result most often with an average percent difference of -4.65%.

Soils properties determined did not correlate well with each other or with erosional properties found by the submerged jet test method. Bulk density does not take into account sediment composition, salinity, or other physiochemical properties of the soil. While previous studies (Wynn and Mosaghimi 2006a; Asare et al. 1997) found a relationship between critical shear stress and bulk density, the results of this experiment failed to do so. It is possible that results from other studies which linked soil properties to the erosive parameters could not be transferred to the soil types tested for this project.

With the closed-loop laboratory flume having zero slope, it was difficult to achieve critical shear stresses that reliably and continually produced a constant rate of erosion. Because a fraction of the samples at most sites experienced some form of erosion in the flume while others samples from the same site location did not, the lack of a measurable pattern of erosion in the laboratory flume suggest that the critical shear stress and erodibility are not the primary considerations when dealing with cohesive sediment. Considering the observations of the two procedures, the submerged jet test device was the

best available testing method. Since the soil structure, soil gradation, and chemistry of the soil and water apparently influenced the erosion of cohesive sediment, any in situ method that had been carefully designed would be the better representation than the laboratory result based upon erosion observations of this experiment. While the submerged jet test device is field intensive, the in situ test uses a practical amount of site water and does not include the sampling or transport disturbance that the laboratory method requires. As for the submerged jet test device not accounting for the viscous sublayer, the results have shown that there are more influential factors on the erosion of cohesive sediment.

Many important advances in understanding the erosive behavior of cohesive sediment have been made in the past decade. However, the connection between values obtained using analytical equations, in situ devices, or laboratory experiments is subject to great uncertainty unless the influential parameters that dominate the behavior of cohesive sediment erosion are measured and detailed along with the experimental results. Judging from experiences with this project, in situ testing over a wide range of soil types with careful accounting of cohesive parameters is recommended for future research on improving erosion prediction and measurement.

References

Alberts, E.E., Laflen, J.M., Rawls, W.J., Simanton, J.R., and Nearing, M.A. (1989). Soil component. *In* "USDA Water Erosion Prediction Project: Hillslope Profile Model Documentation," Chap. 6, NSERL Report No. 2. National Soil Erosion Laboratory, USDA-ARS, W. Lafayette, IN.

Asare, S.N., R.P. Rudra, W.T. Dickinson, and G.J. Wall. (1997). Frequency of Freeze-Thaw Cycles, Bulk Density, and Saturation Effects on Soil Surface Shear and Aggregate Stability in Resisting Water Erosion. *Canadian Agricultural Engineering* 39(4):273-279.

ASTM. (2003). Standard test method for Liquid Limit, Plastic Limit, and Plasticity Index of Soils. No. D4318-00. ASTM International, West Conshohocken, PA. 04.08: 582-595.

ASTM. (2003). Standard test method for Particle-Size Analysis of Soils. No. D422-63. ASTM International, West Conshohocken, PA. 04.08: 10-17.

ASTM. (2003). Standard test method for Unconfined Compressive Strength of Cohesive Soil. No. D2166-00. ASTM International, West Conshohocken, PA. 04.08: 201-204.

Bhasin, R. N., Lovell, C. W., and Toebes, G. R. (1969). *Erodability of sand-clay mixtures as evaluated by a water jet*. Technical Report No. 8, Purdue University Water Resources Research Center, West Lafayette, Indiana.

Blaisdell, F., Clayton, L. A., and G. G. Hebaus. (1981). Ultimate dimension of local scour. *Journal of Hydraulic Division ASCE*. 107(HY3):327-337.

Briaud, J. L., Chen, H. C., Li, Y., Nurtjahyo, P., and J. Wang. (2004). *Pier and Contraction Scour in Cohesive Soils: National Cooperative Highway Research Program Report* 516. Transportation Research Board. 1-136.

Clark, L.A., and Wynn, T.M. (2007). Methods for Determining Streambank Critical Shear Stress and Soil Erodibility: Implications for Erosion Rate Predictions. *Transactions of the ASAE*. Vol. 50 Issue 1, p95-106.

Cornelisse, J. M., Mulder, H. P. J., Houwing, E. J., Williamson, H., and G. Witte. (1994). "On the Development of Instruments for In-Situ Erosion Measurements," in *Cohesive Sediments*, N. Burt, R. Parker, and J. Watts (eds.), John Wiley and Sons Ltd., 175-186.

Dash, U. (1968). *Erosion behavior of cohesive soils*. PhD thesis, Purdue University, West Lafayette, Indiana.

Debnath, K., Nikora, V., Aberle, J., Westrich, B. and M. Muste. Erosion of cohesive sediments: Resuspension, bed load, and erosion patterns from field experiments. *Journal of Hydraulic Engineering*. 133(5):508-520.

Dunn, I. S. (1959). Tractive resistance of cohesive channels. *Journal of Soil Mechanics and Foundations Division*. ASCE, 85(3):1-24.

Foster, G. R. (1982). *Effect of discharge rate on rill erosion*. Paper – American Society of Agricultural Engineers [0145-0166].

Foster, G. R., Meyer, L. D., and Onstad, C. A. (1977). An erosion equation derived from basic erosion principles. *Trans. ASAE* 20(4):678-682.

Haan, C. T., Barfield, B. J., Hayes, J. C. (1994). *Design Hydrology and Sedimentology for Small Catchments*. San Diego: Academic Press, Inc.

Hanson, G. J. (1990). Surface erodibility of earthen channels at high stresses: Part II. Developing an in situ testing device. *Trans. ASAE* 33(1):132-137.

Hanson, G. J., and K. R. Cook. (1997). *Development of excess shear stress parameters for circular jet testing*. ASAE Paper No. 972227. St. Joseph, Michigan: ASAE.

Hanson, G. J., and Cook, K. R. (2004). Apparatus, test procedures, and analytical methods to measure soil erodibility in situ. *Applied Eng. in Agric.* 20(4):455-462.

Hanson, G. J., and A. Simon. (2001). Erodibility of cohesive streambeds in the loess area of the Midwestern USA. *Hydrological Processes*. 15(1):23-38.

Hanson, G.J., Cook, K.R., and Simon, A. (1999). Determining erosion resistance of cohesive materials. In *Proc. ASCE Intl. Water Resources Eng. Conf*., CD-ROM. Seattle, Washington: ASCE.

Hedges, J. D. (1990). *The scour of cohesive soils by an inclined submerged water jet*. MSc thesis, Texas A&M University, College station, Texas.

Hirschi, Michael C., and B. J. Barfield. (1988a). Compaction effects on erosion of mine spoil and reconstructed topsoil. *Transactions of the ASAE* [0001-2351]. 31(2): 447-452.

Hollick, M. (1976). "Towards a routine assessment of the critical tractive forces of cohesive soils." *Transactions of the ASAE*. St. Joseph, Michigan, 19: (1076-1081).

Huang, Jianchun, Hilldale, Robert C., and Blair P. Greimann. (2006). *Erosion and Sedimentation Manual*. Department of the Interior Bureau of Reclamation. Chapter 4: 1-55.

Julian, J.P., and R. Torres. (2006). Hydraulic erosion of cohesive riverbanks. *Geomorphology* 76(1-2): 193-206.

Julien, Pierre E. (1998). Erosion and Sedimentation. Cambridge University Press: Trumpington Street, Cambridge. 1-280.

Krishnappan, Bommanna G., and Ian G. Droppo. (2006). Use of an in situ erosion flume measuring stability of sediment deposits in Hamiliton, Harbour, Canada. *Water, Air, and Soil Pollution: Focus.* 6: 557-567.

Langendoen, E. J. (2000). CONCEPTS – Conservational channel evolution and pollutant transport system: Stream corridor version 1.0. Research Report No. 16. Oxford, Miss.: USDA-ARS.

Lyle, W.M., and Smerdon, E.T. (1965). Relation of compaction and other soil properties to erosion resitance of soils. *Trans. Am. Soc. Agric. Eng.* 8(3):419-421.

Mantz, Peter A. (1977). Incipient transport of fine grains and flakes by fluids em dash extended Shields diagram. *Journal of Hydraulic Division*. 103(6): 601-615.

Mazurek. K. A. (2001). *Scour of clay by jets*. PhD thesis, University of Alberta, Edmonton, Alta., Canada.

Mirtskhulava, Ts. E., Dolidze, I. V. and Magomedova, A. V. (1967). Mechanisms and computation of local and general scour in non-cohesive, cohesive soils, and rock beds. *Proc., 12 Congress of IAHR*, Delft, The Netherlands, 3: 169-176.

Moore, W. L., and Masch, R. D. Jr. (1962). "Experiments on the scour resistance of cohesive sediments." *Journal of Geophysical Resources*, 67(4):1437-1449.

Neill, C.R. (1967). Mean-velocity criterion for scour of coarse uniform bed-material. *Proc. Intl. Assoc. for Hydraulic Res*. 3:46-54.

Neill, C.R. (1973). *Guide to Bridge Hydraulics*. Toronto, Canada: University of Toronto Press.

Pidwirny, Michael. (2006). Soil erosion and deposition. The Encyclopedia of Earth. Sidney Draggan and Cutler J. Cleveland (eds.). Washington, D.C.: Environmental Information Coalition, National Council for Science and the Environment. Image, 1.

Prosser, I. P., Rutherfurd, I. D., Olley, J., Young, W. J., Wallbrink, P.J., and C. J. Moran. (2001). Large-scale patterns of erosion and sediment transport in river networks, with examples from Austrailia. Marine and Freshwater Research. 52: 81-99.

Shields, A. (1936). Application of similarity principles and turbulence research to bed-load movement. Trans. By W. P. Ott and J. C. van Uchelen. Pasadena California: California Institute of Technology, SCS Co-operative Laboratory.

Smerdon, E.T., and Beasley, R.P. (1961). Critical tractive forces in cohesive soils. *Agric. Eng.* 42(1):26-29.

Stein, O. R., Julien, P. Y., and Alonso, C. V. (1993). "Mechanics of jet scour downstream of a headcut." *Journal of Hydraulic Resources*, 31(6), 723-738.

Sturm, Terry W. (2001). *Open Channel Hydraulics*. New York: McGraw-Hill.

Temple, D.M. (1992). Estimating flood damage to vegetated deep soil spillways. *Applied Engineering in Agriculture*. 8(2):237-242.

Tolhurst, T. J., Black, K. S., Shayler, S. A., Black, I., Baker, K., & Paterson, D. S. (1999). Measuring the insitu erosion shear stress of inter tidal sediments with the cohesive strength meter (CSM). *Esuarine, Coastal and Shelf Science*. 49:281-294).

USGS. (2007). USGS Tennessee Water Science Center. Internet reference: http://tn.water.usgs.gov/. Accessed November 20, 2007.

Vanoni, V. A. (1977). *Sedimentation Engineering*. New York, N.Y.: American Society of Civil Engineers.

Wallbrink, P. J., Murray, A. S., Olley, J. M., and L. J. Olive. (1998). Determining sources and transit times of suspended sediment in the Murrumbidgee River, New South Wales, Austrailia, using fallout ^{137}Cs and ^{210}Pb. *Water Resources Research*. 34: 879-887.

Wasson, R. J., Mazari, R. K., Starr, B., and G. Clifton. (1998). The recent history of erosion and sedimentation on the Southern tablelands of southeastern Austrailia: sediment flux dominated by channel incision. *Geomorphology*. 24: 291-308

Widdows, J., Friend, P. L., Bale, A. J., Brinsley, M. D., Pope, N. O., Thompson, C. E. L., (2007). Inter-comparison between five devices for determining erodibility of intertidal sediments. *Continental Shelf Research*. 27:1174:1189.

Winterwerp, J. C., Cornelisse, J. M., and C. Kuijper. (1990). "Parameters to Characterize Natural Muds," in Abstract Volume, Int. Workshop on Cohesive Sediments, Brussels, KBIN, Brussels. 103-105.

Wynn, T. and S. Mostaghimi. (2006a). The Effects of Vegetation and Soil Type on Streambank Erosion, Southwestern Virginia, USA. *Journal of American Water Resources Association*. February: 70-82.

Yalin, M. Selim and Emin Karahan. (1979). Interception of Sediment Transport. *Journal of Hydraulic Division*. 105(11): 1433-1443.

Appendix

Appendix A: Flume Construction and Initial Activation

The closed-loop design was chosen for the laboratory's use of space and for its availability for future sediment transport studies. Once the construction period was finished, a series of tests were preformed to determine the flume's characteristics and capabilities. Equilibrium points and velocity profiles were produced to aid in the development of methodology and provide values required to compute erosive parameters of the sediment core samples.

Flume Construction

Construction began on the flume December 2006 and the bulk of the work continued until March 2007. At first, the support system in Figure 26 needed to be built to hold the flume filled with water and contain a few key features.



Figure 26. Support structure for flume with sediment bed cut-out and hydraulic jack section.



Figure 27. Sediment core jack system.

One of the support tables' components is a sediment core jack system. Figure 27 shows the area for the core sample and jack system to elevate the sediment core. Also, the flume was built to contain an erosion bed test section with a removable plate. In order to build the walls and vanes, sheets of polyvinyl chloride (PVC) were cut and welded together with PVC piping shown in Figure 28.

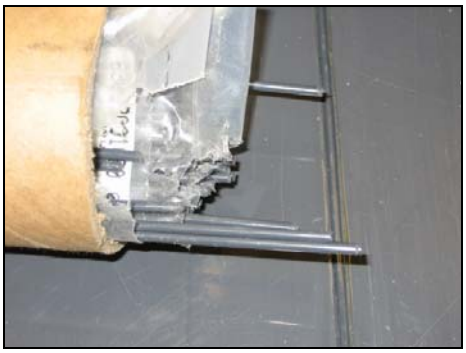


Figure 28. Polyvinyl chloride utilized to weld the sheets of PVC together.

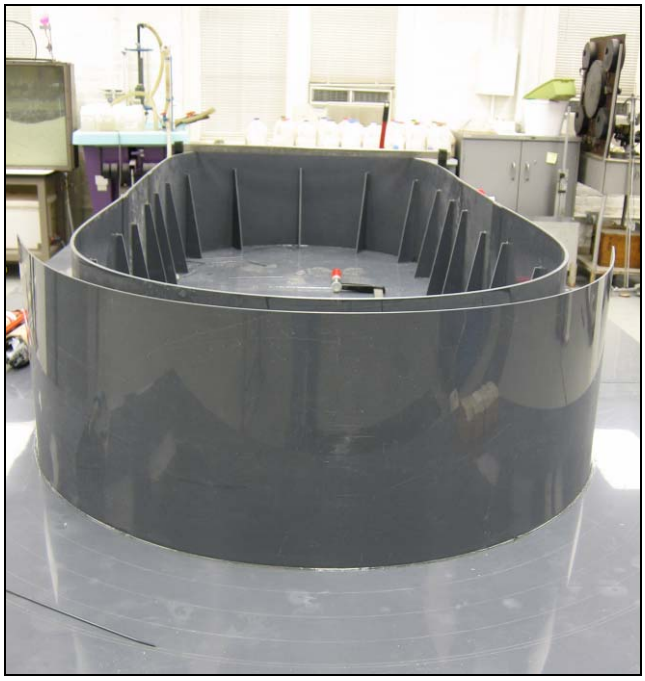


Figure 29. Construction of the inside wall and the first vane.

As seen in Figure 29, the inside wall was welded first, followed by the vanes, and finally the outside of the flume. At the end of the flume's construction, the inside and outside were sealed with silicon to help prevent fluid loss through the joints. Throughout the construction period, the flume was periodically checked for its levelness and its ability to perform under specified conditions.

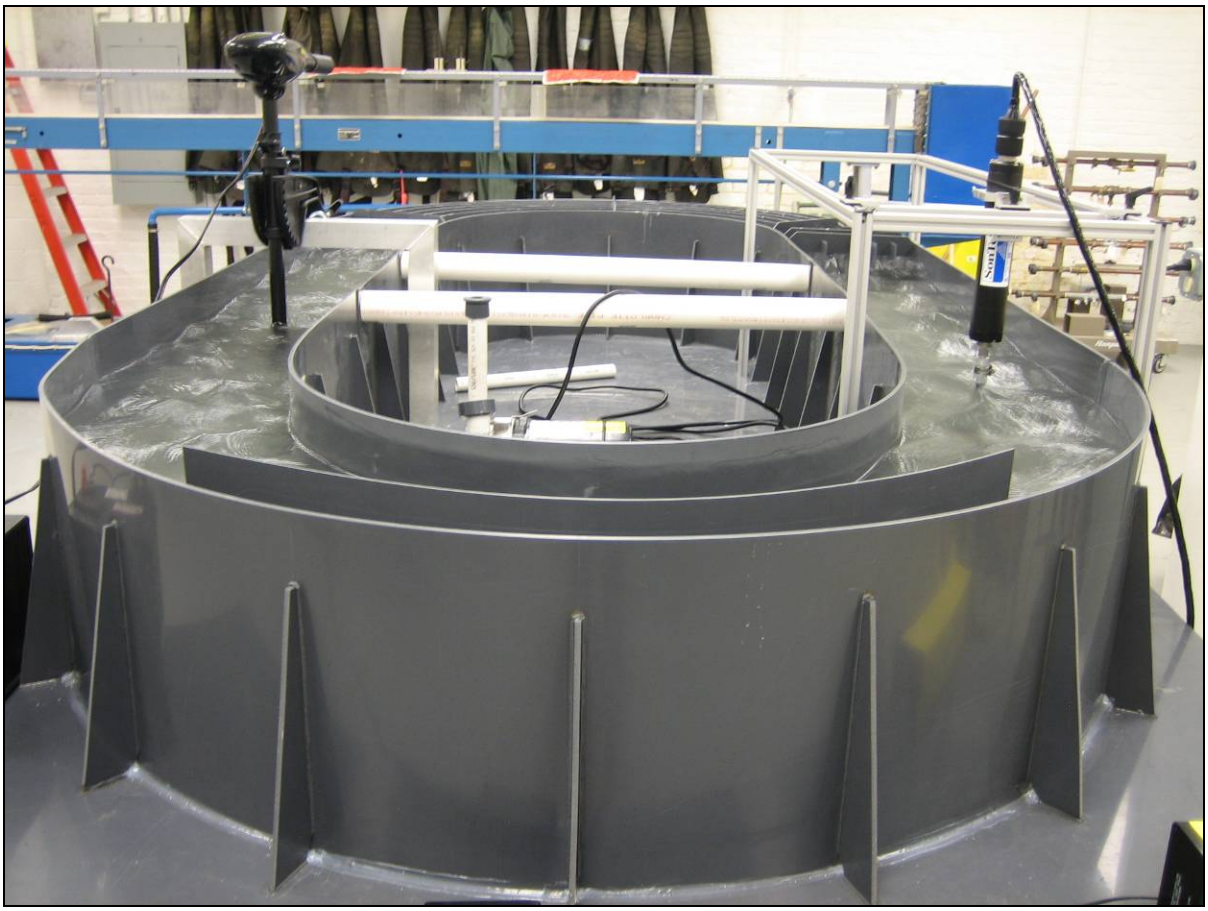


Figure 30. Closed-loop flume during testing procedure.

Alterations of the flume shown from the single-vane side in Figure 30 that came after the substantial completion date were the pump system component for lower flow rates and plexiglass window on wall beside cylindrical test section show with the ADV setup in Figure 31.



Figure 31. Acoustic Doppler Velocimeter over cylindrical test section with plexiglass window.

After final completion of the flume, equilibrium and velocity profile tests could begin and the flume's bed shear capabilities could be quantified.

Equilibrium Test

The point of equilibrium defines where the state of balance between opposing forces or actions is equal. In this case, the point of equilibrium needing to be defined considers the force generated by the trolling motor and the momentum developed from the water recirculating around the flume. Using an Acoustic Doppler Velocimeter, the mean velocity at a single point is measured from the moment the trolling motor is turned until it reaches a peak value. For the equilibrium profile, the HorizonADV software is set up to record the ADV measurements. The ADV is placed 10-cm above the flume bed and velocity measurements are recorded for a duration of 10 minutes. The output plots developed at settings #1, #2, #3, and #4 are seen in the following four figures (Figure 32, Figure 33, Figure 34, and Figure 35).

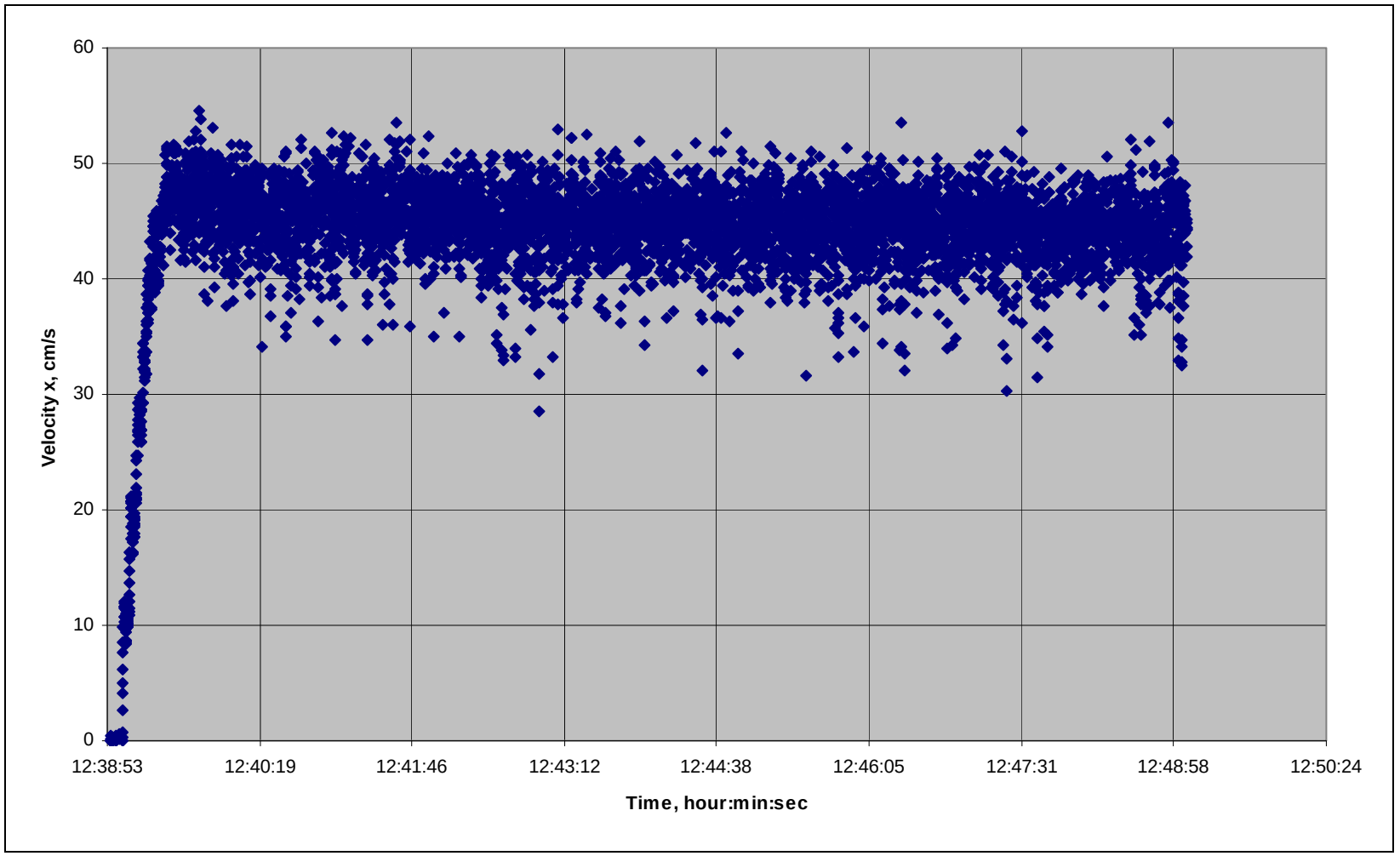


Figure 32. Equilibrium profile for trolling motor setting #1.

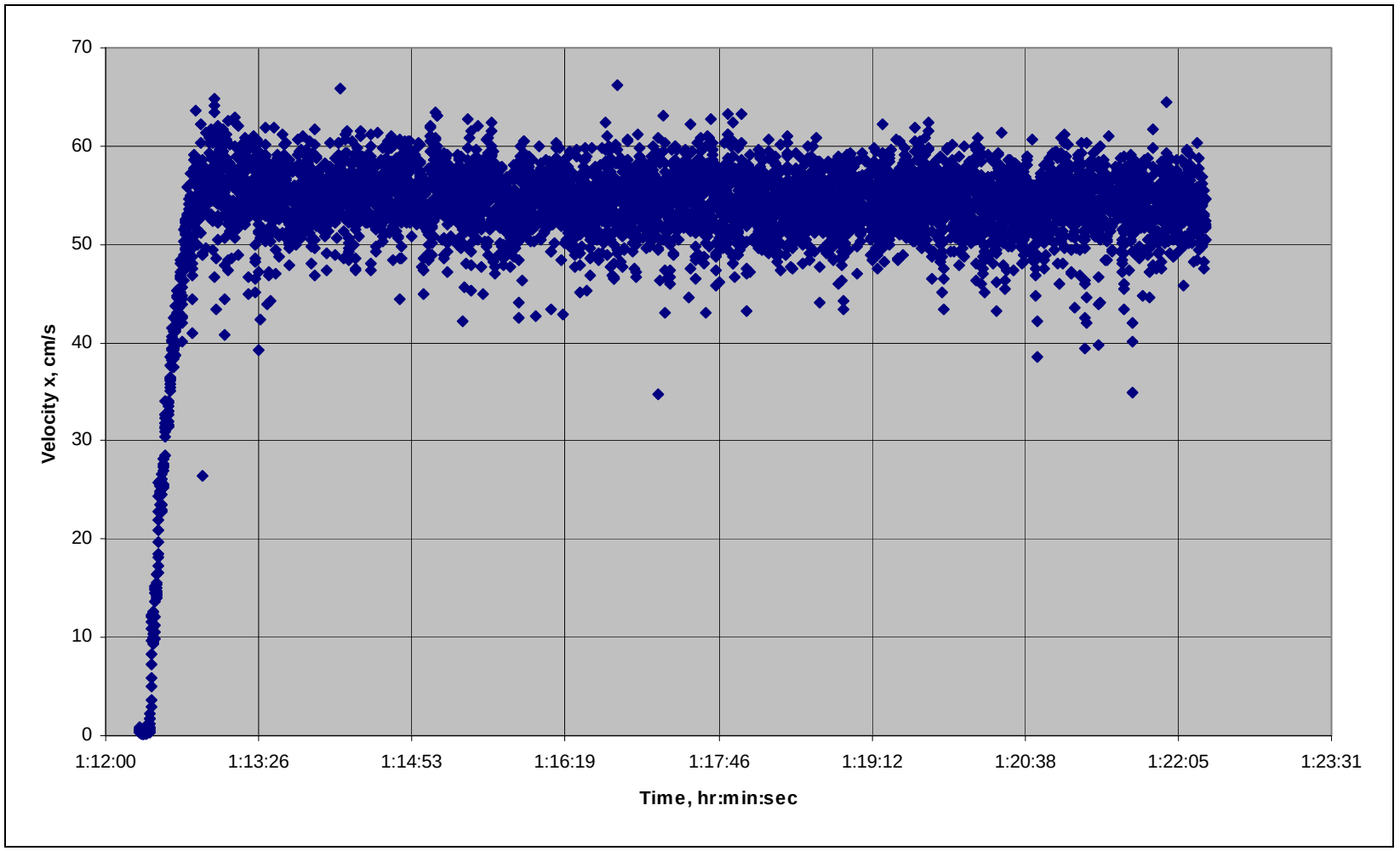


Figure 33. Equilibrium profile for trolling motor setting #2.

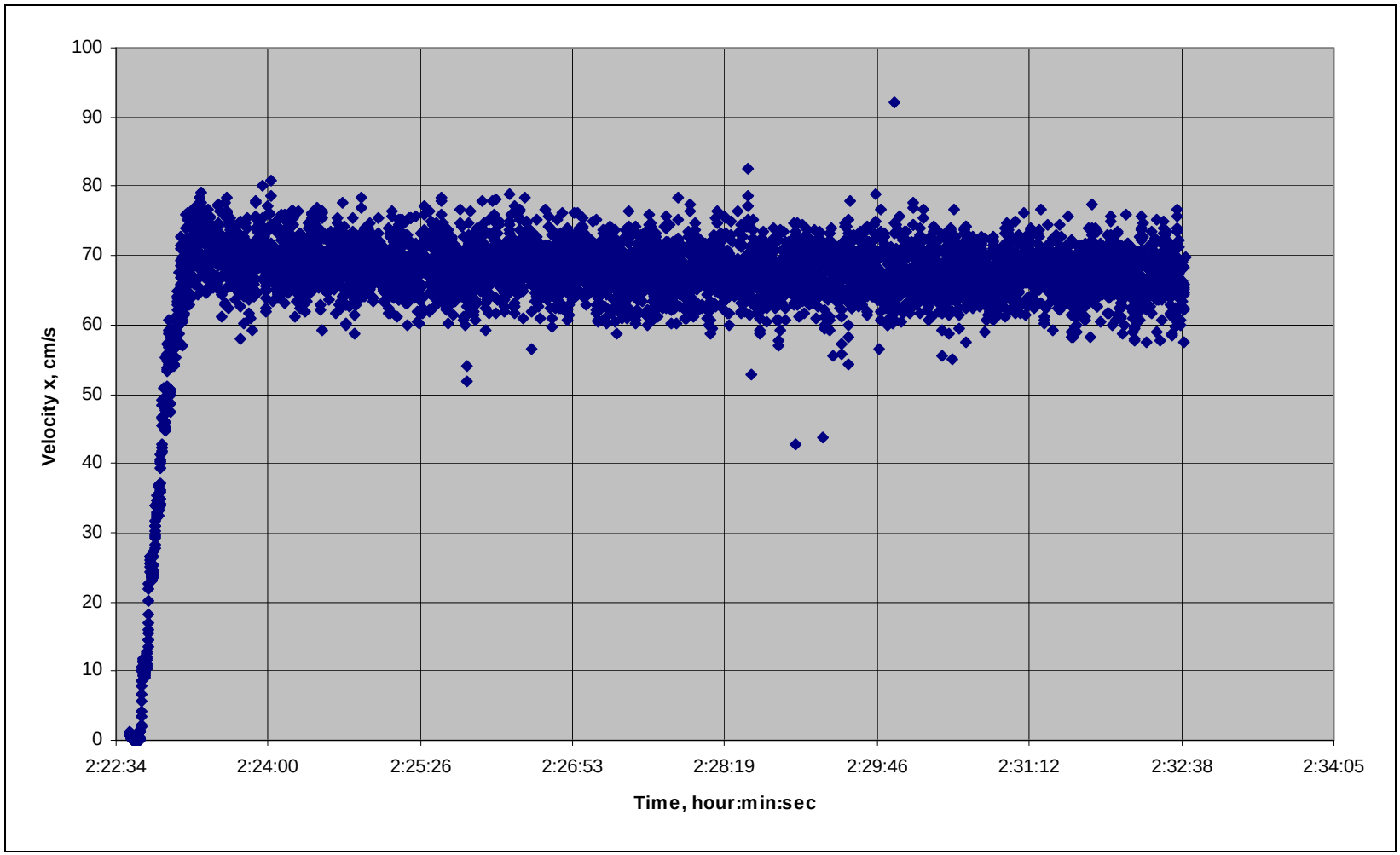


Figure 34. Equilibrium profile with trolling motor setting #3.

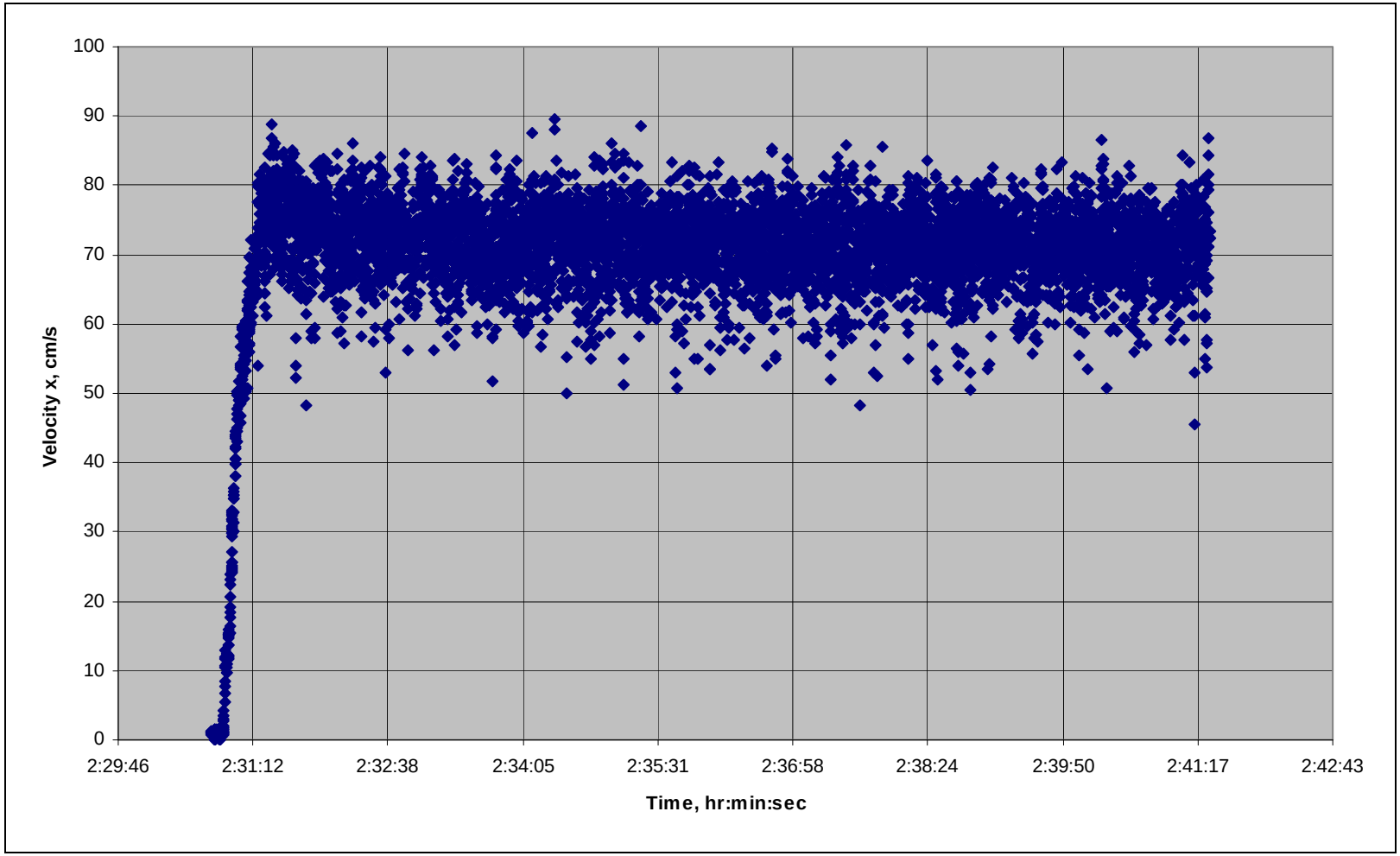


Figure 35. Equilibrium profile with trolling motor setting #4.

The equilibrium point is the cumulative time the flume requires in order for the velocity to reach a steady rate. From the four equilibrium tests, the time required for the closed-loop flume to reach equilibrium was 2 minutes for all of the trolling motor settings. In order to check this point of equilibrium over the long duration of a sediment core erosison test, the same procedure is run over the course of one and a half hours with the ADV 10-cm above the bed. The graphical result is shown in Figure 36. The long duration equilibrium profile showed a slight decrease in velocity magnitude over time. The change is not large enough to change the outcome significantly since most of the tests do not require that length of time. Multiple equilibrium tests are preformed for each motor setting and length and the results are consistent.

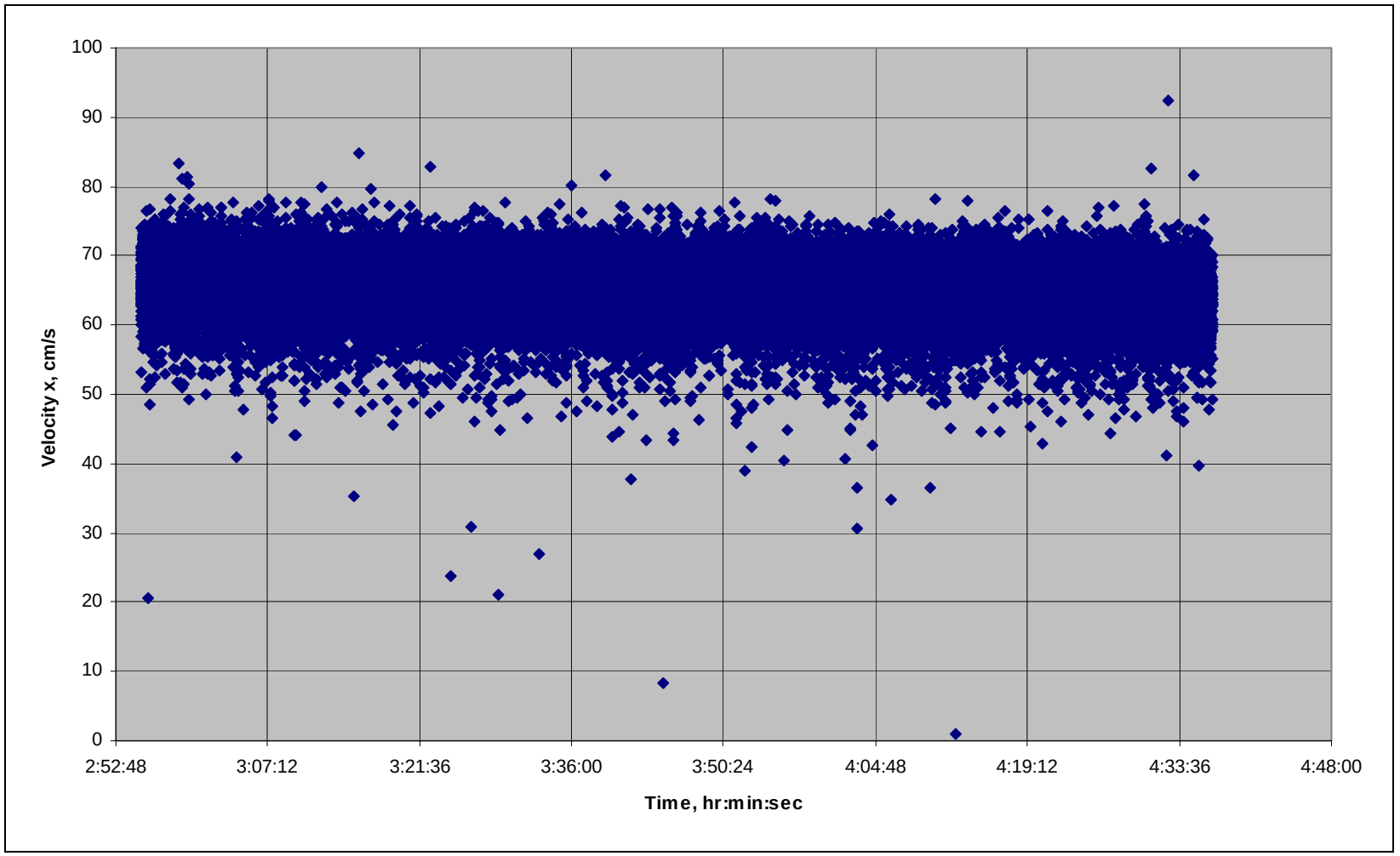


Figure 36. Long duration equilibrium profile with trolling motor on setting #3.

Velocity Profiles

After the point of equilibrium is determined, the velocity profiles are produced for the trolling motor settings #1, #2, #3, #4, and #5 for the half propeller and settings #1, #2, #3, and #4 for the full propeller. The trolling motor is turned on to the respective setting and left to run for 5 minutes. After 5 minutes, the data collection begins and the velocities are collected at different elevations to produce the velocity profiles. The temperature is measured and the HorizonADV software is set up to record the velocity for 1 minute at each of the following intervals: 10, 6, 4, 2, 1, and 0.3 cm above the bed. In some cases, additional velocity and elevation measurements are collected. For analysis, the top of the viscous sublayer is assumed to be the location of zero velocity. The following tables (Table 12 through Table 20) and figures (Figure 37 through Figure 54) summarize the data that is collected from the velocity profile test runs.

Table 12. Velocity data for trolling motor with half propeller on setting #1.

Elevation z, cm	Velocity x, cm/s	Elevation z, ft	Velocity, ft/s	LOG Elevation z, ft
22.00	34.06	0.72	1.12	-0.14
20.00	33.42	0.66	1.10	-0.18
18.00	33.19	0.59	1.09	-0.23
16.00	33.32	0.52	1.09	-0.28
14.00	32.99	0.46	1.08	-0.34
10.00	31.94	0.33	1.05	-0.48
6.00	29.57	0.20	0.97	-0.71
4.00	26.77	0.13	0.88	-0.88
2.00	24.81	0.07	0.81	-1.18
1.00	23.13	0.03	0.76	-1.48
0.30	20.51	0.01	0.67	-2.01
0.011	0.00	0.00	0.00	-3.44

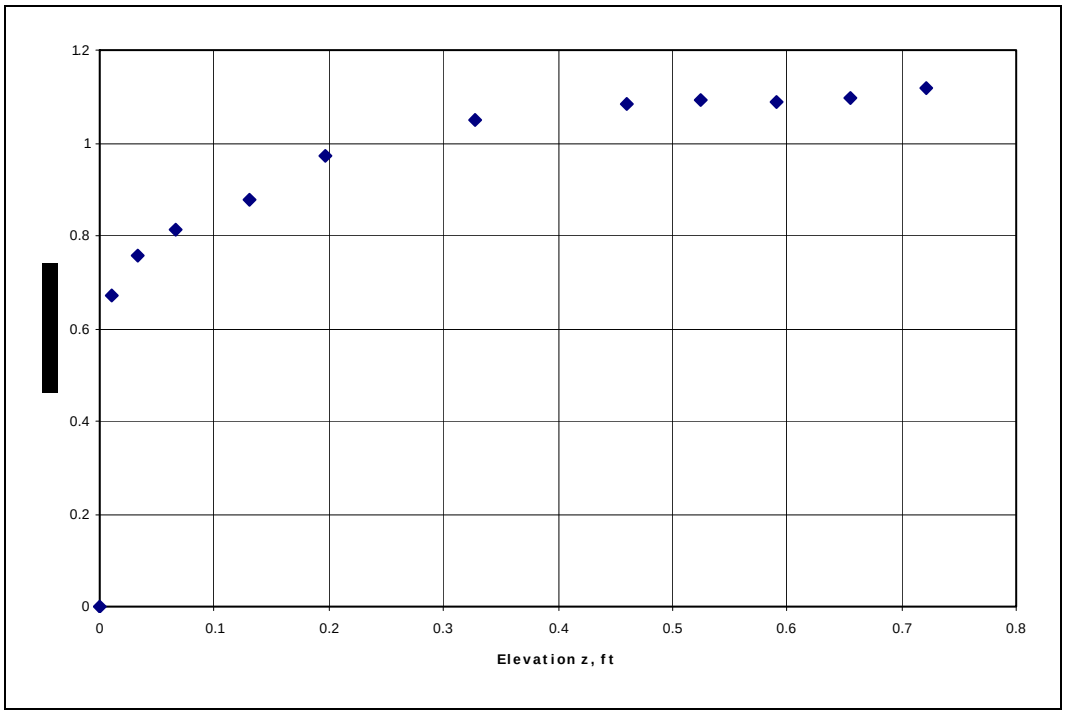


Figure 37. Velocity profile for trolling motor with half propeller on setting #1.

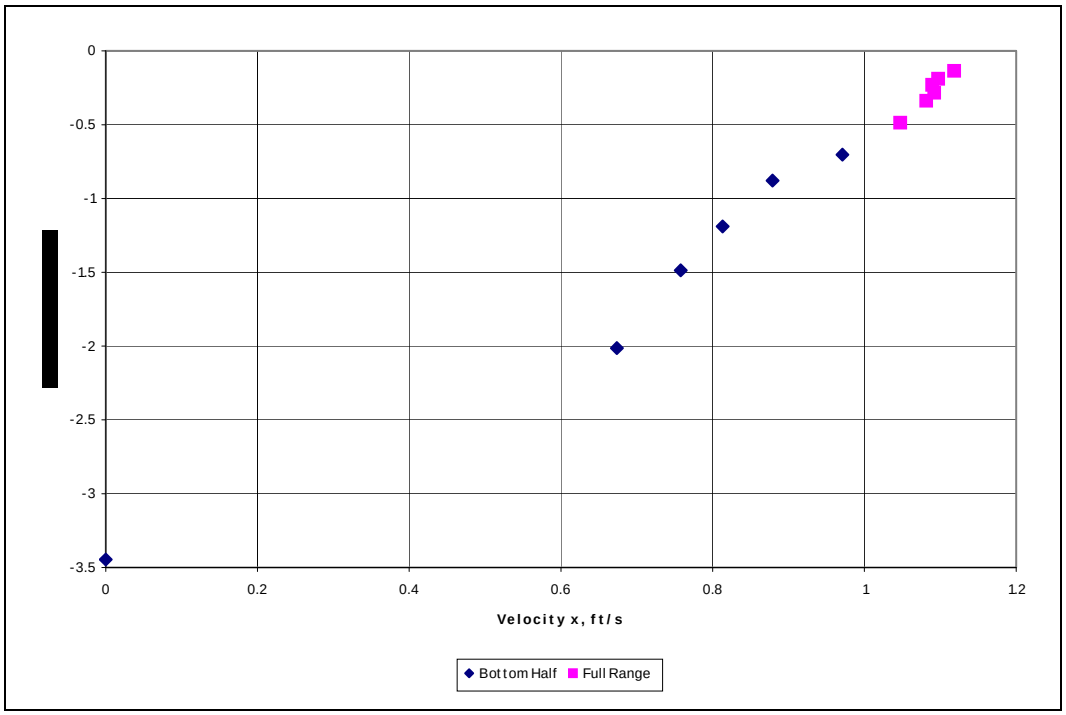


Figure 38. Velocity distribution for trolling motor with half propeller on setting #1.

Table 13. Velocity data for trolling motor with half propeller on setting #2.

Elevation z, cm	Velocity x, cm/s	Elevation z, ft	Velocity, ft/s	LOG Elevation z, ft
22.00	40.79	0.72	1.34	-0.14
20.00	39.77	0.66	1.30	-0.18
18.00	39.52	0.59	1.30	-0.23
16.00	38.85	0.52	1.27	-0.28
14.00	39.00	0.46	1.28	-0.34
10.00	37.74	0.33	1.24	-0.48
6.00	35.06	0.20	1.15	-0.71
4.00	32.35	0.13	1.06	-0.88
2.00	29.45	0.07	0.97	-1.18
1.00	27.65	0.03	0.91	-1.48
0.30	23.73	0.01	0.78	-2.01
0.01	0.00	0.00	0.00	-3.48

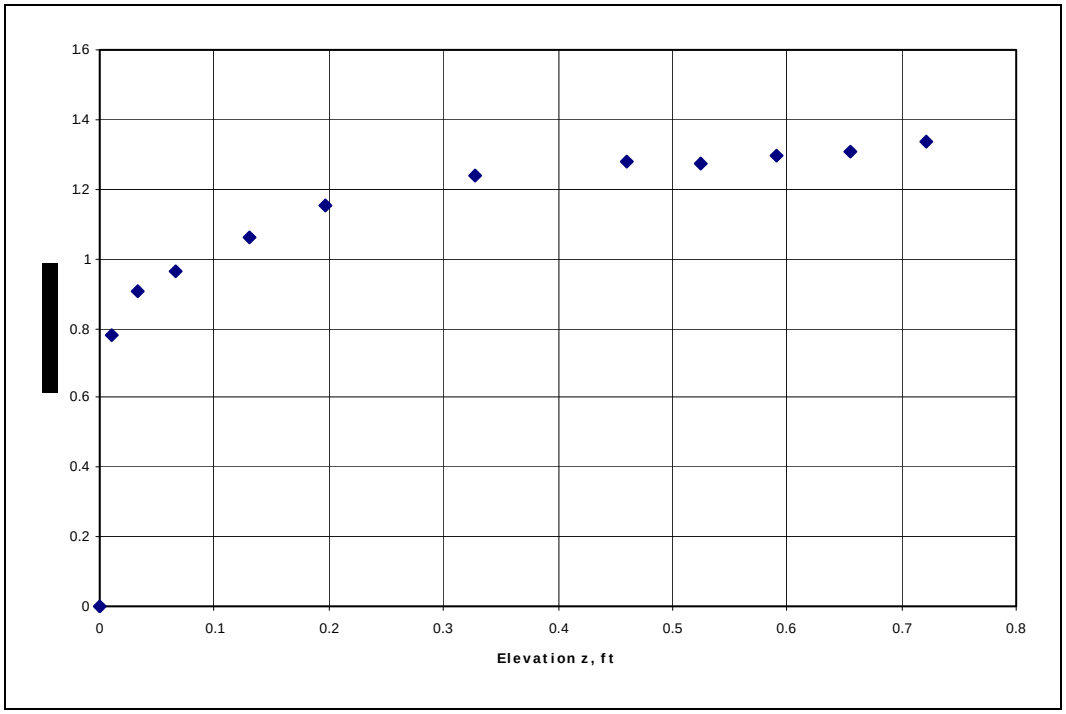


Figure 39. Velocity profile for trolling motor with half propeller on setting #2.

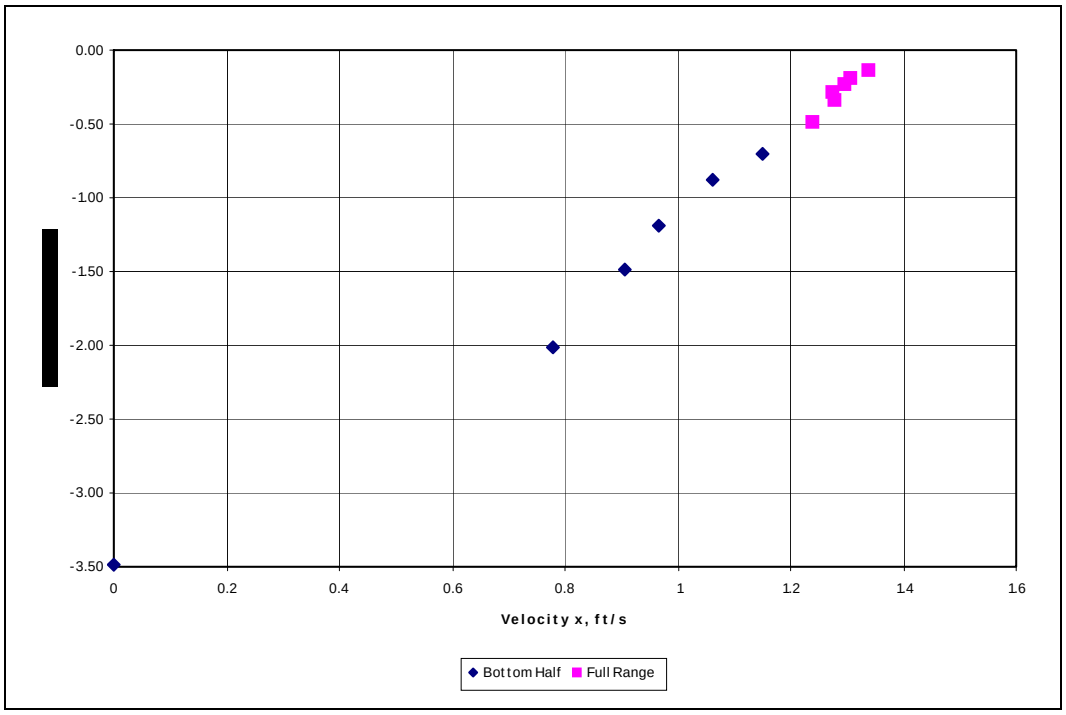


Figure 40. Velocity distribution for trolling motor with half propeller on setting #2.

Table 14. Velocity data for trolling motor with half propeller on setting #3.

Elevation z, cm	Velocity x, cm/s	Elevation z, ft	Velocity, ft/s	LOG Elevation z, ft
22.00	47.25	0.72	1.55	-0.14
20.00	47.26	0.66	1.55	-0.18
18.00	46.91	0.59	1.54	-0.23
16.00	46.01	0.52	1.51	-0.28
14.00	46.29	0.46	1.52	-0.34
10.00	45.52	0.33	1.49	-0.48
6.00	42.34	0.20	1.39	-0.71
4.00	40.69	0.13	1.33	-0.88
2.00	36.68	0.07	1.20	-1.18
1.00	34.75	0.03	1.14	-1.48
0.30	28.60	0.01	0.94	-2.01
0.008	0.00	0.00	0.00	-3.58

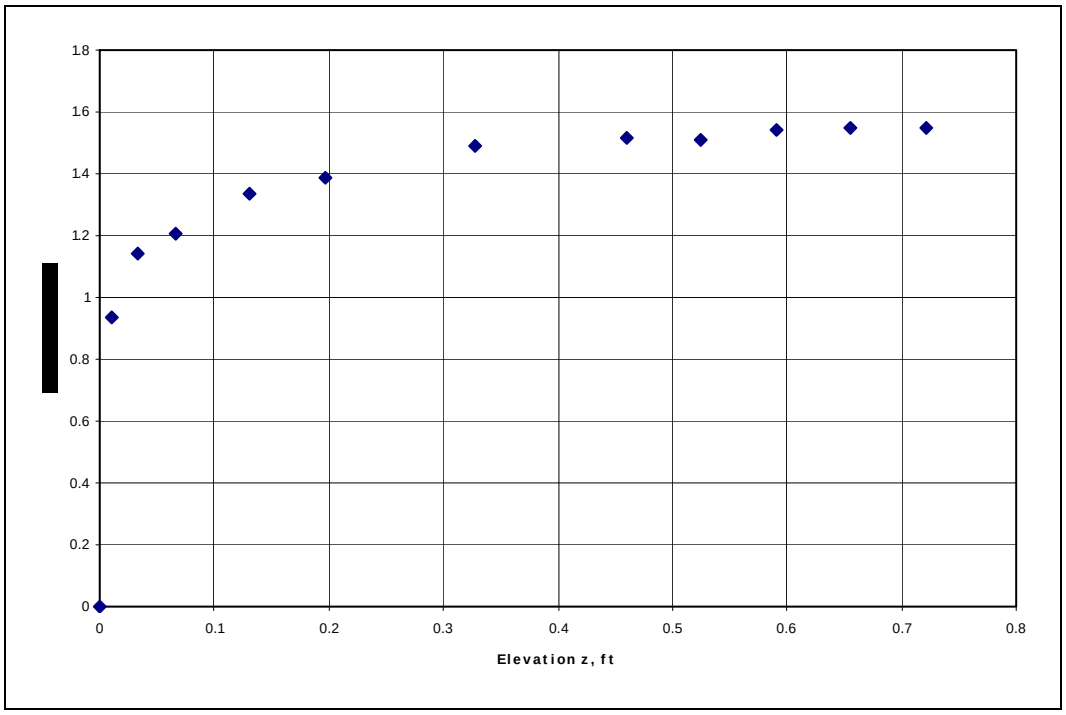


Figure 41. Velocity profile for trolling motor with half propeller on setting #3.

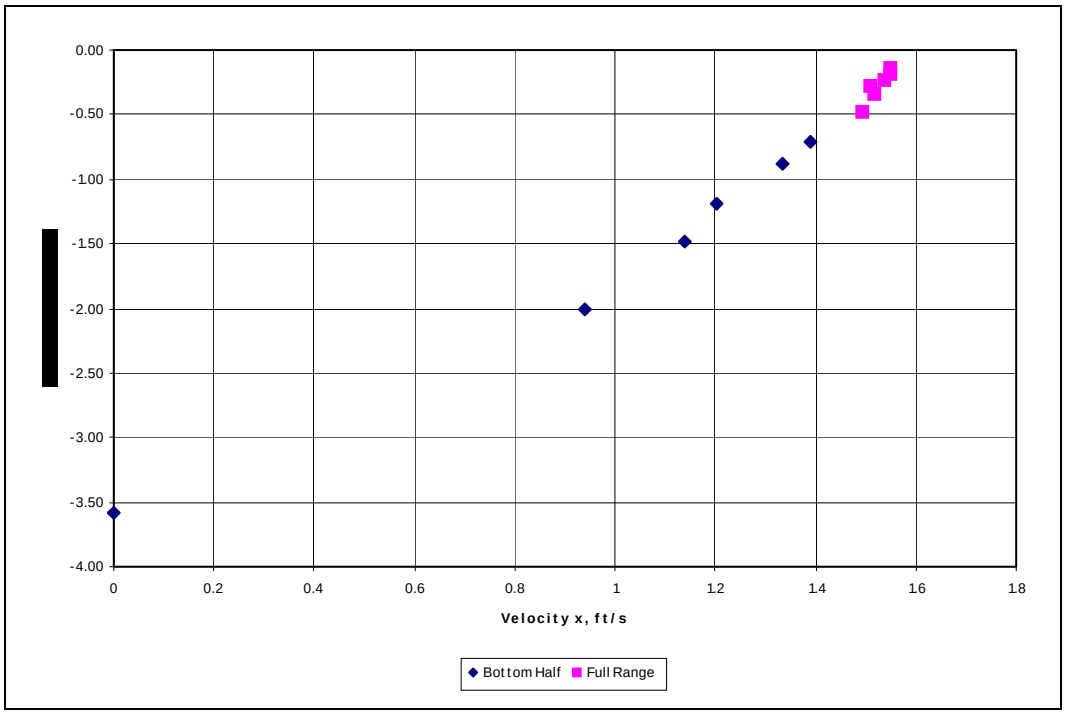


Figure 42. Velocity distribution for trolling motor with half propeller on setting #3.

Table 15. Velocity data for trolling motor with half propeller on setting #4.

Elevation z, cm	Velocity x, cm/s	Elevation z, ft	Velocity, ft/s	LOG Elevation z, ft
22.00	52.63	0.72	1.73	-0.14
20.00	52.86	0.66	1.73	-0.18
18.00	52.68	0.59	1.73	-0.23
16.00	52.01	0.52	1.71	-0.28
14.00	52.26	0.46	1.71	-0.34
10.00	50.97	0.33	1.67	-0.48
6.00	48.63	0.20	1.60	-0.71
4.00	45.28	0.13	1.49	-0.88
2.00	42.54	0.07	1.40	-1.18
1.00	39.75	0.03	1.30	-1.48
0.30	34.79	0.01	1.14	-2.01
0.007	0.00	0.00	0.00	-3.64

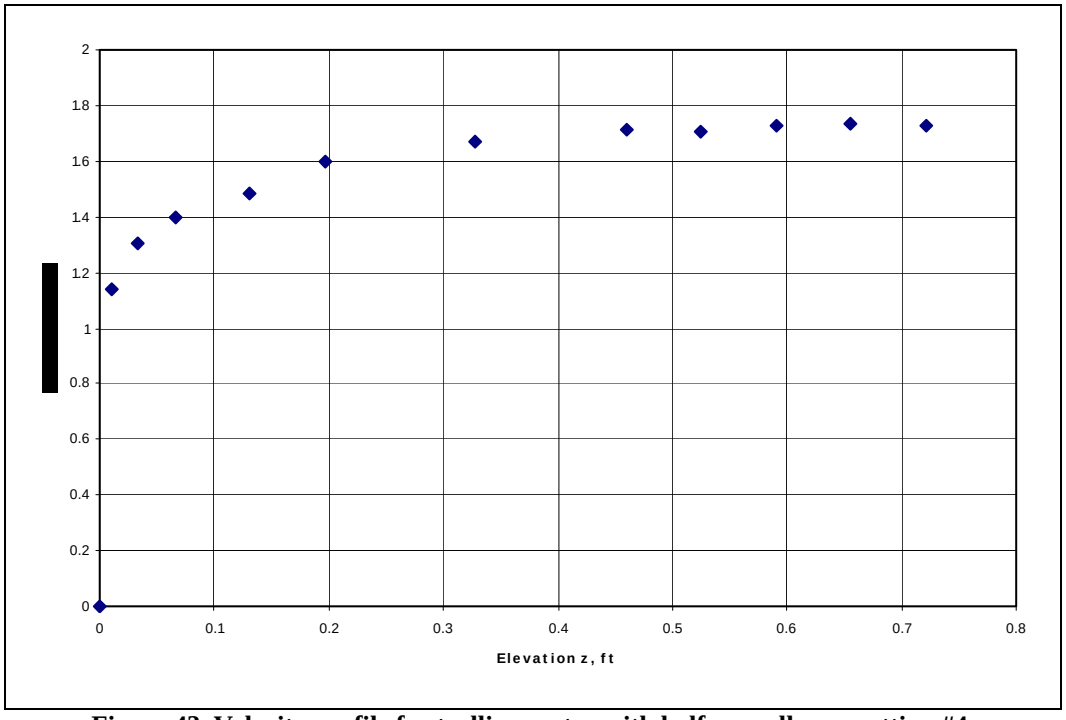


Figure 43. Velocity profile for trolling motor with half propeller on setting #4.

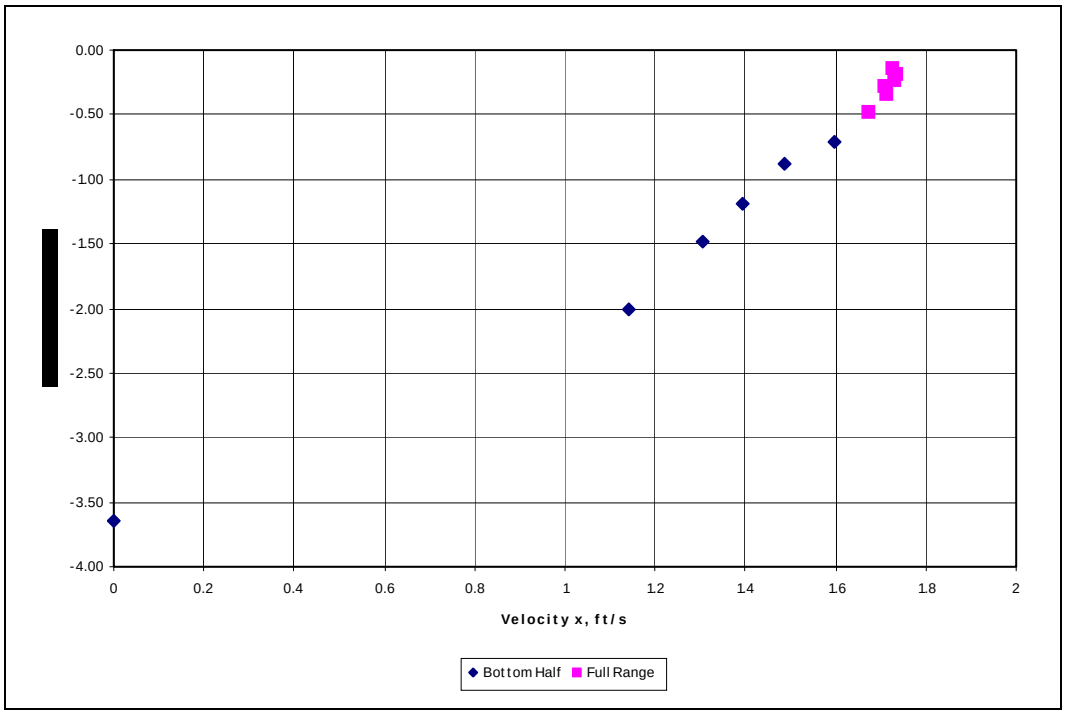


Figure 44. Velocity distribution for trolling motor with half propeller on setting #4.

Table 16. Velocity data for trolling motor with half propeller on setting #5.

Elevation z, cm	Velocity x, cm/s	Elevation z, ft	Velocity, ft/s	LOG Elevation z, ft
22.00	66.92	0.72	2.20	-0.14
20.00	66.80	0.66	2.19	-0.18
18.00	68.23	0.59	2.24	-0.23
16.00	66.48	0.52	2.18	-0.28
14.00	67.45	0.46	2.21	-0.34
10.00	66.71	0.33	2.19	-0.48
6.00	63.49	0.20	2.08	-0.71
4.00	59.91	0.13	1.97	-0.88
2.00	56.18	0.07	1.84	-1.18
1.00	53.18	0.03	1.74	-1.48
0.30	43.38	0.01	1.42	-2.01
0.006	0.00	0.00	0.00	-3.71

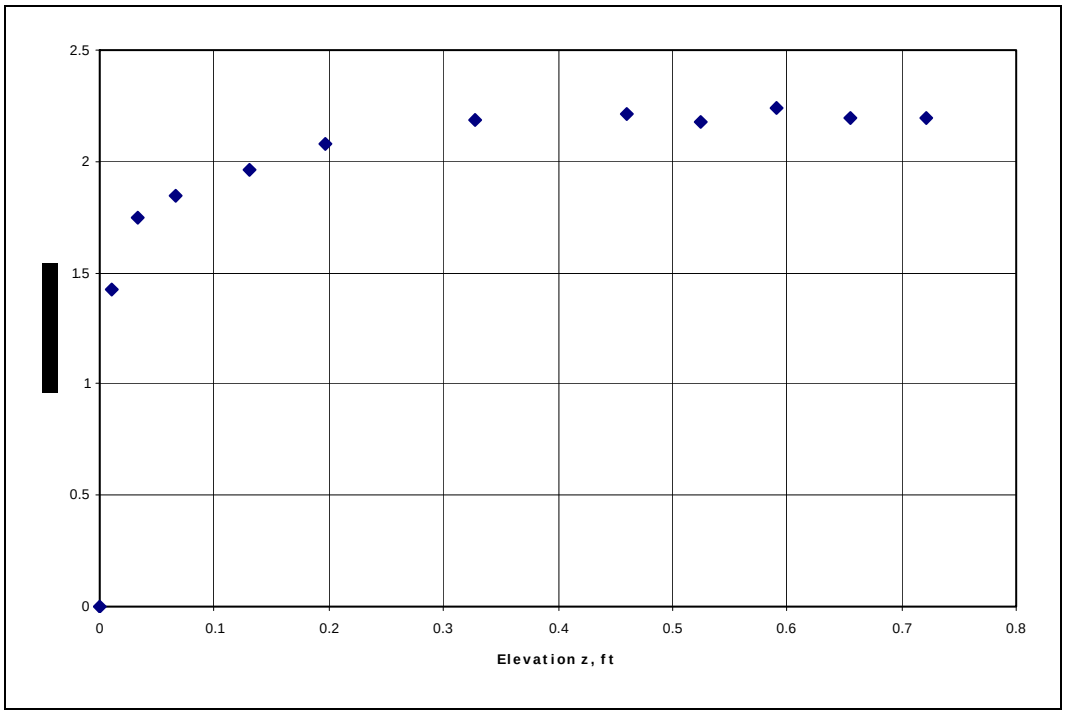


Figure 45. Velocity profile for trolling motor with half propeller on setting #5.

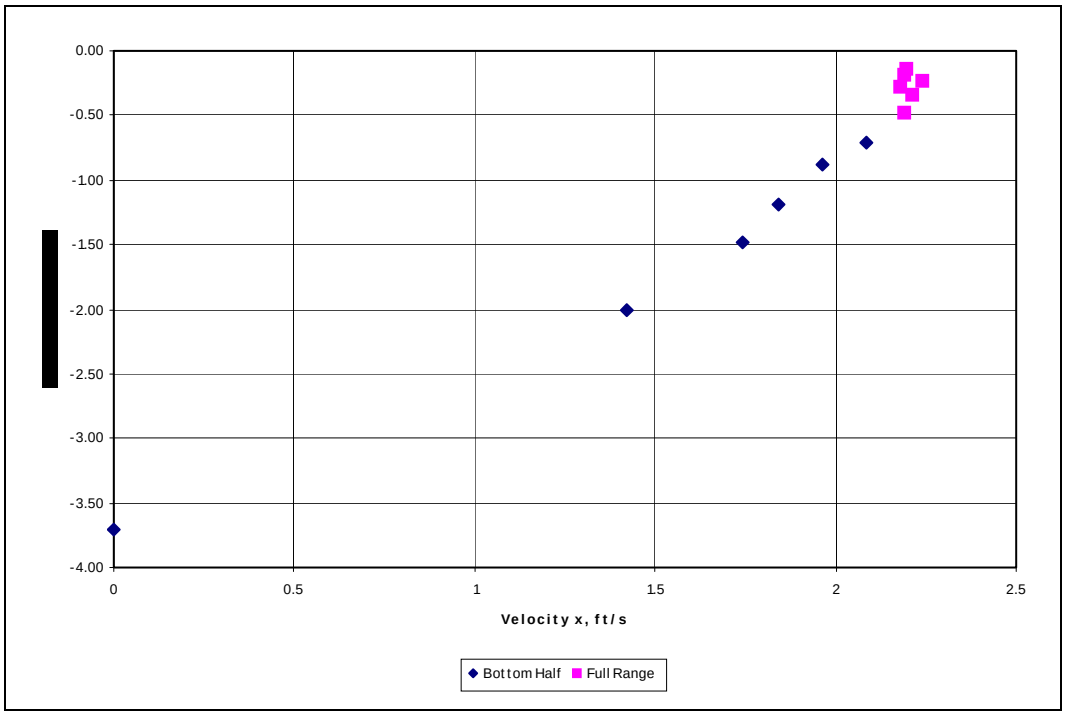


Figure 46. Velocity distribution for trolling motor with half propeller on setting #5.

Table 17. Velocity data for trolling motor with full propeller on setting #1.

Elevation z, cm	Velocity x, cm/s	Elevation z, ft	Velocity, ft/s	LOG Elevation z, ft
10.00	44.02	0.33	1.44	-0.48
6.00	42.33	0.20	1.39	-0.71
4.00	40.18	0.13	1.32	-0.88
2.00	36.71	0.07	1.20	-1.18
1.00	34.69	0.03	1.14	-1.48
0.30	31.60	0.01	1.04	-2.01
0.008	0.00	0.00	0.00	-3.58

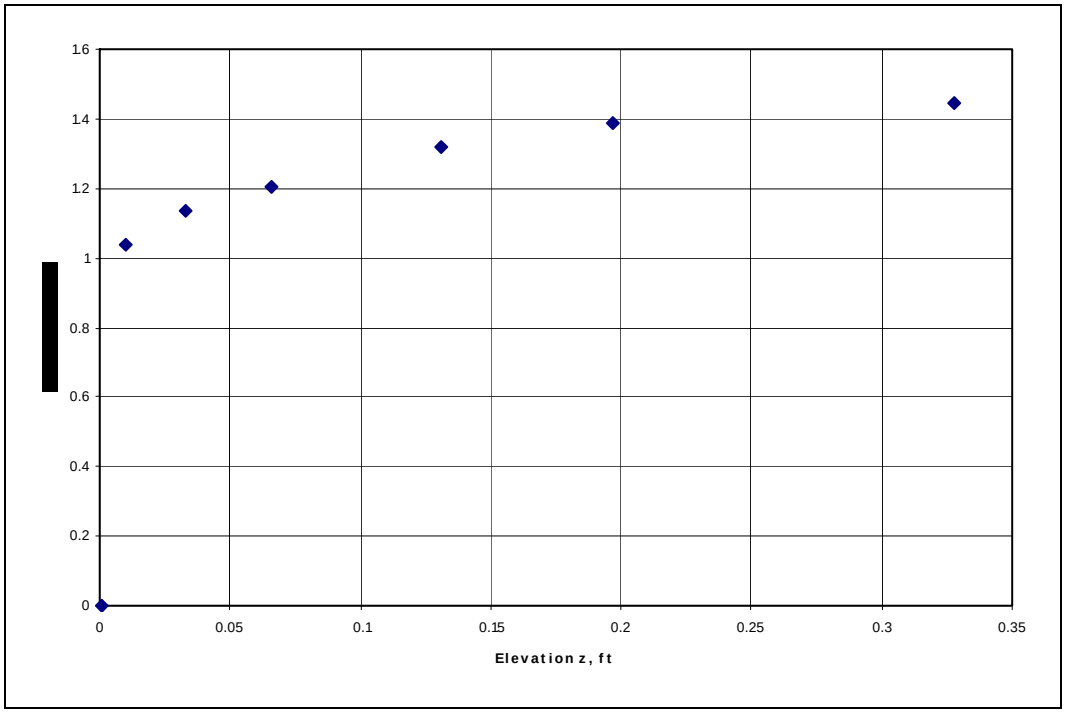


Figure 47. Velocity profile for trolling motor with full propeller on setting #1.

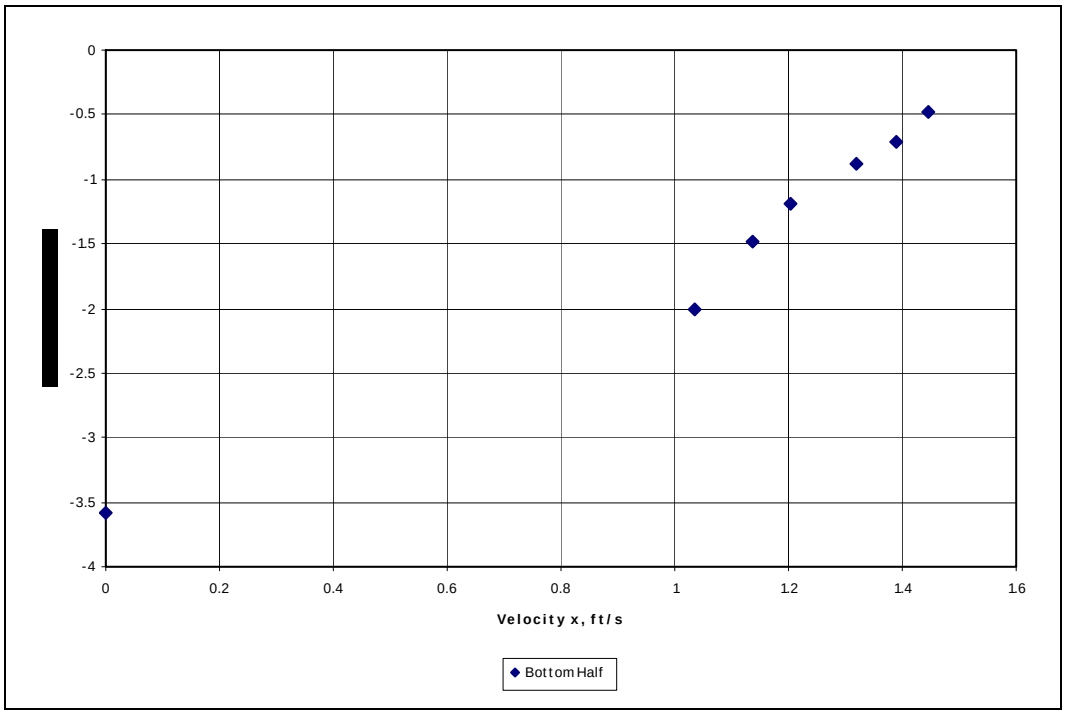


Figure 48. Velocity distribution for trolling motor with full propeller on setting #1.

Table 18. Velocity data for trolling motor with full propeller on setting #2.

Elevation z, cm	Velocity x, cm/s	Elevation z, ft	Velocity, ft/s	LOG Elevation z, ft
10.00	52.51	0.33	1.72	-0.48
6.00	50.13	0.20	1.64	-0.71
4.00	47.11	0.13	1.55	-0.88
2.00	43.22	0.07	1.42	-1.18
1.00	40.52	0.03	1.33	-1.48
0.30	31.92	0.01	1.05	-2.01
0.007	0.00	0.00	0.00	-3.64

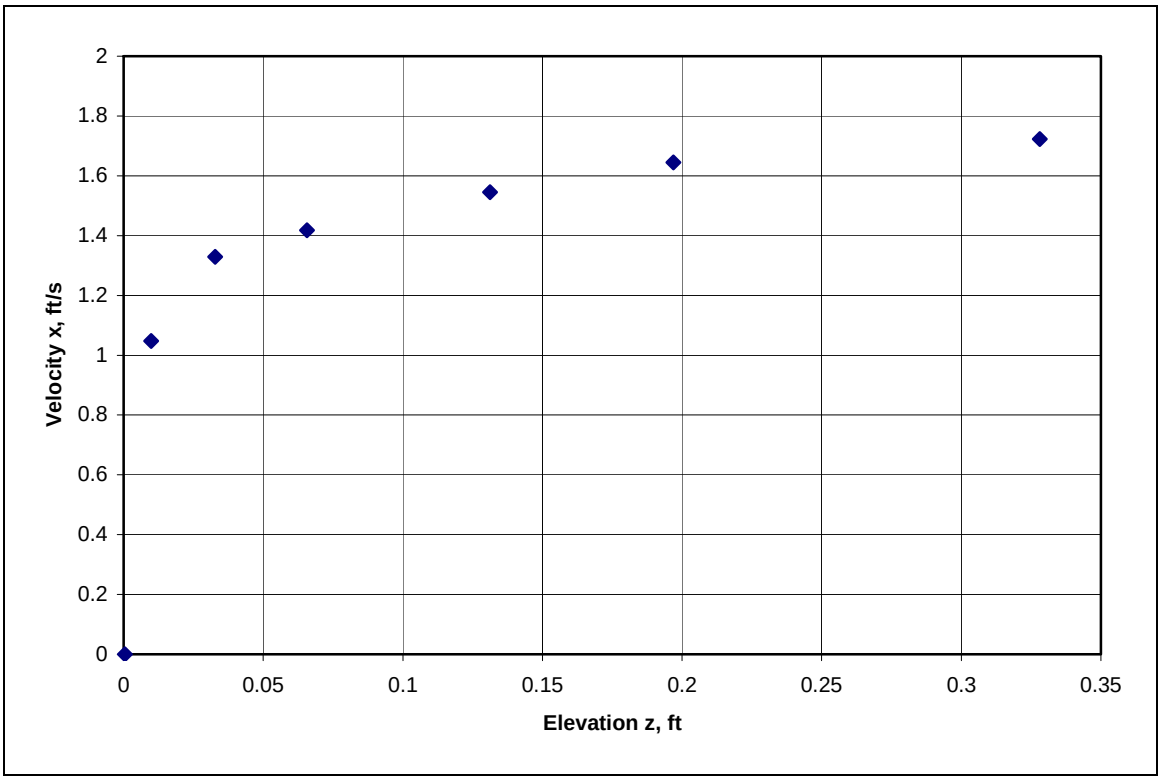


Figure 49. Velocity profile for trolling motor with full propeller on setting #2.

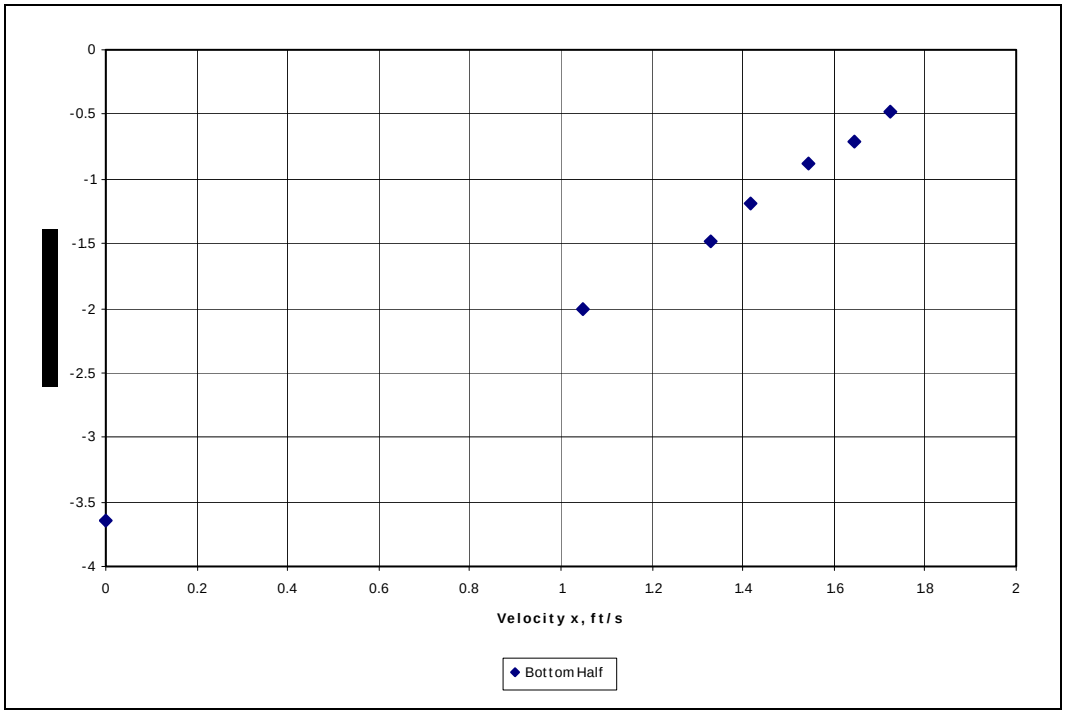


Figure 50. Velocity distribution for trolling motor with full propeller on setting #2.

Table 19. Velocity data for trolling motor with full propeller on setting #3.

Elevation z, cm	Velocity x, cm/s	Elevation z, ft	Velocity, ft/s	LOG Elevation z, ft
10.00	64.31	0.33	2.11	-0.48
6.00	63.00	0.20	2.07	-0.71
4.00	59.62	0.13	1.96	-0.88
2.00	54.39	0.07	1.78	-1.18
1.00	51.15	0.03	1.68	-1.48
0.30	44.44	0.01	1.46	-2.01
0.006	0.00	0.00	0.00	-3.71

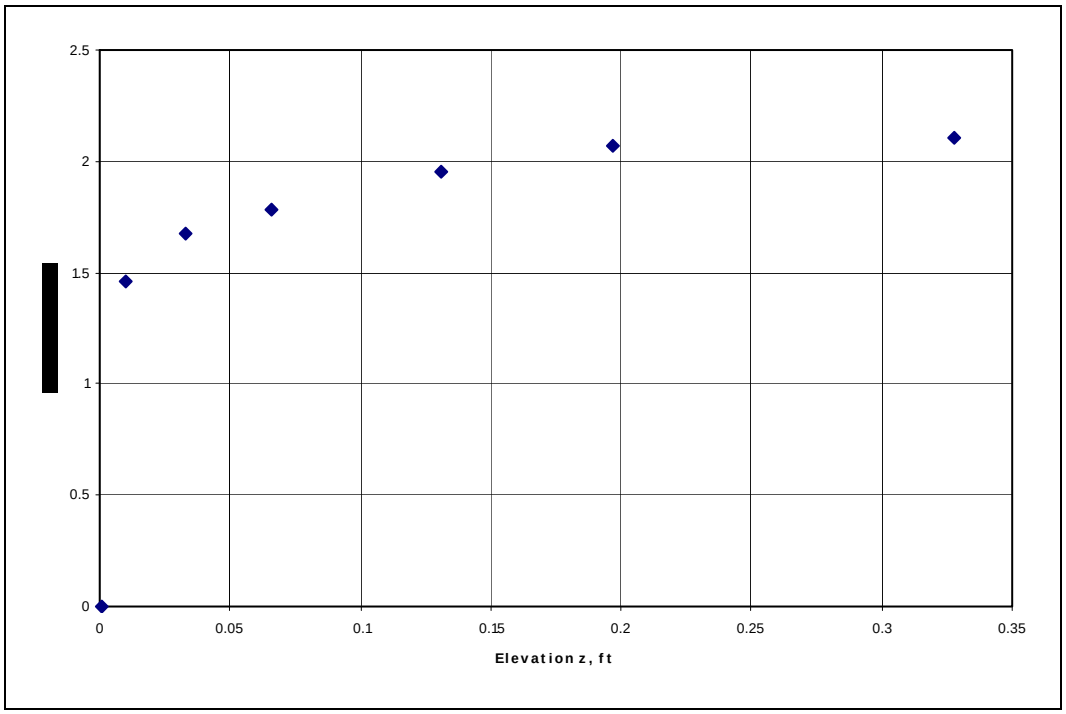


Figure 51. Velocity profile for trolling motor with full propeller on setting #3.

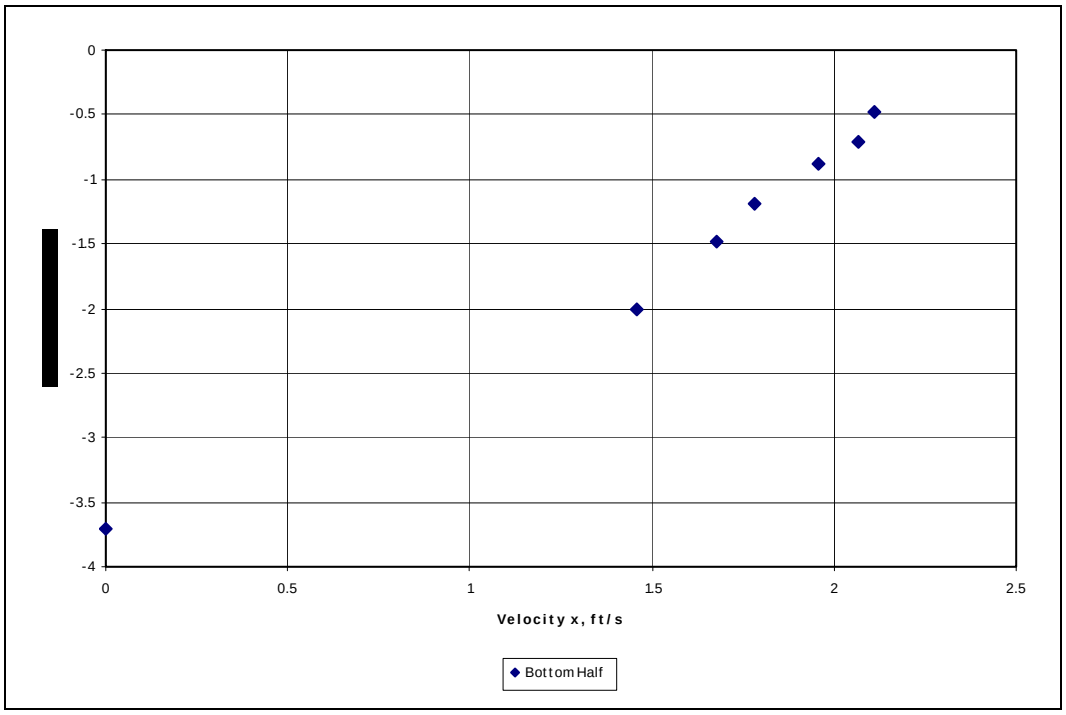


Figure 52. Velocity distribution for trolling motor with full propeller on setting #3.

Table 20. Velocity data for trolling motor with full propeller on setting #4.

Elevation z, cm	Velocity x, cm/s	Elevation z, ft	Velocity, ft/s	LOG Elevation z, ft
16.00	77.84	0.52	2.55	-0.28
14.00	78.62	0.46	2.58	-0.34
10.00	78.05	0.33	2.56	-0.48
6.00	75.98	0.20	2.49	-0.71
4.00	72.79	0.13	2.39	-0.88
2.00	68.96	0.07	2.26	-1.18
1.00	64.73	0.03	2.12	-1.48
0.30	53.74	0.01	1.76	-2.01
0.005	0.00	0.00	0.00	-3.79

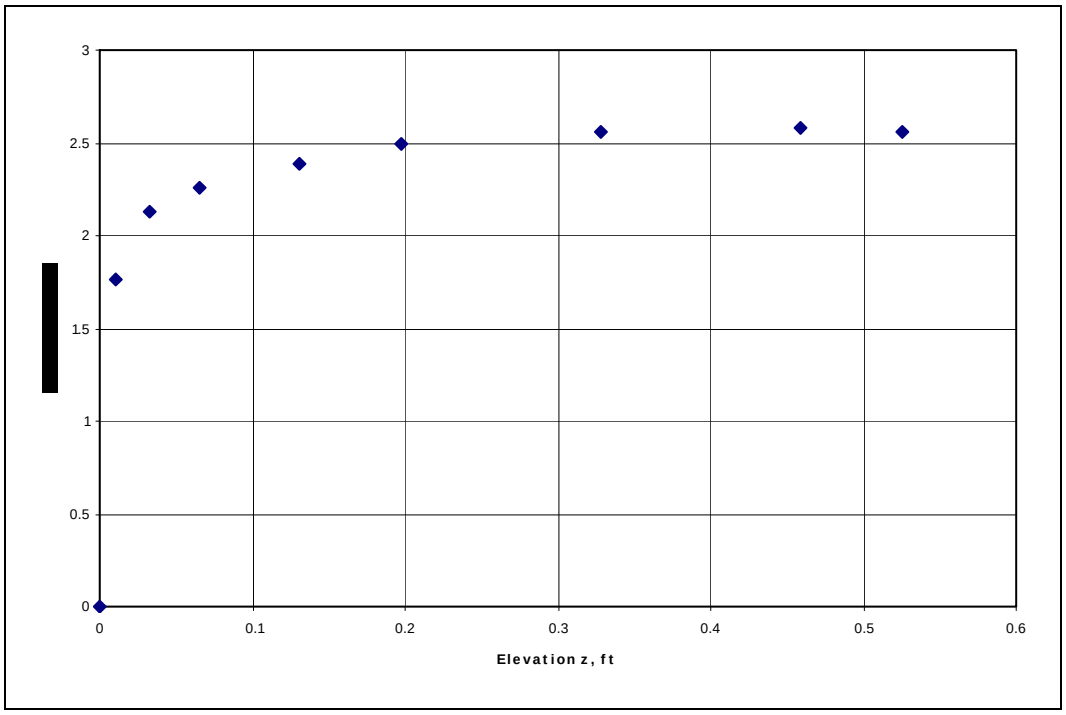


Figure 53. Velocity profile for trolling motor with full propeller on setting #4.

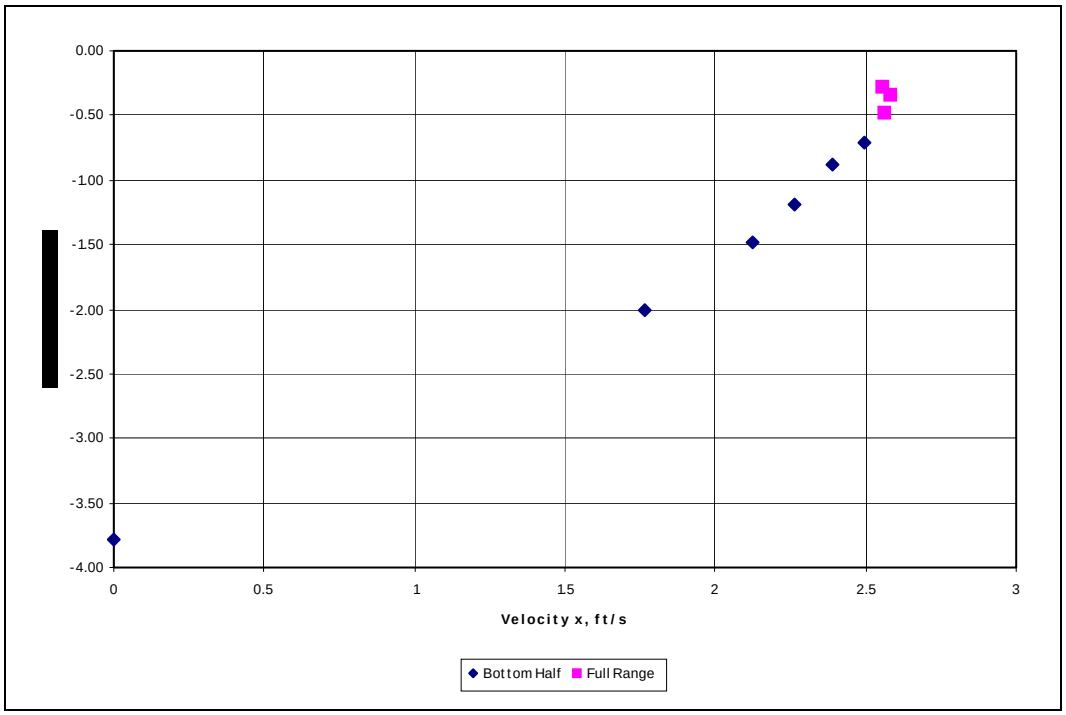


Figure 54. Velocity distribution for trolling motor with full propeller on setting #4.

Bed Shear Computation

After the velocity profiles were created, the shear at the bed could be computed. To solve for the slope of the velocity profile three scenarios were explored: determine the slope by including only the measured values of velocity, determine the slope by assuming no-slip condition and including all the measured values of velocity, and determining the slope by assuming no-slip condition and using the bottom half of data. The second analysis occurred since the top half of the flow does not contribute to shear distribution and it was recommended that the top half of the velocities be removed prior to analysis. Then, the third analysis was preformed because the selection of the depth for zero velocity strongly influences the estimated bed shear. Therefore, the top of the viscous sublayer was calculated for each condition and assumed to be the location of zero velocity for the third bed shear determination. The following is a presentation of the regression analysis for each trolling motor type and setting.

Regression Analysis for trolling motor with half propeller on setting #1:

1) Measured values full range SUMMARY OUTPUT **Slope = 3.814523**

Regression Statistics	
Multiple R	0.988389391
R Square	0.976913589
Adjusted R Square	0.974348432
Standard Error	0.097950824
Observations	11

	Coefficients	*Standard Error*	*P-value*	*Lower 95%*	*Upper 95%*	*Lower 95.0%*	*Upper 95.0%*
Intercept	-4.40260092	0.191016726	2.58987E-09	-4.834711104	-3.970490736	-4.834711104	-3.970490736
X Variable 1	3.814522541	0.19546503	1.12727E-08	3.372349585	4.256695496	3.372349585	4.256695496

2) Measured values full range with estimated no-slip condition SUMMARY OUTPUT **Slope = 3.046066**

Viscous sublayer depth estimated at, assuming 70F water:

v = 0.00000041m^2/s

v = 4.4132E-06ft^2/s

for shear velocities computed ….

1) delta-v = 0.000484ft
2) delta-v = 0.000386ft
3) delta-v = 0.000364ft

1) delta-v = 0.147519mm
2) delta-v = 0.1178mm
3) delta-v = 0.110906mm

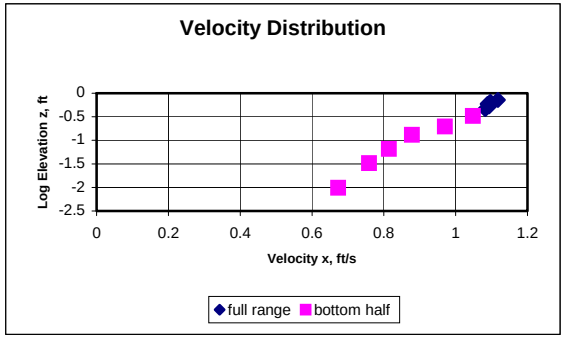
6.1.1.1	*Regression Statistics*
Multiple R	0.986709158
R Square	0.973594962
Adjusted R Square	0.970954458
Standard Error	0.166799495
Observations	12

	Coefficients	*Standard Error*	*P-value*	*Lower 95%*	*Upper 95%*	*Lower 95.0%*	*Upper 95.0%*
Intercept	-3.642492806	0.148423145	2.8797E-10	-3.973200239	-3.311785374	-3.973200239	-3.311785374
X Variable 1	3.046066223	0.158633017	3.19425E-09	2.692609773	3.399522673	2.692609773	3.399522673

3) Measured values bottom-half range

SUMMARY OUTPUT

Slope = **2.867793**



Regression Statistics	
Multiple R	0.983387149
R Square	0.967050285
Adjusted R Square	0.960460342
Standard Error	0.201519861
Observations	7

	Coefficients	*Standard Error*	*P-value*	*Lower 95%*	*Upper 95%*	*Lower 95.0%*	*Upper 95.0%*
Intercept	-3.562101819	0.189850406	7.91958E-06	-4.050127027	-3.074076611	-4.050127027	-3.074076611
X Variable 1	2.867792698	0.236735863	6.77155E-05	2.259244783	3.476340613	2.259244783	3.476340613

Shear Velocity		Bed Shear		Bed Shear	
u*		tau-0		tau-0	
0.04559	ft/s	0.004032604	lb/ft^2	0.19	Pa
0.05709	ft/s	0.006323935	lb/ft^2	0.30	Pa
0.06064	ft/s	0.007134613	lb/ft^2	0.34	Pa

Regression Analysis for trolling motor with half propeller on setting #2:

1) Measured values full range SUMMARY OUTPUT **Slope = 3.206872**

Regression Statistics	
Multiple R	0.993926966
R Square	0.987890815
Adjusted R Square	0.98654535
Standard Error	0.070939373
Observations	11

	Coefficients	*Standard Error*	*P-value*	*Lower 95%*	*Upper 95%*	*Lower 95.0%*	*Upper 95.0%*
Intercept	-4.391717986	0.137191902	1.39E-10	-4.702067866	-4.081368106	-4.702067866	-4.081368106
X Variable 1	3.206872083	0.118348668	6.15E-10	2.939148593	3.474595574	2.939148593	3.474595574

SUMMARY OUTPUT **Slope = 2.59659**

Viscous sublayer depth estimated at, assuming 70F water:

v = 0.00000041m^2/s

v = 4.4132E-06ft^2/s

for shear velocities computed ….

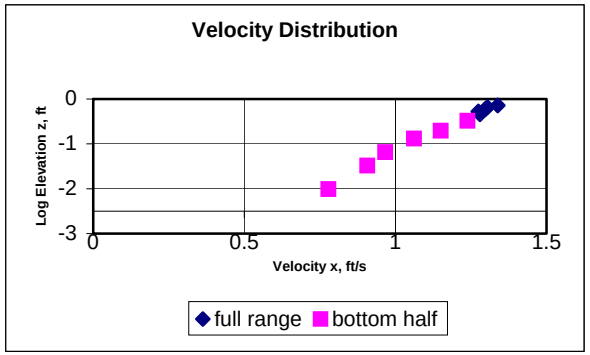
1) delta-v = 0.000407ft
2) delta-v = 0.000329ft
3) delta-v = 0.000311ft

1) delta-v = 0.124019mm
2) delta-v = 0.100418mm
3) delta-v = 0.094855mm

Regression Statistics	
Multiple R	0.989751348
R Square	0.979607732
Adjusted R Square	0.977568505
Standard Error	0.148024314
Observations	12

	Coefficients	*Standard Error*	*P-value*	*Lower 95%*	*Upper 95%*	*Lower 95.0%*	*Upper 95.0%*
Intercept	-3.67550978	0.131486393	7.97E-11	-3.968479772	-3.382539788	-3.968479772	-3.382539788
X Variable 1	2.596589659	0.118470437	8.75E-10	2.332621031	2.860558288	2.332621031	2.860558288

3) Measured values bottom-half range SUMMARY OUTPUT **Slope = 2.452739**



Regression Statistics	
Multiple R	0.987882368
R Square	0.975911573
Adjusted R Square	0.971093888
Standard Error	0.174609291
Observations	7

	Coefficients	*Standard Error*	*P-value*	*Lower 95%*	*Upper 95%*	*Lower 95.0%*	*Upper 95.0%*
Intercept	-3.599376459	0.164074924	3.65E-06	-4.021143788	-3.177609129	-4.021143788	-3.177609129
X Variable 1	2.452739099	0.172331765	3.08E-05	2.009746918	2.895731279	2.009746918	2.895731279

Shear Velocity		Bed Shear		Bed Shear	
u*		tau-0		tau-0	
0.05423	ft/s	0.005705619	lb/ft^2	0.27	Pa
0.06698	ft/s	0.008702806	lb/ft^2	0.42	Pa
0.07091	ft/s	0.009753565	lb/ft^2	0.47	Pa

Regression Analysis for trolling motor with half propeller on setting #3:

1) Measured values full range … SUMMARY OUTPUT **Slope = 2.979383**

Regression Statistics	
Multiple R	0.996171417
R Square	0.992357493
Adjusted R Square	0.991508325
Standard Error	0.056356992
Observations	11

	Coefficients	*Standard Error*	*P-value*	*Lower 95%*	*Upper 95%*	*Lower 95.0%*	*Upper 95.0%*
Intercept	-4.827826632	0.121367924	2E-11	-5.102380159	-4.553273105	-5.102380159	-4.553273105
X Variable 1	2.979383016	0.087154324	7.74E-11	2.782226088	3.176539944	2.782226088	3.176539944

2) Measured values full range with estimated no-slip condition SUMMARY OUTPUT **Slope =2.250058**

Viscous sublayer depth estimated at, assuming 70F water:

v = 0.00000041m^2/s

v = 4.4132E-06ft^2/s

for shear velocities computed ….

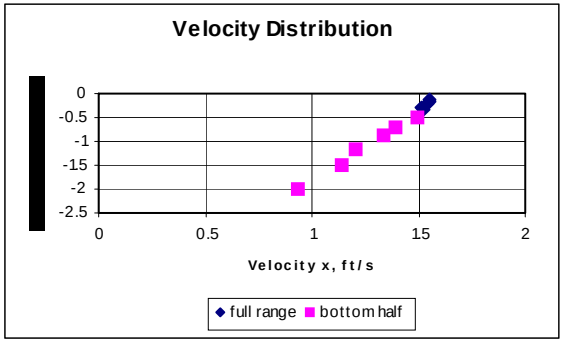
1) delta-v = 0.000378Ft
2) delta-v = 0.000285Ft
3) delta-v = 0.000263Ft

1) delta-v = 0.115221mm
2) delta-v = 0.087016mm
3) delta-v = 0.080149mm

Regression Statistics	
Multiple R	0.986373554
R Square	0.972932789
Adjusted R Square	0.970226068
Standard Error	0.174459103
Observations	12

	Coefficients	*Standard Error*	*P-value*	*Lower 95%*	*Upper 95%*	*Lower 95.0%*	*Upper 95.0%*
Intercept	-3.802093013	0.158232187	3.55E-10	-4.154656357	-3.449529669	-4.154656357	-3.449529669
X Variable 1	2.250058409	0.118679068	3.62E-09	1.985624921	2.514491896	1.985624921	2.514491896

3) Measured values bottom-half range SUMMARY OUTPUT **Slope = 2.072479**



Regression Statistics	
Multiple R	0.990298065
R Square	0.980690257
Adjusted R Square	0.976828308
Standard Error	0.161199118
Observations	7

	Coefficients	*Standard Error*	*P-value*	*Lower 95%*	*Upper 95%*	*Lower 95.0%*	*Upper 95.0%*
Intercept	-3.695555438	0.152071499	2.2E-06	-4.086467033	-3.304643843	-4.086467033	-3.304643843
X Variable 1	2.072479427	0.130055146	1.77E-05	1.738162577	2.406796278	1.738162577	2.406796278

Shear Velocity		Bed Shear		Bed Shear	
u*		tau-0		tau-0	
0.05837	ft/s	0.006610181	lb/ft^2	0.32	Pa
0.07729	ft/s	0.011589871	lb/ft^2	0.55	Pa
0.08392	ft/s	0.013661103	lb/ft^2	0.65	Pa

Regression Analysis for trolling motor with half propeller on setting #4:

1) Measured values full range SUMMARY OUTPUT **Slope = 2.97447**

Regression Statistics	
Multiple R	0.995221835
R Square	0.990466502
Adjusted R Square	0.989407224
Standard Error	0.062944245
Observations	11

	Coefficients	*Standard Error*	*P-value*	*Lower 95%*	*Upper 95%*	*Lower 95.0%*	*Upper 95.0%*
Intercept	-5.371978942	0.153321311	6.21E-11	-5.718816108	-5.025141775	-5.718816108	-5.025141775
X Variable 1	2.974470165	0.097273516	2.09E-10	2.754422016	3.194518315	2.754422016	3.194518315

2) Measured values full range with estimated no-slip condition SUMMARY OUTPUT **Slope = 2.040766**

Viscous sublayer depth estimated at, assuming 70F water:

v = 0.00000041m^2/s

v = 4.4132E-06ft^2/s

for shear velocities computed ….

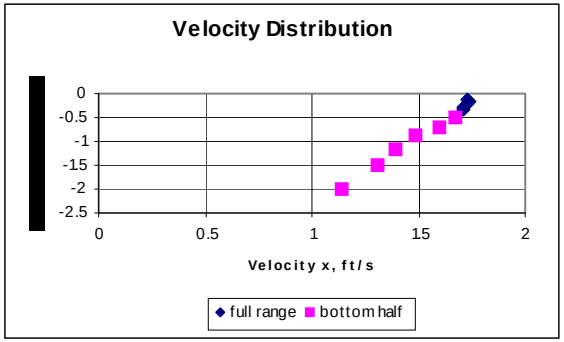
1) delta-v = 0.000377Ft
2) delta-v = 0.000259Ft
3) delta-v = 0.000236Ft

1) delta-v = 0.115031mm
2) delta-v = 0.078922mm
3) delta-v = 0.072006mm

Regression Statistics	
Multiple R	0.979496105
R Square	0.95941262
Adjusted R Square	0.955353882
Standard Error	0.216531845
Observations	12

	Coefficients	*Standard Error*	*P-value*	*Lower 95%*	*Upper 95%*	*Lower 95.0%*	*Upper 95.0%*
Intercept	-3.888880624	0.200308646	2.87E-09	-4.335196177	-3.442565071	-4.335196177	-3.442565071
X Variable 1	2.040766294	0.132735187	2.76E-08	1.745013815	2.336518772	1.745013815	2.336518772

3) Measured values bottom-half range SUMMARY OUTPUT **Slope = 1.861916**



Regression Statistics	
Multiple R	0.983957963
R Square	0.968173274
Adjusted R Square	0.961807928
Standard Error	0.21071833
Observations	7

	Coefficients	*Standard Error*	*P-value*	*Lower 95%*	*Upper 95%*	*Lower 95.0%*	*Upper 95.0%*
Intercept	-3.769550987	0.201746299	8.08E-06	-4.28815551	-3.250946463	-4.28815551	-3.250946463
X Variable 1	1.861915724	0.150971322	6.21E-05	1.47383222	2.249999228	1.47383222	2.249999228

Shear Velocity		Bed Shear		Bed Shear	
u*		tau-0		tau-0	
0.05847	ft/s	0.006632036	lb/ft^2	0.32	Pa
0.08522	ft/s	0.014088982	lb/ft^2	0.67	Pa
0.09341	ft/s	0.01692567	lb/ft^2	0.81	Pa

Regression Analysis for trolling motor with half propeller on setting #5:

1) Measured values full range SUMMARY OUTPUT **Slope = 2.323005392**

Regression Statistics	
Multiple R	0.98283334
R Square	0.96596137
Adjusted R Square	0.9621793
Standard Error	0.1189367
Observations	11

	Coefficients	*Standard Error*	*P-value*	*Lower 95%*	*Upper 95%*	*Lower 95.0%*	*Upper 95.0%*
Intercept	-5.42232878	0.296432553	1.99E-08	-6.092906317	-4.751751248	-6.092906317	-4.751751248
X Variable 1	2.32300539	0.145356716	6.5E-08	1.994185404	2.651825379	1.994185404	2.651825379

2) Measured values full range with estimated no-slip condition SUMMARY OUTPUT **Slope = 1.603363**

Viscous sublayer depth estimated at, assuming 70F water:

v = 0.00000041m^2/s

v = 4.4132E-06ft^2/s

for shear velocities computed ….

1) delta-v = 0.000295ft

2) delta-v = 0.000203ft

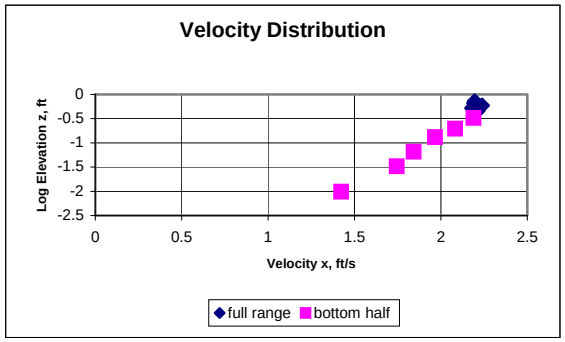
3) delta-v = 0.000184ft

1) delta-v = 0.089837mm
2) delta-v = 0.062007mm
3) delta-v = 0.056055mm

Regression Statistics	
Multiple R	0.97725385
R Square	0.95502508
Adjusted R Square	0.95052759
Standard Error	0.23148295
Observations	12

	Coefficients	*Standard Error*	*P-value*	*Lower 95%*	*Upper 95%*	*Lower 95.0%*	*Upper 95.0%*
Intercept	-3.94387038	0.21483552	4.95E-09	-4.422553827	-3.465186926	-4.422553827	-3.465186926
X Variable 1	1.60336269	0.11002961	4.62E-08	1.358201397	1.848523982	1.358201397	1.848523982

3) Measured values bottom-half range SUMMARY OUTPUT **Slope = 1.449465**



Regression Statistics	
Multiple R	0.98910294
R Square	0.97832462
Adjusted R Square	0.97398955
Standard Error	0.17750368
Observations	7

	Coefficients	*Standard Error*	*P-value*	*Lower 95%*	*Upper 95%*	*Lower 95.0%*	*Upper 95.0%*
Intercept	-3.82224227	0.168937288	3.14E-06	-4.256508686	-3.387975856	-4.256508686	-3.387975856
X Variable 1	1.44946512	0.096486064	2.37E-05	1.201440204	1.697490041	1.201440204	1.697490041

Shear Velocity		Bed Shear		Bed Shear	
u*		tau-0		tau-0	
0.07487	ft/s	0.010873406	lb/ft^2	0.52	Pa
0.10847	ft/s	0.022824555	lb/ft^2	1.09	Pa
0.11998	ft/s	0.027928691	lb/ft^2	1.34	Pa

Regression Analysis for trolling motor with full propeller on setting #1:

1) Measured values full range SUMMARY OUTPUT **Slope = 3.538248**

Regression Statistics	
Multiple R	0.989083684
R Square	0.978286535
Adjusted R Square	0.972858168
Standard Error	0.0918931
Observations	6

	Coefficients	*Standard Error*	*P-value*	*Lower 95%*	*Upper 95%*	*Lower 95.0%*	*Upper 95.0%*
Intercept	-5.56509122	0.332918623	7.5E-05	-6.48942341	-4.64075902	-6.48942341	-4.64075902
X Variable 1	3.538248219	0.263566272	0.000178	2.806469417	4.270027022	2.806469417	4.270027022

2) Measured values full range with estimate no-slip condition SUMMARY OUTPUT **Slope = 2.08792**

Viscous sublayer depth estimated at, assuming 70F water:

v = 0.00000041m^2/s

v = 4.4132E-06ft^2/s

for shear velocities computed ….

1) delta-v = 0.000449Ft

2) delta-v = 0.000265Ft

3) delta-v = 0.000265Ft

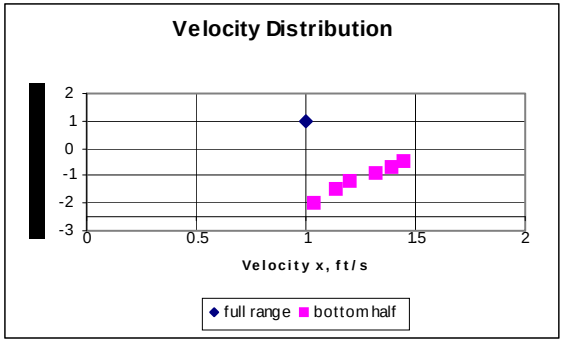
1) delta-v = 0.136834mm

2) delta-v = 0.080746mm
3) delta-v = 0.080746mm

Regression Statistics	
Multiple R	0.976497684
R Square	0.953547727
Adjusted R Square	0.941934659
Standard Error	0.233334101
Observations	6

	Coefficients	*Standard Error*	*P-value*	*Lower 95%*	*Upper 95%*	*Lower 95.0%*	*Upper 95.0%*
Intercept	-3.7213936	0.24098455	2.07E-05	-4.340863091	-3.101924101	-4.340863091	-3.101924101
X Variable 1	2.087919561	0.206069796	0.000161	1.558201153	2.617637969	1.558201153	2.617637969

3) Measured values bottom-half range SUMMARY OUTPUT **Slope = 2.08792**



Regression Statistics	
Multiple R	0.976497684
R Square	0.953547727
Adjusted R Square	0.941934659
Standard Error	0.233334101
Observations	6

	Coefficients	*Standard Error*	*P-value*	*Lower 95%*	*Upper 95%*	*Lower 95.0%*	*Upper 95.0%*
Intercept	-3.7213936	0.24098455	2.07E-05	-4.340863091	-3.101924101	-4.340863091	-3.101924101
X Variable 1	2.087919561	0.206069796	0.000161	1.558201153	2.617637969	1.558201153	2.617637969

Shear Velocity		Bed Shear		Bed Shear	
u*		tau-0		tau-0	
0.04915	ft/s	0.004686941	lb/ft^2	0.22	Pa
0.08329	ft/s	0.013459791	lb/ft^2	0.64	Pa
0.08329	ft/s	0.013459791	lb/ft^2	0.64	Pa

Regression Analysis for trolling motor with full propeller on setting #2:

1) Measured values full range SUMMARY OUTPUT **Slope = 2.272635032**

Regression Statistics	
Multiple R	0.996725315
R Square	0.993461354
Adjusted R Square	0.991826692
Standard Error	0.050426897
Observations	6

	Coefficients	*Standard Error*	*P-value*	*Lower 95%*	*Upper 95%*	*Lower 95.0%*	*Upper 95.0%*
Intercept	-4.422516577	0.135363248	5.23E-06	-4.798345982	-4.046687172	-4.798345982	-4.046687172
X Variable 1	2.272635032	0.09218667	1.61E-05	2.016683272	2.528586792	2.016683272	2.528586792

2) Measured values full range with estimated no-slip condition SUMMARY OUTPUT **Slope = 1.809464758**

Viscous sublayer depth estimated at, assuming 70F water:

v = 0.00000041m^2/s

v = 4.4132E-06ft^2/s

for shear velocities computed ….

1) delta-v = 0.000288ft

2) delta-v = 0.00023ft

3) delta-v = 0.00023ft

1) delta-v = 0.087889mm

2) delta-v = 0.069977mm

3) delta-v = 0.069977mm

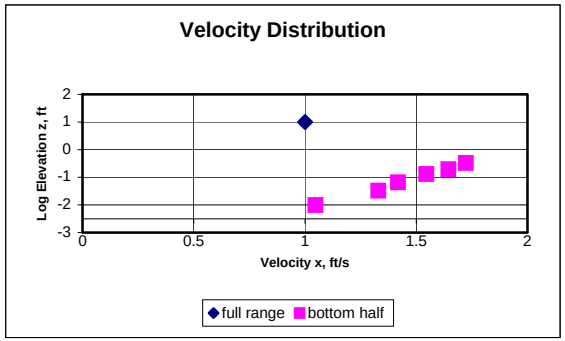
Regression Statistics	
Multiple R	0.993888614
R Square	0.987814576
Adjusted R Square	0.985377492
Standard Error	0.130384705
Observations	7

	Coefficients	*Standard Error*	*P-value*	*Lower 95%*	*Upper 95%*	*Lower 95.0%*	*Upper 95.0%*
Intercept	-3.734411309	0.122181927	7.03E-07	-4.048489439	-3.42033318	-4.048489439	-3.42033318
X Variable 1	1.809464758	0.089876827	5.59E-06	1.578429398	2.040500119	1.578429398	2.040500119

3) Measured values bottom-half range

SUMMARY OUTPUT

Slope = 1.809465



Regression Statistics	
Multiple R	0.993888614
R Square	0.987814576
Adjusted R Square	0.985377492
Standard Error	0.130384705
Observations	7

	Coefficients	*Standard Error*	*P-value*	*Lower 95%*	*Upper 95%*	*Lower 95.0%*	*Upper 95.0%*
Intercept	-3.734411309	0.122181927	7.03E-07	-4.048489439	-3.42033318	-4.048489439	-3.42033318
X Variable 1	1.809464758	0.089876827	5.59E-06	1.578429398	2.040500119	1.578429398	2.040500119

Shear Velocity		Bed Shear		Bed Shear	
u*		tau-0		tau-0	
0.07652	ft/s	0.01	lb/ft^2	0.54	Pa
0.09611	ft/s	0.02	lb/ft^2	0.86	Pa
0.09611	ft/s	0.02	lb/ft^2	0.86	Pa

Regression Analysis for trolling motor with full propeller on setting #3:

1) Measured values full range SUMMARY OUTPUT **Slope = 2.219036092**

Regression Statistics	
Multiple R	0.995351297
R Square	0.990724204
Adjusted R Square	0.988405255
Standard Error	0.060061189
Observations	6

	Coefficients	*Standard Error*	*P-value*	*Lower 95%*	*Upper 95%*	*Lower 95.0%*	*Upper 95.0%*
Intercept	-5.21229887	0.199293637	1.27E-05	-5.765627859	-4.658969881	-5.765627859	-4.658969881
X Variable 1	2.219036092	0.107357794	3.24E-05	1.920962453	2.517109731	1.920962453	2.517109731

2) Measured values full range with estimated no-slip condition SUMMARY OUTPUT **Slope = 1.480751663**

Viscous sublayer depth estimated at, assuming 70F water:

v = 0.00000041m^2/s

v = 4.4132E-06ft^2/s

for shear velocities computed ….

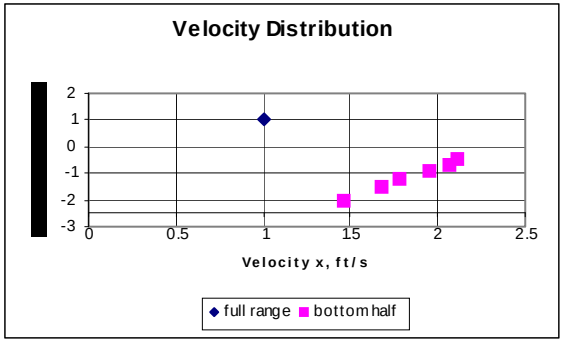
1) delta-v = 0.000282Ft
2) delta-v = 0.000188Ft
3) delta-v = 0.000188Ft

1) delta-v = 0.085817mm
2) delta-v = 0.057265mm
3) delta-v = 0.057265mm

Regression Statistics	
Multiple R	0.985909394
R Square	0.972017334
Adjusted R Square	0.966420801
Standard Error	0.201682671
Observations	7

	Coefficients	*Standard Error*	*P-value*	*Lower 95%*	*Upper 95%*	*Lower 95.0%*	*Upper 95.0%*
Intercept	-3.83129235	0.193103981	6.01E-06	-4.327681126	-3.334903578	-4.327681126	-3.334903578
X Variable 1	1.480751663	0.112358198	4.49E-05	1.19192619	1.769577135	1.19192619	1.769577135

3) Measured values bottom-half range SUMMARY OUTPUT **Slope = 1.480752**



Regression Statistics	
Multiple R	0.985909394
R Square	0.972017334
Adjusted R Square	0.966420801
Standard Error	0.201682671
Observations	7

	Coefficients	*Standard Error*	*P-value*	*Lower 95%*	*Upper 95%*	*Lower 95.0%*	*Upper 95.0%*
Intercept	-3.83129235	0.193103981	6.01E-06	-4.327681126	-3.334903578	-4.327681126	-3.334903578
X Variable 1	1.480751663	0.112358198	4.49E-05	1.19192619	1.769577135	1.19192619	1.769577135

Shear Velocity		Bed Shear		Bed Shear	
u*		tau-0		tau-0	
0.07837	ft/s	0.011916187	lb/ft^2	0.57	Pa
0.11745	ft/s	0.026760953	lb/ft^2	1.28	Pa
0.11745	ft/s	0.026760941	lb/ft^2	1.28	Pa

Regression Analysis for trolling motor with full propeller on setting #4:

1) Measured values full range SUMMARY OUTPUT **Slope = 2.089576238**

Regression Statistics	
Multiple R	0.9809405
R Square	0.962244265
Adjusted R Square	0.955951643
Standard Error	0.12678738
Observations	8

	Coefficients	*Standard Error*	*t Stat*	*P-value*	*Lower 95%*	*Upper 95%*	*Lower 95.0%*	*Upper 95.0%*
Intercept	-5.81111309	0.398028068	-14.5998	6.48E-06	-6.785053396	-4.837172778	-6.785053396	-4.837172778
X Variable 1	2.089576238	0.168978477	12.36593	1.71E-05	1.676100497	2.503051979	1.676100497	2.503051979

2) Measured values full range with estimate no-slip condition SUMMARY OUTPUT **Slope = 1.313635616**

Viscous sublayer depth estimated at, assuming 70F water:

v = 0.00000041m^2/s

v = 4.4132E-06ft^2/s

for shear velocities computed ….

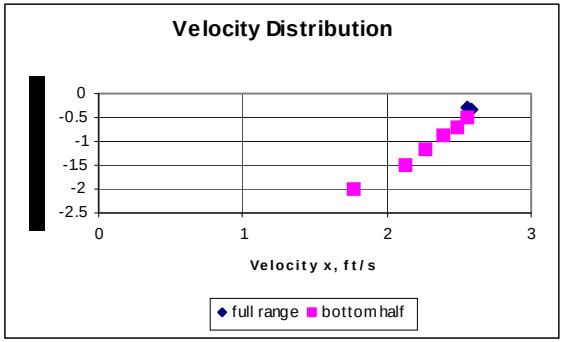
1) delta-v = 0.000265ft
2) delta-v = 0.000167ft
3) delta-v = 0.000157ft

1) delta-v = 0.08081mm
2) delta-v = 0.050802mm
3) delta-v = 0.047893mm

Regression Statistics	
Multiple R	0.97560828
R Square	0.951811517
Adjusted R Square	0.944927448
Standard Error	0.260383721
Observations	9

	Coefficients	*Standard Error*	*P-value*	*Lower 95%*	*Upper 95%*	*Lower 95.0%*	*Upper 95.0%*
Intercept	-3.97168603	0.248100758	9.01E-07	-4.558350684	-3.385021385	-4.558350684	-3.385021385
X Variable 1	1.313635616	0.111717715	7.29E-06	1.049465386	1.577805846	1.049465386	1.577805846

3) Measured values bottom-half range SUMMARY OUTPUT **Slope = 1.238416353**



Regression Statistics	
Multiple R	0.976497684
R Square	0.953547727
Adjusted R Square	0.941934659
Standard Error	0.233334101
Observations	6

	Coefficients	*Standard Error*	*P-value*	*Lower 95%*	*Upper 95%*	*Lower 95.0%*	*Upper 95.0%*
Intercept	-3.90884848	0.203953573	7.13E-06	-4.433126974	-3.384569988	-4.433126974	-3.384569988
X Variable 1	1.238416353	0.096587704	5.14E-05	0.99013016	1.486702545	0.99013016	1.486702545

Shear Velocity		Bed Shear		Bed Shear	
u*		Tau-0		tau-0	
0.08323	ft/s	0.013438463	lb/ft^2	0.64	Pa
0.13239	ft/s	0.03400292	lb/ft^2	1.63	Pa
0.14043	ft/s	0.038258918	lb/ft^2	1.83	Pa

From the prior regression analyses, it was recommended that the third option be the procedure followed to calculate the shear at the bed. The top half of the flow did not contribute to shear distribution and the top of the viscous layer was assumed to be the location of zero velocity. Table 21 is a summary of the device shear capabilities.

Table 21. Flume bed shear stress values.

Propeller	Setting	Bed Shear Stress (lb/ft^2)	Bed Shear Stress (Pa)
Half	1	0.0071	0.34
Half	2	0.0098	0.47
Full	1	0.0135	0.64
Half	3	0.0137	0.65
Half	4	0.0169	0.81
Full	2	0.0179	0.86
Full	3	0.0268	1.28
Half	5	0.0279	1.34
Full	4	0.0383	1.83

All velocities used to compute the bed shear stresses were collected utilizing the Acoustic Doppler Velocimeter (ADV). For the flume portion of the research project, the bed shear stress was assumed equal to the shear stress on the soil surface and, therefore, equal to the critical shear stress.

Vita



Tara Liyana Mallison, originally named Tara Teresa Liyana, was born in Moberly, Missouri, to parents Andrew and Loretta Liyana. One of five children, Tara Mallison is a middle child and full of spirit. She grew up in Kingwood, Texas, and attended Bear Branch Elementary. Twelve years later, her family moved to Hendersonville, Tennessee, where she graduated from Robert E. Ellis Middle School and Hendersonville High School with honors in academics and athletics.

Tara's undergraduate alma mater is Auburn University (AU) where she spent four years studying Civil Engineering. While she attended the university in the loveliest village on the plains, Tara was awarded a Juniors Honors Certificate for passing challenging core classes in Honors Chemistry, World Literature, World History and Political Science, and earned the James E. Martin Initiative Award. As an active member of a mentoring community, Vice-President of AU Chi-Epsilon, Treasurer of AU American Society of Civil Engineering, Public Relations Chair of Representatives of the Auburn University Swimming & Diving Team, Indian Lake Swim & Tennis Club swim coach, swim technique instructor, and undergraduate research assistant overseen by Dr. David H. Timm, Mallison also kept busy with athletics and friends. All the while, Tara maintained her course towards graduating Magna Cum Laude.

After leaving Alabama, Tara Mallison moved back to Tennessee to attend the University of Tennessee in Knoxville. She spent her first summer in the city coaching at the Gulfwood Swim Team, aiding graduate research assistants on-campus, and falling in love with the east Tennessee community. During her graduate degree, she married William Tyler Mallison, worked as a graduate research/teaching assistant for Dr. John S. Schwartz at the University of Tennessee, and interned at CH2M HILL. In May 2008, Tara Mallison earned her Master of Science degree in Environmental Engineering with a concentration in Water Resources. Hopefully, her future experiences will remain as bright and challenging as her past endeavors.